FACULTY OF MATHEMATICS, PHYSICS AND INFORMATICS
COMENIUS UNIVERSITY
BRATISLAVA

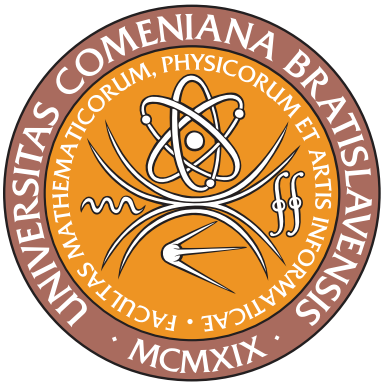

Department of Nuclear Physics and Biophysics

Gamma-spectroscopy of K-isomers and Non-yrast States in ^{254}No - Influence of Deformed Shell Gaps $Z = 100$ and $N = 152$

Academic Dissertation
for the Degree of
Doctor of Philosophy

by

Martin Venhart

Supervisor: prof. RNDr. Š. Šáro DrSc. Bratislava 2008

This is not the end. It is not even the beginning of the end. But it is, perhaps, the end of the beginning.

sir Winston Leonard Spencer Churchill
(1874 - 1965)

Abstract

Spectroscopic studies of K-isomers in transfermium nucleus ^{254}No have been carried out at Accelerator Laboratory of the University of Jyväskylä employing the RITU gas-filled separator. Along with the separator, two very efficient spectrometer, the JUROGAM at target position and the GREAT at focal plane have been used. Combination of both detection systems allowed the powerfull recoil-electron tagging techniques to be used.

The decay scheme of known K-isomeric state with half-life of 264.6 ms has been discovered and in addition new short-lived isomer with the half-life of 184.8 μs has been identified. New $K^{\pi} = 3^{+}$ rotational band has been observed for the first time. Structure of this band provides unambiguous assumption of two-quasiproton structure to the band-head. This state involves the $2f_{5/2}$ proton orbital which properties are crucial for prediction of position of next proton spherical shell.

The results presented extend the knowledge of isomeric and non-yrast structures in transfermium nuclei and therefore provide valuable input to nuclear structure calculations in the heavy element region.

Acknowledgement

First of all I would like to thank to my official supervisor Prof. Štefan Šáro. Without him, things would look very different. I am also deeply indebted to Prof. Matti Leino and Prof. Rauno Julin for their strong support and for the possibility to work in the laboratory located in one of the most beautiful places I have ever seen. I am grateful to Paul Greenlees for help during the data analysis, introducing me into the heavy nuclei problematics and answering my neverending questions. He is a great teacher! I want to thank also to all the people that made my often trips to Finnland very beautiful, namely Cath, Panu, Pete, Sarah, Jan, Janne, Tuomas, Markus, Steffen, Ari-Pekka, Sakari and Juha. Kiitos! If I have missed anyone out I apologise myself... I really love Jyväskylä and I miss its wonderful white nights!

Another big thank you goes to GSI Darmstadt, namely to Prof. Sigurd Hofmann for the possibility to work in his group during exciting super-heavy elements experiments. I thank to Dr. Fritz Peter Heßberger and to Dr. Dieter Ackermann for the advises that they always gave me. Very special "Grazie" goes to Barbara. Every day when I met this wonderfull Italian girl was brighter for me!

I am indebted to Dr. Andrei Andreyev and Dr. Teng Lek Khoo for support, advises and help. I am grateful to my colleagues Braňo, Stano and Janka for discussions and smooth atmosphere during working days in Bratislava or abroad.

I thank to all my friends, especially to Majo, Tomáš, Slavo and other for cycling and beautiful moments that we spent at l'Alpe d'Huez, Mont Ventoux or Col du Tourmalet. One thank you goes also to the ballet and opera ensemble of the Slovak National Theatre for glorious experiences.

And at last, but not at least my biggest "Ďakujem!" goes to my family - my parents, my sister and to my grandparents for their love and continual strong support during whole my life.

Martin
In Trnava, 16^{th} of January 2008

Contents

Chapter 1

Introduction

Atomic nucleus has been under intensive investigation since its discovery by Ernst Rutherford in early years of the 20^{th} century. Despite this fact, many nuclear properties still remain unclear. There exist many theoretical approaches for description of fundament of matter forming atomic nucleus in the present. The nuclei with proton number around 100 were a good field for testing of nuclear models in the past decade and therefore many experiments oriented to spectroscopy of transfermium nuclei were performed. This region of the table of isotopes became accessible thanks to the great challenge in heavy ions acceleration technology.

First steps in an in-beam γ-spectroscopy were experiments oriented to even-even nuclei which have started with pioneering studies of ^{254}No [Rei99, Lei99] employing the GAMMASPHERE and the SARI spectrometers at ANL and JYFL respectively. These experiments yield an information about parameters such as the moments of inertia, deformation and stability against fission. Later the in-beam experiments continued at JYFL utilising target position γ-spectrometers - the JUROSPHERE, the JUROSPHERE II. and the JUROGAM. Until these days even-even isotopes ^{248}Fm [Her07], ^{250}Fm [Bas06] and ^{252}No [Lep06] were studied at JYFL. In the future there is a plan to investigate ^{256}Rf employing new JUROGAM II. array equipped with fully digital data acquisition system. Another important role in the in-beam research play studies of odd-mass nuclei. Measurement of branching ratios of mixed M1/E2 and stretched E2 transitions within the rotational bands based on the ground-state or excited states allows the insight into the band-head structure. Several of these experiments were performed at JYFL and ANL. The datasets for isotopes ^{251}Md [Cha07], ^{255}Lr [Gre05] and ^{253}No [Rei05, Her02] were obtained.

The γ-spectroscopy of heavy nuclei is often very complicated due to the strong internal conversion of low-energy transitions. This is the most marginal in the case of odd-mass isotopes due to the presence of M1 transitions. Therefore the SACRED conversion electrons target position array has been constructed and several experiments complementary to γ-spectroscopy were performed (see e. g. [Hum04]). Each nucleus needs thus to be studied twice - γ-rays and electrons. To avoid this problem the combined SAGE spectrometer for simultaneous measurements of γ-rays

and electrons was proposed and will operate at JYLF.

The in-beam experiments are complemented with decay studies performed by detector systems placed at the focal plane of separators. The GREAT spectrometer at JYLF heralds complex system of detectors of different types. It can be employed as a powerfull standalone device or as a tagging unit during in-beam experiments. Another strong experimental facility is active in the GSI at kinematic separator SHIP. Its main advantage is possibility of using of very intensive heavy ions beams (ones of the most intensive worldwide in the present). Many successfull alpha-gamma decay studies have been performed there - see e.g. [Hes05] and references therein.

Theoretical calculations predict large quadrupole deformation for the ground-state of nuclei in the region of ^{252}Fm. As the largest deformations, β_2 values of about 0.25 [Nil69, Sob89, Cwi94, Sob01] were calculated. The reason was found in a compression of single-particle energy levels below and above proton number of Z = 100 and a neutron number of N = 152. Due to the bunching of levels at low energy, the (negative) binding energy is decreased and nuclei in the region of the level gap gain stability.

At which proton or neutron numbers the energy gaps appear, depends on details of the single-particle level scheme. Whereas the macroscopic-microscopic models predict the largest energy gap at Z = 100 and N = 152 [Nil69, Sob89, Cwi94, Sob01], some self consistent mean field calculations, as e.g. [Ben03], predict large gaps at Z = 104 and N = 150, at β_2 values of 0.28. In order to obtain a unique and the most precise description of these heavy nuclei, detailed spectroscopic information is needed. This effort is especially important, because the same models are used for prediction of properties of superheavy nuclei.

K-isomers in even-even nuclei are formed with the multi-quasiparticle states. The decay of these states proceeds via K-hindered (usually M1 or E1) transitions to rotational states. Strength of K-hindrance is proportional to change of spin orientation, therefore the high-spin states are needed to form the isomeric state. According to this, the necessary conditions are strong quadrupole deformation as well as presence of high-Ω orbitals close to Fermi surface. Studies of properties of two-quasiparticle states yields information about the single-particle energies and the pair gap.

This work originates in the close cooperation with experimental groups at JYFL. It deals with analysis of two experimental runs performed at JYFL utilising the RITU gas-filled separator in conjunction with the GREAT and the JUROGAM. During both experiments K-isomers in ^{254}No were studied. First indirect observation of K-isomer in ^{254}No was reported in [Ghi73] but the decay scheme, the excitation energy and the nucleonic structure remained unclear. Now, more than 30 years later we were able to build full decay scheme and tentatively assign two-quasiproton structure to isomer. In addition new previously unknown four-quasiparticle isomeric state was observed.

Experiments discussed in the present work were carried out as a part of K-isomers in the nobelium region research program. This covers up studies of

^{248,250}Fm [Her07, Gre07] and ^{252}No [Sul07b]. Obtained data allowed to build limited systematics of two-quasiparticle levels and fix single-particle energies of some important orbitals. These results provide a valuable input for existing theoretical calculations probing their predictive power.

Main goals of the presented thesis are:

- Confirmation of existence of the K-isomer in ^{254}No
- Evidence for new isomeric states.
- Obtaining of the basic spectroscopic properties like excitation energy, spin, parity and decay scheme of observed isomers.
- Assignment of the nucleonic configurations to the observed multi-quasiparticle states deduced from the rotational bands properties.
- Improving the systematics of multi-quasiparticle states in even-even nuclei in the nobelium region.
- Comparison of the experimental results with existing theoretical models.

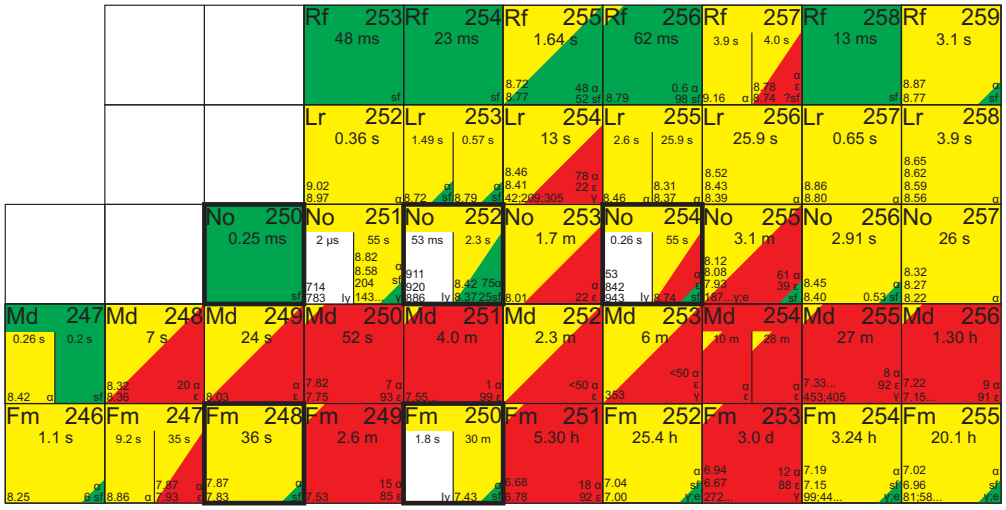

Figure 1.1: Excerpt from chart of nuclei in the area of interest. In present work K-isomers in ^{254}No were studied. In the picture there are marked isotopes where K-isomers were identified and investigated during past years.

Chapter 2

Nuclear properties

This chapter is based upon [Kra88, Hey04, Pau02, Nil95, Hod97].

2.1 The nuclear shell model

Shell model was developed in the late 1940s [May49, Hax49]. Previous models (liquid drop model, Fermi gas model etc.) could not describe several nuclear phenomenas like e. g. :

- Existence of magic numbers
- First excited states of doubly magic nuclei are anomalously high (> 1.5 MeV)
- Neutron induced reaction resonance structure
- Series of nuclei with same spin and parity of lowest excited states
- Discontinuities in nucleon binding energy

2.1.1 Single-particle spherical shell model

Single-particle spherical shell model ignores nucleon-nucleon interactions and describes the nucleus as a system of independent nucleons in a central potential. Hamiltonian for a system of interacting nucleons is

$$\hat{H} = \sum_i \hat{T}_i + \sum_{i<j} V_{ij}, \tag{2.1}$$

where $\hat{T}_i$ is a kinetic energy operator and V_{ij} is a nucleon-nucleon potential. Hamiltonian can be split into two components: central part $\hat{H}_0$ and a residual non-central part $\hat{H}_{res}$

$$\hat{H} = \hat{H}_0 + \hat{H}_{res}, \tag{2.2}$$

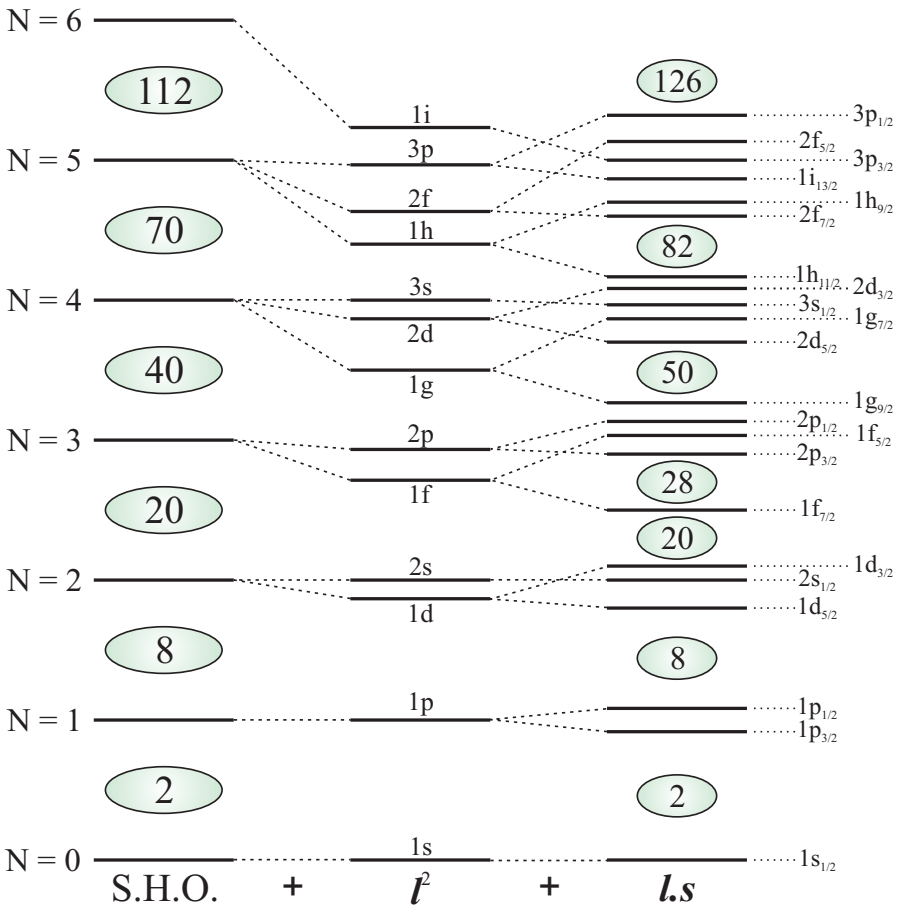

Figure 2.1: Sequence of single-particle energy levels for spherical harmonic oscillator (S.H.O.) potential with the addition of flat bottom and spin-orbital terms.

where

$$\hat{H}_0 = \sum_i (\hat{T}_i + V_i) = \sum_i \hat{h}_i \tag{2.3}$$

and

$$\hat{H}_{res} = \sum_{i<j} (V_{ij} - V_i), \tag{2.4}$$

where V_i is a central potential. If residual effects are small, the nucleus is well described only by central potential. The single-particle wave functions $|\varphi_i\rangle$ are then the solution of Schrödinger equation

$$\hat{h}_i|\varphi_i\rangle = \epsilon_i|\varphi_i\rangle. \tag{2.5}$$

The wave function $|\Psi\rangle$ of a system of independent particles is then the linear combination of the single-particle wave functions. Several descriptions for the

central potential are used. The most simple are the finite square well

$$V(r) = \begin{cases} -V_0 & \text{if } r < R \\ 0 & \text{if } r > R, \end{cases} \tag{2.6}$$

and the harmonic oscillator potential

$$V(r) = \begin{cases} -V_0\left[1 - \frac{r^2}{R^2}\right] & \text{if } r < R \\ 0 & \text{if } r > R \end{cases} \tag{2.7}$$

More realistic is the Woods-Saxon potential[Woo54]

$$V(r) = \frac{-V_0}{1 + \exp(\frac{r-R}{a})}, \tag{2.8}$$

where R is the half-density radius and a is the diffuseness parameter.

Basic potentials as they were given above could not explain the existence of magic numbers. Therefore Mayer [May49] and Haxel, Jensen and Suess [Hax49], following a suggestion of E. Fermi, proposed an additional spin-orbital term to central potential in order to reproduce magic numbers

$$V_i(r) = V_0 + V_S(r)\langle ls \rangle. \tag{2.9}$$

Spin-orbital potential arises from coupling between intristic (**s**) and orbital (**l**) angular momentum.

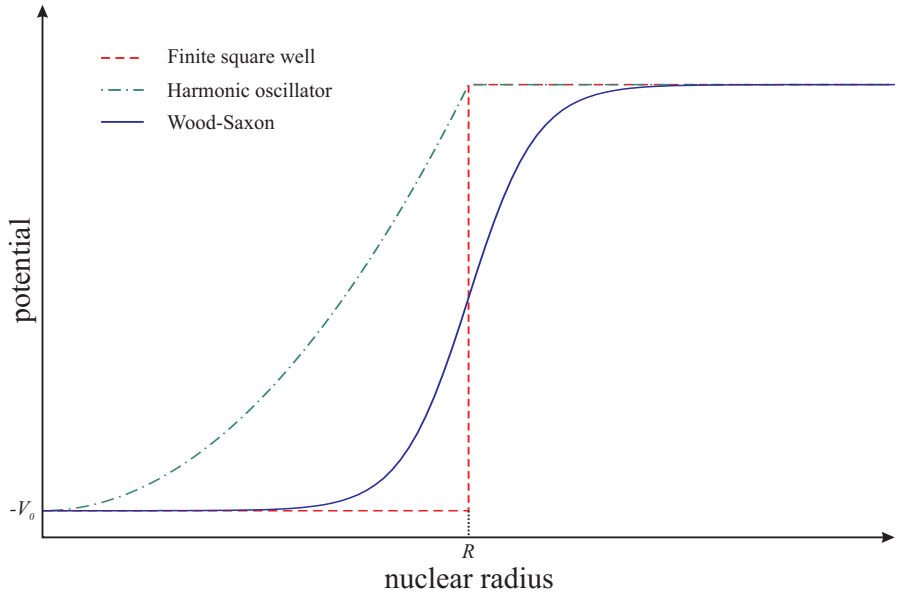

Figure 2.2: Potentials used in single-particle shell models.

2.1.2 Deformed shell model - Nillson model

In 1955 S. G. Nilsson introduced the shell model describing ellipsoidally deformed nuclei [Nil55]. Nilsson used axially symmetric deformed harmonic oscillator, which enables much of the calculation to be done analytically

$$V = \frac{m(\omega_x^2 x^2 + \omega_y^2 y^2 + \omega_z^2 z^2)}{2} - \kappa\hbar\omega_0\left[2\vec{ls} + \mu\vec{l^2}\right]. \tag{2.10}$$

First term represents deformed oscillator potential: $\omega_x^2 = \omega_y^2 = \omega_0^2(1 + \frac{2}{3}\epsilon_2)$ and $\omega_z^2 = \omega_0^2(1 - \frac{4}{3}\epsilon_2)$, where ω_0 is the spherical oscillator frequency and ϵ_2 is the Nilsson deformation parameter - see formula 2.21. Parameters κ and μ are introduced to adjust strength of ls and l^2 term.

In the Nilsson model each orbital is characterised by a set of asymptotic (as they become "good" only in the case of infinitive deformation of the nucleus) quantum numbers Ω^π[N,n_z,Λ]:

- Ω - the projection of the total angular momentum on the symmetry axis.
- π - the parity of the state.
- N - the total oscillator shell quantum number.
- n_z - the number of oscillator quanta in the z direction.
- Λ - the projection of angular momentum along the symmetry axis, Ω=Λ+Σ, where Σ is the projection of the intristic spin along the symmetry axis.

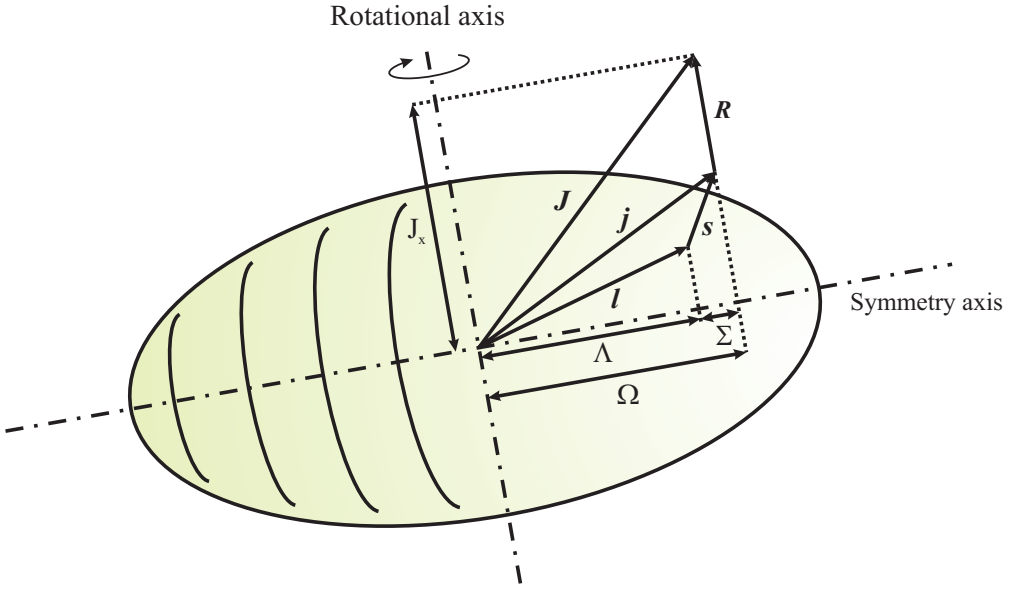

Figure 2.3: Asymptotic quantum numbers in the Nilsson model.

Plots of energy levels versus quadrupole deformation parameter are generally called Nilsson diagrams (whatever type of potential is used). An example of the Nilsson diagram is shown in Fig. 2.4.

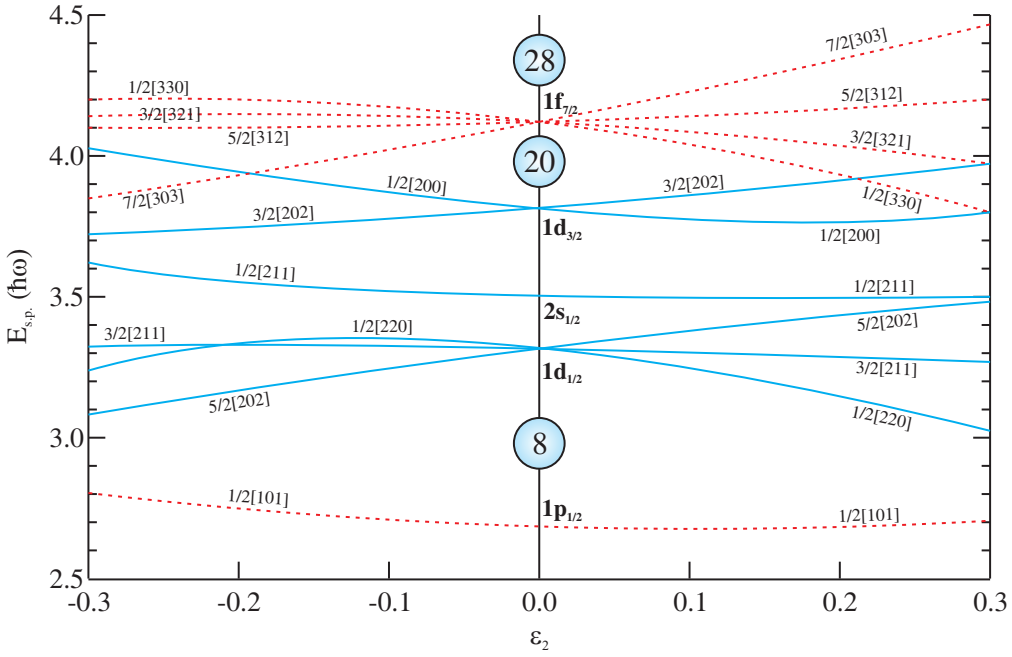

Figure 2.4: Nilsson diagram for protons, $8 \leq Z \leq 28$.

2.1.3 Cranked shell model

Cranked shell model was introduced by Inglis [Ing54] (later improved by Bengtsson and Frauendorf [Ben79]) in order to describe a nucleus rotating around an axis perpendicular to the symmetry axis, at a fixed rotational frequency ω. The cranked Hamiltonian (or called Routhian) is then

$$H^{\omega} = H_{int} - \hbar\omega J_x, \tag{2.11}$$

where H_{int} is the intristic single-particle Hamiltonian and J_x is the aligned angular momentum

$$J_x = \sqrt{J(J+1) - K^2}. \tag{2.12}$$

The second term in equation 2.11 describes the rotational perturbation due to the Coriolis and centrifugal forces in the rotating frame. The presence of this term in the Hamiltonian brakes symmetries. Cranking Hamiltonian is only symmetric for rotation about the axis perpendicular to the symmetry axis. This is described by:

$$R_x(\pi)|\Psi\rangle = r|\Psi\rangle = e^{-i\pi J_x}|\Psi\rangle. \tag{2.13}$$

Rotation of 2π leaves the wavefunction unchanged for even-A nuclei, while for odd-A nucleus it changes sign. Hence

$$R_x^2(\pi)|\Psi\rangle = r^2|\Psi\rangle = (-1)^A|\Psi\rangle. \tag{2.14}$$

Eigenvalues of operator R_x are then

$$\begin{aligned} r &= \pm 1 \text{ for even A} \\ r &= \pm i \text{ for odd A.} \end{aligned} \tag{2.15}$$

Widely used is the signature quantum number α, which is additive and is defined as

$$r = e^{-i\pi\alpha}. \tag{2.16}$$

This gives possible two-possible spin sequences for rotational bands

$$I = \alpha \bmod 2 \tag{2.17}$$

and thus there are two signature partners evident.

2.2 Macroscopic properties of the nuclei

2.2.1 Nuclear deformation

Existence of single-particle properties which cannot be interpreted in the framework of spherical shell model or large quadrupole moments for nuclei away from closed shell can be explained with static nuclear deformation. The surface of the nucleus can be expressed in the terms of spherical harmonic functions

$$R(\Theta, \Phi) = R_0\Big(1 + \sum_{\lambda=0}^{\infty}\sum_{\mu=-\lambda}^{\lambda} a_{\lambda\mu} Y_\lambda^\mu(\Theta, \Phi)\Big), \tag{2.18}$$

where R_0 is the radius of the sphere and coefficients $a_{\lambda\mu}$ represents abberation from spherical shape. $\lambda = 2$ represents quadrupole , $\lambda = 3$ octupole deformation etc.

The most important deformation from the point of view of present work is the quadrupole deformation. The system of principal axes five $a_{\lambda\mu}$ coefficients reduce to only two independent ones (a_{20} and a_{22}) because of

$$\begin{aligned} a_{22} &= a_{2-2} \\ a_{21} &= a_{2-1} = 0. \end{aligned} \tag{2.19}$$

In the system of principal axes parametrisation using polar coordinates can be introduced

$$\begin{aligned} a_{20} &= \beta_2 \cos\gamma \\ a_{22} &= -\frac{\sqrt{2}}{2}\beta_2 \sin\gamma, \end{aligned} \tag{2.20}$$

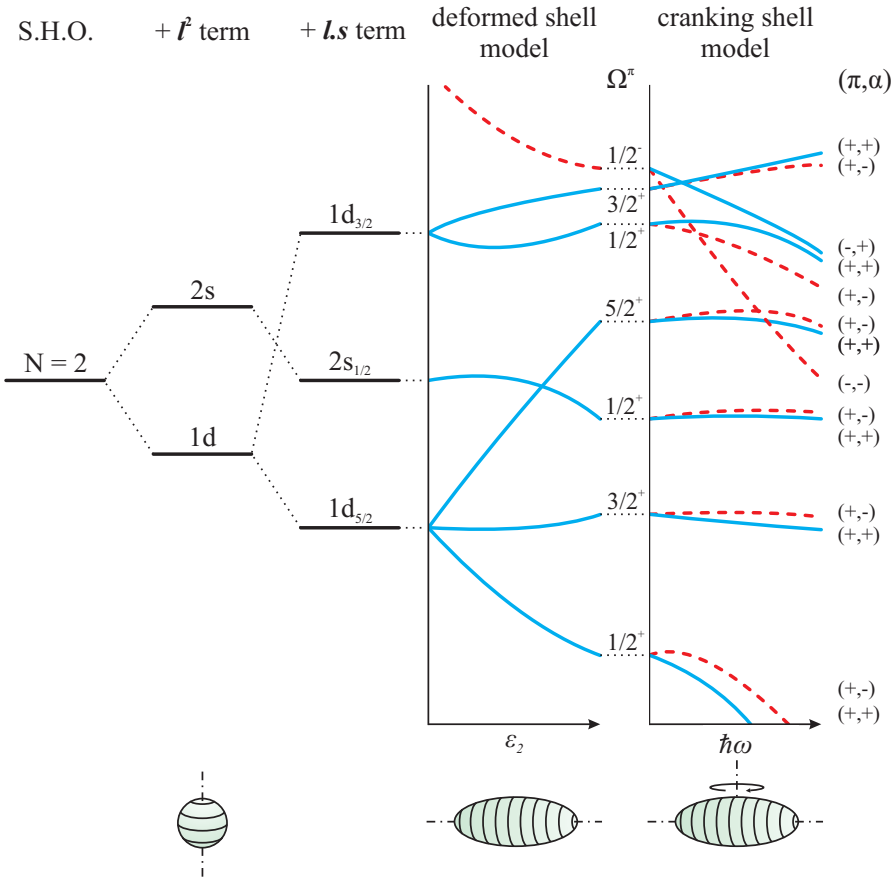

Figure 2.5: Evolution of single-particle orbitals using different shell model approaches. Figure adapted from [Pau02].

where β_2 is the quadrupole deformation parameter and γ describes deviation from axial symmetry. For axially symmetric nuclei ($\gamma = 0$) the Nilsson deformation parameter ϵ_2 is introduced and is related to β_2:

$$\beta_2 = \sqrt{\pi/5}\left(\frac{4}{3}\epsilon_2 + \frac{4}{9}\epsilon_2^2 + \frac{4}{27}\epsilon_2^3 + \frac{4}{81}\epsilon_2^4 + ...\right) \tag{2.21}$$

Different possible shapes of an axially symmetric nucleus are shown in Fig. 2.6. In some nuclei in the neutron deficient lead region the shape coexistence phenomenon is known [And00].

2.2.2 Rotation

Properties of nuclei around the closed shells are quite well described by the spherical shell model. As we move away from the closed shell, the situation becomes more and more complicated. For strongly deformed nuclei, the collective excitations such as rotation and vibration become to play very important role.

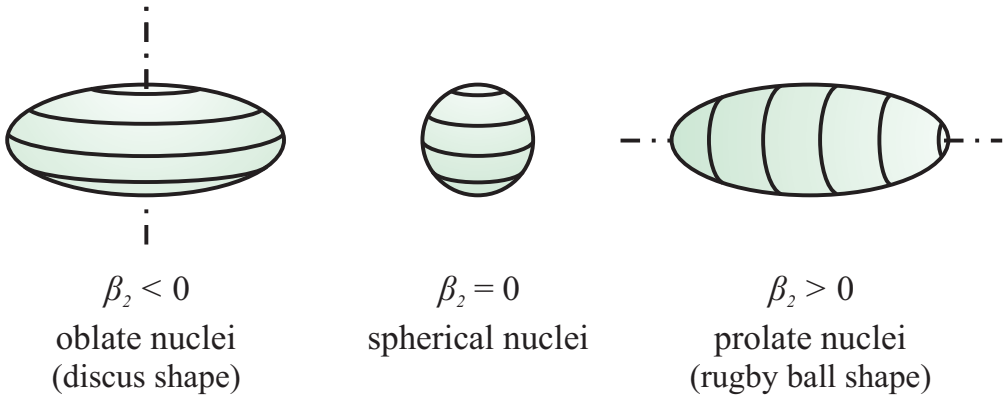

Figure 2.6: Quadrupole deformation shapes of axially symmetric nuclei.

Deformation allows the definition of a nuclear orientation and the possibility of observing the effect of rotation around an axis perpendicular to the symmetry axis. The total angular momentum $\vec{J}$ is then

$$\vec{J} = \vec{j} + \vec{R}, \tag{2.22}$$

where $\vec{j}$ is the intristic angular momentum and $\vec{R}$ is the collective angular momentum (see Fig. 2.3). Quantum number K is the projection of total angular momentum $\vec{J}$ onto the symmetry axis.

Classically, the rotation energy of a body with moment of inertia $\mathcal{J}$ is

$$E_{rot} = \frac{1}{2}\mathcal{J}\omega^2 = \frac{J^2}{2\mathcal{J}}, \tag{2.23}$$

where ω is the angular velocity. Low-lying rotational states in even-even nuclei follow the quantum mechanical equivalent of formula 2.23

$$E_{rot} = \frac{\hbar^2 J(J+1)}{2\mathcal{J}}. \tag{2.24}$$

Going to higher values of J one can see that the energies depart somewhat from the above formula. Higher rotational velocity increases the centrifugal force and therefore an improved formula

$$E_{rot} = \frac{\hbar^2}{2\mathcal{J}}\big(J(J+1) - \alpha J^2(J+1)^2\big) \tag{2.25}$$

is necessary.

In the case of rotational band based on the band-head with non-zero intristic angular momentum (K $\neq$ 0), the excitation energy of the states is

$$E_{rot} = \frac{\hbar^2}{2\mathcal{J}}\big(J(J+1) - K(K+1)\big). \tag{2.26}$$

In all formulas above, $\mathcal{J}$ defines the static moment of inertia, but due to the residual interactions it strictly differs from the value calculated for a rigid rotor body

$$\mathcal{J}_{rig} = \frac{2}{5} AMR_0^2(1 + 0.31\beta), \tag{2.27}$$

where β is the deformation parameter and R_0 is the radius of the nucleus ($R_0 \sim A^{1/3}$).

The rotating nucleus can be described in term of its angular velocity

$$\hbar\omega = \frac{dE}{dJ_x}, \tag{2.28}$$

where J_x is the projection of the total angular momentum onto the rotational axis (so called aligned angular momentum)

$$J_x = \sqrt{J(J+1) - K^2}. \tag{2.29}$$

In order to describe the collective motion two moments of inertia are introduced:

- **Kinematic moment of inertia**

$$\mathcal{J}^{(1)} = J_x \Big(\frac{dE}{dJ_x}\Big)^{-1} \hbar^2 = \hbar \frac{J_x}{\omega} \tag{2.30}$$

- **Dynamic moment of inertia**

$$\mathcal{J}^{(2)} = \Big(\frac{d^2E}{dJ_x^2}\Big)^{-1} \hbar^2 = \hbar \frac{dJ_x}{d\omega} \tag{2.31}$$

Both moments of inertia can be related as follows

$$\mathcal{J}^{(2)} = \frac{dJ_x}{d\omega} = \frac{d}{d\omega}(\omega \mathcal{J}^{(1)}) = \mathcal{J}^{(1)} + \omega \frac{d\mathcal{J}^{(1)}}{d\omega}. \tag{2.32}$$

2.3 Microscopic correction method

Previously mentioned model approaches can describe satisfactorily many of nuclear properties but fails for example in reproduction of the binding energy of a nucleus.

Therefore microscopic-macroscopic model, incorporating both approaches, has been introduced by Strutinsky [Str67]. The total energy of a nucleus is expressed as follows

$$E = E_{mac.} + E_{mic.}, \tag{2.33}$$

where $E_{mac.}$ is the macroscopic energy (most common calculated by the liquid drop model - see [Nil95] and references therein) and $E_{mic.}$ represents the shell plus

pairing correction. Microscopic correction was calculated on the basis of finite-range liquid drop model and droplet model by Möller *et al.* [Mol97] - see Fig. 2.7.

Existence of shell effects is crucial for the stability of transfermium nuclei. In the Strutinsky model is the shell defined as a large inhomogeneity within the single-particle orbitals distribution. Following this definition, shells may be expected at any nuclear shape and in the region of nobelium deformed ground state is prefered.

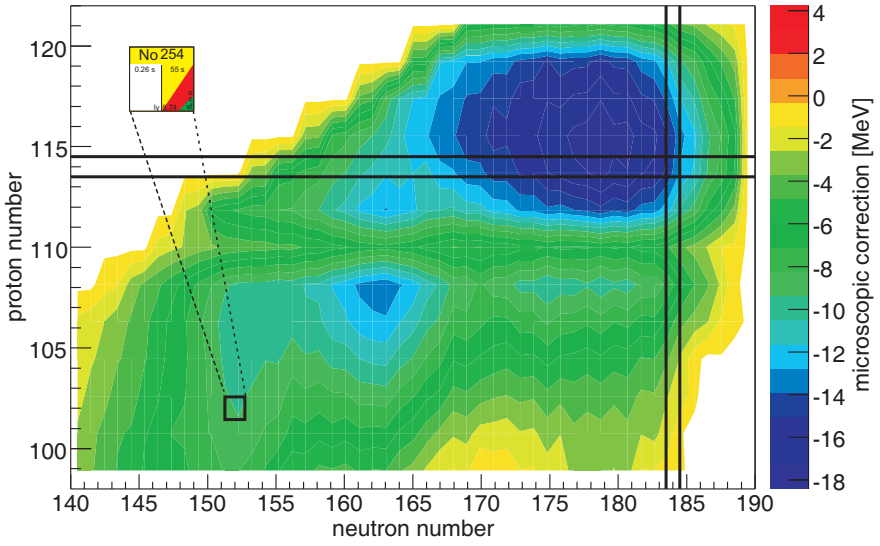

Figure 2.7: Microscopic correction calculated by [Mol97] in superheavy region. Position of the studied ^{254}No and of the expected doubly-magic nucleus ^{298}114 is marked.

2.4 Pairing interaction

One of the most important residual interaction is the pairing interaction. There are several experimental evidences for pairing interaction:

- The ground state of all even-even nuclei is $J^{\pi} = 0^{+}$.
- There are missing low-energy non-collective excitations in even-even nuclei.
- The ground state spin of odd mass nucleus is determined by the spin of the last unpaired nucleon.
- Nuclear moments of inertia are lower than expected rigid-body values.

Interaction energy of the nucleon-nucleon pair is given only with spatial overlap of the wave functions of both nucleons. The greatest overlap would occur if both nucleons orbit the nucleus in the same level. This is strictly forbidden by Pauli's principle thus the greatest allowed overlap occurs for particles in time-reversed orbits.

Due to the strong overlap of the wave functions, pairs of particles can scatter to another orbit. Following the angular momentum conservation law particles are still in time-reversed orbits with $J^\pi = 0^+$, only the plane of orbits has slewed.

Theoretically is the pair interaction described by an operator $\hat{G}$ with following properties

$$\langle m_2, m_2'|\hat{G}|m_1, m_1'\rangle = -G\delta_{m_1,-m_1'}\delta_{m_2,-m_2'}, \tag{2.34}$$

where G is the pair energy. This interaction effects between the states $|m_1, -m_1\rangle$ and $|m_2, -m_2\rangle$ also when they belongs to shells with different j. As a consequence of this is an existence of the configuration mixing - the pair of the valence nucleons occurs with certain amplitude in more than one shell. This leads to smearing of the Fermi surface. In the absence of pairing the Fermi surface would be a diving line between filled and unfilled states (see Figure 2.9 part a).

It was found that the first non-collective excitation level is in even-even nuclei located very high (~ 1 MeV). In odd-mass case it is at the half of this value. These gaps are completely missing in odd-odd nuclei - see Figure 2.8. Thus even-even nuclei are more bound than odd-mass ones (and odd-mass more than odd-odd cases). Based on these binding energy differences between even and odd-mass neighbouring nuclei simple expressions have been derived [Jen84]. The simplest is the three-point mass formula

$$\Delta^{(3)}(N) = \frac{(-1)^N}{2}[E(N+1) - 2E(N) + E(N-1)], \tag{2.35}$$

where N is the number of protons or neutrons and E is the ground state binding energy. In some cases the five-point mass formula

$$\Delta^{(5)}(N) = -\frac{(-1)^N}{8}[E(N+2) - 4E(N+1) + 6E(N) - 4E(N-1) + E(N-2)] \tag{2.36}$$

is better approximation of pair gap - e.g. isotopes in tin region [Ben00].

The odd-even mass staggering in nuclei in the context of self-consisted mean-field calculations was analysed and referred by [Dug01]. Additional mean-field contributions with realistic pairing were used for modification of the standard three-point mass formula.

2.4.1 Quasiparticles

To explain the existence of energy gaps in non-collective excitations of nuclei the concept of quasiparticles was suggested [Boh58]. It is based on an analogy between this effect and the character of an electronic excitation of a superconducting metal.

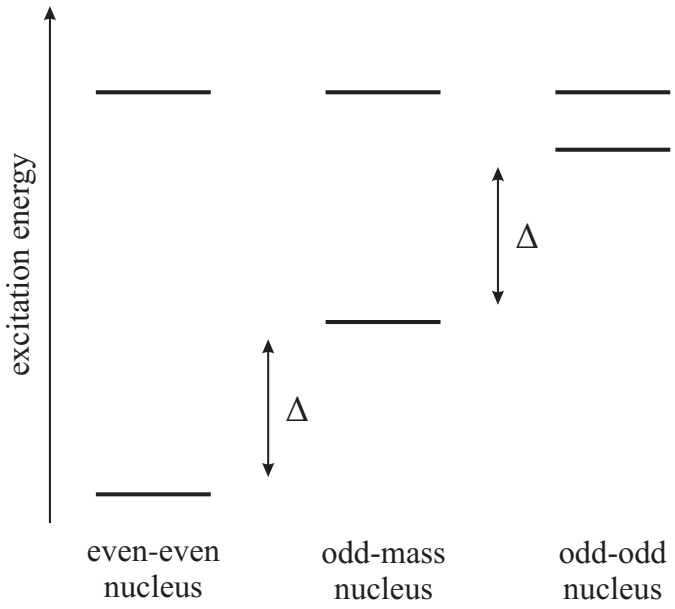

Figure 2.8: Schematic drawing of excitation energy of the first non-collective excitation level in even-even, odd-mass and odd-odd nuclei, respectively.

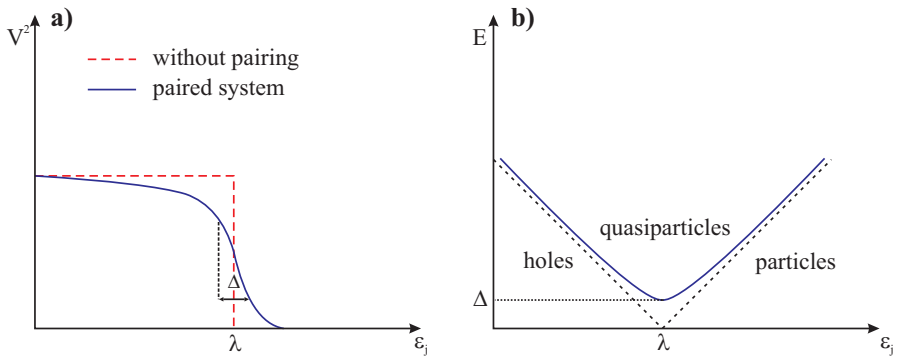

Figure 2.9: a) Occupation probability of single-particle states. While in unpaired system the Fermi surface presents sharp border between filled and unfilled states, pairing leads to the smearing of the Fermi surface. b) Excitation energy of quasiparticle states.

The quasiparticle is a mixture of particle and hole states (see Fig. 2.9 part b). Excitation energy of the quasiparticle occupying the j-shell of the nucleus is

$$E_j = \sqrt{(\epsilon_j - \lambda)^2 + \Delta^2}, \tag{2.37}$$

where ϵ_j is the single-particle energy, λ is the chemical potential and Δ is the pair gap parameter. The probability that a state j is occupied by a particle (V_j) or by

a hole (U_j) is given by expressions

$$V_j = \frac{1}{\sqrt{2}}\Big[1 + \frac{\epsilon_j - \lambda}{E_j}\Big]^{1/2}$$
$$U_j = \frac{1}{\sqrt{2}}\Big[1 + \frac{\epsilon_j + \lambda}{E_j}\Big]^{1/2} \tag{2.38}$$

and hence

$$|V_j|^2 + |U_j|^2 = 1. \tag{2.39}$$

In the terms of occupation probabilities the pair gap may be expressed as

$$\Delta = G\sum_j U_j V_j. \tag{2.40}$$

2.4.2 Orbital blocking

If some unpaired nucleons are presented, the pairing interaction is affected due to the reduction of possible single-particle states that can by occupied by a pair of nucleons. If twice-degenerated level is filled by a single nucleon then Pauli principle forbids occupation by a pair. This is known as orbital blocking (because orbitals are "blocked"). Blocking reduces the magnitude of pair gap - it depends sensitively on the number of blocked levels, their location and the single-particle levels distribution near Fermi surface.

2.4.3 Two-quasiparticle states in even-even nuclei

Low-lying non-collective excitations are in even-even formed by two-quasiparticle states. Such a state origanates by braking of a pair o valence nucleons. Spin degeneracy is removed by residual spin dependet forces. Coupling rules for a lower-lying state were suggested by Gallagher [Gal62]

$$J = |\Omega_1 - \Omega_2| \quad \text{if} \quad \Omega_1 = \Lambda_1 \pm \frac{1}{2}, \Omega_2 = \Lambda_2 \pm \frac{1}{2}$$
$$J = \Omega_1 + \Omega_2 \quad \text{if} \quad \Omega_1 = \Lambda_1 \pm \frac{1}{2}, \Omega_2 = \Lambda_2 \mp \frac{1}{2}. \tag{2.41}$$

The g_k factor of a such state is given by the Landé formula:

$$g_K = \frac{g_{K1} + g_{K2}}{2} + \frac{\Omega_1(\Omega_1+1)(g_{K2} - g_{K1}) - \Omega_2(\Omega_2+1)(g_{K1} + g_{K2})}{2J(J+1)}. \tag{2.42}$$

When the spin-singlet two-quasiparticle state is performed, the excitation energy is lowered due to the residual spin-spin interaction. This has a value of 40 - 120 keV in U and Cf nuclei [Kat73]. In ^{254}No it is expected to be about 100 keV [Tan06].

If both two-quasineutron and two-quasiproton states are presented (and forming four-quasiparticle state) additional residual proton-neutron interaction needs to be taken into account. This lowers the excitation energy of the state by about 200 keV [Kho75].

2.5 The α decay

Many heavy nuclei decay through the α decay. It is a spontaneous emission of $^4He^{2+}$ ion, it can be schematically represented as

$$^{A}_{Z}\mathrm{X}_{N} \rightarrow {}^{A-4}_{Z-2}\mathrm{Y}_{N-2} + \alpha.$$

The kinetic energy of an α particle is characteristic for a certain isotope and is often used for identification. The energy released in the α decay, called the Q value is

$$Q = (m_X - m_Y - m_\alpha)c^2 \tag{2.43}$$

The decay will occur spontaneously only if $Q > 0$.

If the α decay occurs between states with $J_i^{\pi_i}$ and $J_f^{\pi_f}$ a selection rules

$$\begin{aligned} &|J_i - J_f| \leqq L \leqq J_i + J_f \\ &\pi_f = (-1)^L \pi_i, \end{aligned} \tag{2.44}$$

where L is the angular momentum carried by the α particle, must be fullfilled. Spin of the α particle is 0 therefore the total carried angular momentum has purely orbital character.

Quantum mechanical theory was developed in 1928 simultaneously by Gamow [Gam28] and by Gurney and Condon [Con28]. Central feature of this one-body model is that the α particle is formed inside the parent nucleus and could penetrate through the barrier. In this theory the disintegration constant is given by

$$\lambda = \omega P \tag{2.45}$$

where ω is the frequency with which the α particle occur at the barrier and P is the probability of penetration through the barrier. The probability to penetrate the barrier is

$$P = e^{-2G} \tag{2.46}$$

where G is the Gamow factor and it can be expressed in the WKB approximation [Boh55, Fro57] as

$$G = \sqrt{\frac{2m}{\hbar^2}} \int_a^b [V(r) - Q]^{1/2} dr \tag{2.47}$$

According to previous formulas it is possible to show that the disintegration probability λ depends on the Q-value like

$$\lambda = A + \frac{B}{\sqrt{Q}}, \tag{2.48}$$

where A and B are constants depending on the proton number. This is the Geiger-Nuttall law [Gei11] of the spherical even-even nuclei α decay.

Half-life of the α decay strongly depends on the structure of the initial and the final level. According to Rassmusen formalism [Ras59] the reduced width of the α decay δ^2 is introduced as follows:

$$\delta^2 = \frac{h\lambda}{P}, \tag{2.49}$$

where λ is the decay constant and P is the probability of penetration through the barrier, calculated using WKB integral (see 2.47) with additional term to describe the centrifugal barrier

$$V_{centr.}(r) = \frac{\hbar^2 l(l+1)}{2mr^2}. \tag{2.50}$$

Nuclear-α potential was derived from optical model [Igo58] to be

$$V_{nucl.-\alpha}(r) = -1100\exp\Big(-\frac{r - 1.17A^{1/3}}{0.574}\Big)[\mathrm{MeV}]. \tag{2.51}$$

Widely used spectroscopical constant is the hindrance factor of the α decay. It is defined as

$$HF = \frac{\delta^2_{g.s.}}{\delta^2_{exc.s.}}, \tag{2.52}$$

where $\delta^2_{g.s.}$ is the reduced width of ground-state to ground-state decay, while $\delta^2_{exc.s.}$ corresponds to ground-state to excited state transition. Measurement of the hindrance factor is a powerfull method for the determination of the spin of the excited states.

2.6 Electromagnetic processes

The energy of an electromagnetic radiation can be described mathematically in terms of a multipole moment expansion. This expansion converges rapidly and consequently only the lower orders are of importance. The terms correspond to 2^L-poles formalism, where L is the multipolarity of the transition. The electric multipole moments are related to the charge distribution and the magnetic ones to current densities.

2.6.1 Transition probabilities

The decay probality from initial $|\Psi_i\rangle$ to the final state $|\Psi_f\rangle$ is described by the matrix element of multipole operator

$$m_{fi}(\sigma L) = \langle \Psi_f | m(\sigma L) | \Psi_i \rangle, \tag{2.53}$$

where $m(\sigma L)$ is the operator of a multipole of the order L and σ characterizes the electric or the magnetic character of multipole. Function $m(\sigma L)$ changes the nuclear state from initial to final and produces a photon of correct energy, parity

and multipole order. The γ-ray transition probability for radiation of energy E_γ is

$$\lambda(\sigma L) = \frac{8\pi(L+1)}{\hbar L((2L+1)!!)^2}\Big(\frac{E_\gamma}{\hbar c}\Big)^{2L+1} B(\sigma L : I_i \to I_f), \tag{2.54}$$

where $B(\sigma L : I_i \to I_f)$ is the reduced transition probability. The reduced transition probability can be used to compare the strength of transition over the nuclear chart without the effect of transition energy.

For the γ-ray transition probabilities see Tab. 2.1. The single-particle probabilities were calculated by Weisskopf [Fir96] and the collective ones by Bohr and Mottelson [Boh75].

Table 2.1: The γ-rays transition probabilities estimations for single-particle [Fir96] and collective [Boh75] transitions. Transition energy is in MeV, $B(EL)$ in $\mathrm{e^2fm^{2L}}$, $B(ML)$ in $\mu_N^2\mathrm{fm}^{2L-2}$ and resulting probability in s^{-1}.

Multipolarity	**Half-life [s]**	
	Electric	**Magnetic**
Single-particle transitions		
1	$1.03 \times 10^{14} E_\gamma^3 A^{2/3}$	$3.15 \times 10^{13} E_\gamma^3$
2	$7.28 \times 10^{7} E_\gamma^5 A^{4/3}$	$2.24 \times 10^{7} E_\gamma^5 A^{2/3}$
3	$3.40 \times 10^{1} E_\gamma^7 A^{2}$	$1.04 \times 10^{1} E_\gamma^7 A^{4/3}$
4	$1.07 \times 10^{-5} E_\gamma^9 A^{8/3}$	$3.27 \times 10^{-6} E_\gamma^9 A^{2}$
5	$2.40 \times 10^{-12} E_\gamma^{11} A^{10/3}$	$7.36 \times 10^{-13} E_\gamma^{11} A^{8/3}$
Collective transitions		
1	$1.59 \times 10^{15} B(E1) E_\gamma^3$	$1.76 \times 10^{13} B(M1) E_\gamma^3$
2	$1.23 \times 10^{9} B(E2) E_\gamma^5$	$1.36 \times 10^{7} B(M2) E_\gamma^5$
3	$5.71 \times 10^{2} B(E3) E_\gamma^7$	$6.31 \times 10^{0} B(M3) E_\gamma^7$

2.6.2 Selection rules

A classical electromagnetic field that is produced by oscillating charges and currents transmits angular momentum as well as the energy. Multipole transition of the order of L transfers an angular momentum of $L\hbar$. Angular momentum must be conserved. This means that the initial angular momentum, $\overrightarrow{J_i}$, must equal to $\overrightarrow{J_f} + \overrightarrow{L}$. Thus the angular momentum selection rule is

$$|J_i - J_f| \leqq L \leqq J_i + J_f. \tag{2.55}$$

Transitions when $J_i = J_f$ and $L = 0$ proceed only via conversion electron emission - E0 decay (emission of γ-quantum is strictly forbidden because the intristic spin of photon equals to 1).

The additional selection rule is that for parity

$$\pi_f(\mathrm{M}L) = (-1)^{L+1}\pi_i,$$
$$\pi_f(\mathrm{E}L) = (-1)^{L}\pi_i. \tag{2.56}$$

Allowed multipolarities against parity and angular momentum change are shown in Tab. 2.2.

Table 2.2: Allowed multipolarities for some transitions. Transitions $0 \rightarrow 0$ are allowed only via non-radiative E0 decay. The magnetic transitions in brackets are allowed for given combinations of spin and parity changes but they are less probable than the electric ones.

ΔJ	**0**	**1**	**2**	**3**	**4**
$\pi_i\pi_f$ = **-1**	E1 (M2)	E1 (M2)	M2 E3	E3 (M4)	M4 E5
$\pi_i\pi_f$ = **+1**	M1 E2	M1 E2	E2 (M3)	M3 E4	E4 (M5)

2.6.3 Internal conversion

A competing electromagnetic process to γ-ray emission is that of internal conversion (IC). In this process the excited atomic nucleus interacts with one of the atomic electrons, transmits the excitation energy to it and the electron is ejected from the atom. The kinetic energy T_e of the electron depends upon the electron binding energy B_e in the atomic shell and the transition energy ΔE.

$$T_e = \Delta E - B_e. \tag{2.57}$$

Energetic threshold for IC is equal to the electron binding energy in a particular shell. Nobelium electrons binding energies are given in Tab. 2.3.

Table 2.3: Binding energies of electron in nobelium atomic shells [Fir96].

Shell	K	L_1	L_2	L_3	M_1	M_2	M_3	M_4	M_5
B_e **[keV]**	149.2	29.2	28.3	21.9	7.7	7.2	5.7	5.0	4.7

The internal conversion coefficient (ICC) is defined as the ratio of probability of conversion electron emission from particular subshell to the γ-ray emission probability:

$$\alpha = \frac{\lambda_e}{\lambda_\gamma}. \tag{2.58}$$

A total ICC is the sum of all partial ICC's

$$\alpha_t = \sum_i \alpha_i, \tag{2.59}$$

where i = K, L_1, L_2 ... The total decay probability is then

$$\lambda_t = \lambda_\gamma(1 + \alpha_t). \tag{2.60}$$

ICC increases with Z^3 (thus it becomes very important for heavy nuclei) and with the multipolarity of transition. It also decreases with increasing of the transition energy. For ICC for E1, E2, M1 and M2 in nobelium see Fig. 2.10. ICC used in this work were calculated using BRICC software [Kib05]. Measurement of ICC allows by comparing with theoretical values to deduce the multipolarity of the transition.

When the electron is emitted the vacancy is filled by an electron from a higher shell therefore characteristic X-rays or Augere electrons are emitted.

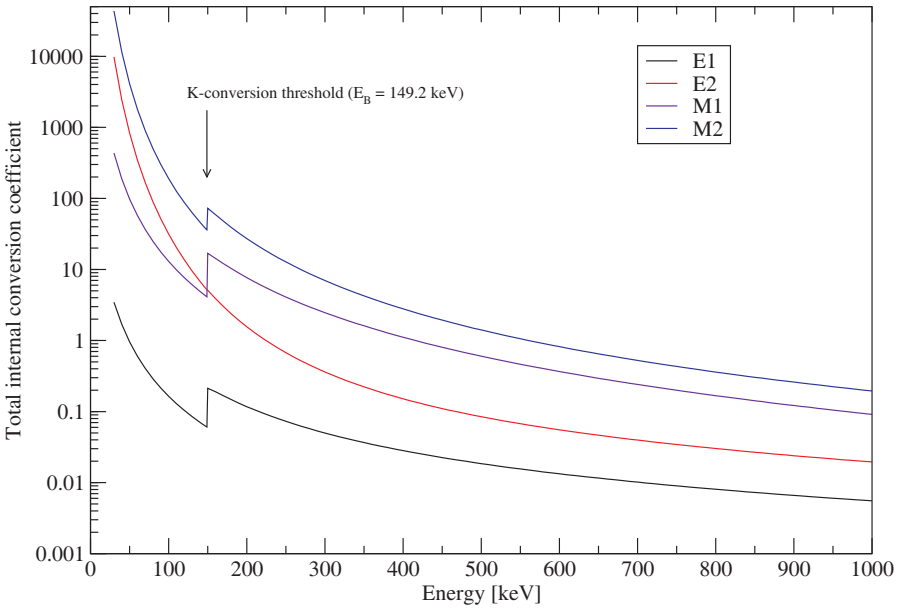

Figure 2.10: Total ICC for nobelium - E1, E2, M1 and M2 transition respectively. Values were calculated using BRICC software [Kib05].

2.6.4 Rotational bands - branching ratios and g-factors

States of rotational bands with both signature partners can decay via $\Delta J = 2$ transition (stretched E2) or via $\Delta J = 1$ transition (mixed M1/E2) respectively. Admixture of higher multipolarity in stretched E2 transitions is very small. Crossover-to-cascade (stretched E2 to mixed M1/E2) γ-rays branching ratio yields information about structure of the band-head. In the case of collective M1 and E2 transitions (if K $\neq$ 1/2) γ-ray reduced transition probability is given by formulas

$$B(\mathrm{M1} : |J\rangle \rightarrow |J-1\rangle) = \frac{3}{4\pi}(g_K - g_R)^2 K^2 |\langle JK10|J-1K\rangle|^2 \mu_N^2 \tag{2.61}$$

and

$$B(\mathrm{E2} : |J\rangle \rightarrow |J-2\rangle) = \frac{5}{16\pi} Q_0^2 |\langle JK20|J-2K\rangle|^2 [(eb)^2], \tag{2.62}$$

where Q_0 is the intristic electric quadrupole moment, g_R is the rotational gyromagnetic ratio (g-factor) and g_K is the intristic g-factor. In general, rotational g-factor is given by $g_R = \frac{Z}{A}$. However g_R can differ from this depending on configuration (see [Bel59, Mig59] for more detailed discussion). Intristic g_K-factor is related to the band-head structure and when it is extracted from measured band properties it can be compared with theoretically obtained values. The following formula can be derived for g_K

$$\frac{|g_K - g_R|}{Q_0} = 0.933 \frac{E_1}{\delta\sqrt{(J^2-1)}}, \tag{2.63}$$

where q is the quadrupole mixing ratio of $\Delta J = 1$ transition and is given as follows

$$\frac{\delta^2}{\delta^2+1} = \frac{2K^2(2J-1)}{(J-K-1)(J+K-1)(J+1)} \frac{E_1^5}{E_2^5} \lambda_\gamma. \tag{2.64}$$

For meaning of quantities in both formulas above see Fig. 2.11.

2.7 Nuclear isomerism

In general, isomers are excited, metastable quantum states of atomic nuclei. Depending on the structure and excitation energy isomers can decay via alpha, beta decay, spontaneous fission, proton emission or via electromagnetic transition into ground state or excited state of the same nucleus. It is open question what is the minimal half-life of a level to qualify it as an isomer. There is no "official" suggestion for it. In this work we decided to consider a level as an isomeric when the half-life is longer than 10 ns - minimal time difference that can be distinguished by Total data readout (TDR) acquisition system. This is much longer than a typical half-life of an excited nuclear state ($\sim 10^{-12}$ s). Isomers can be formed by various energy traps in atomic nuclei - see e.g. [Wal99, Wal01] and references therein for more detailed discussion.

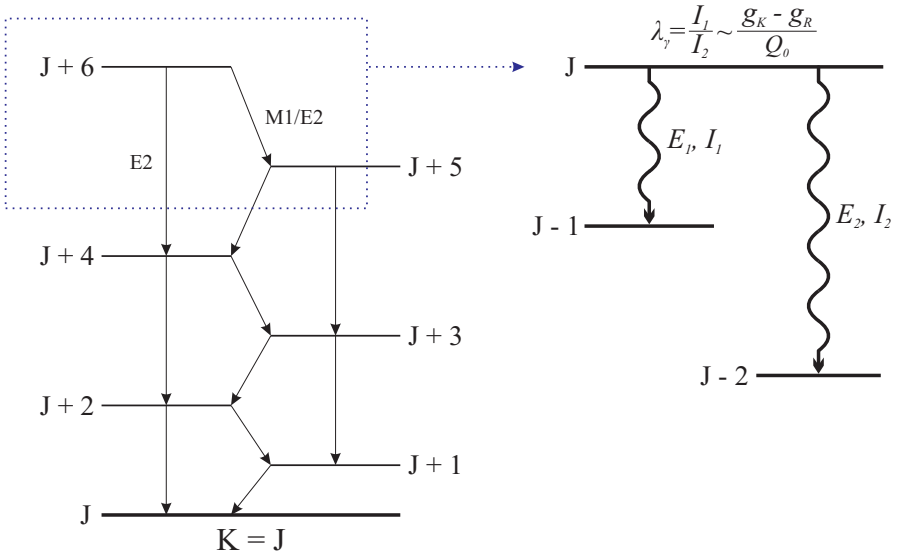

Figure 2.11: Rotational band and decay of rotational state.

2.7.1 Isomers as energy traps in atomic nuclei

- **Shape isomers**

  The existence of short-lived, spontaneously fissioning isomers is understood as population of a state in a second well of a double-humped fission barrier (see. Fig. 2.12). This isomeric state has a much lower barrier to penetrate resulting into much shorter spontaneous fission half-life. Backward γ-decay is hindered due to the different quadrupole deformation. Many shape isomers were observed in the region of Pu, Am and Cm isotopes - see e.g. [Fle67, Pol70].

- **Spin isomers**

  All known isomers in spherical or nearly-spherical nuclei are spin isomers - trapped high-spin levels. Decay into the lower energy states requires a large change of spin, therefore emission of radiation with high multipolarity is needed. Illustrative example is an isomer in ^{180}Ta. It is a $J^\pi = 9^-$ state with excitation energy of 75.3 keV and half-life of $>1.3\times10^{15}$ years [Fir96]. The ground-state is $J^\pi = 1^+$ state, thus emission of the highly improbable M8 radiation is required.

- **K-isomers**

  A special form of a spin trap is the K-isomer. Its existence depends also on orientation of the spin vector. K-isomers are excited states with large value of K quantum number (projection of spin onto nucleus symmetry axis). These states decay via K-forbidden low-multipolarity transitions [Wal97] into collective states based on rotation of lower-lying intristic configurations. Thus

the deformation plays an important role, because only deformed nuclei can generate angular momentum via collective excitation. In deformed even-even nuclei there are K-isomers formed by high-spin multi-quasiparticle states, therefore the existence of high Ω-orbitals close to Fermi level is crucial.

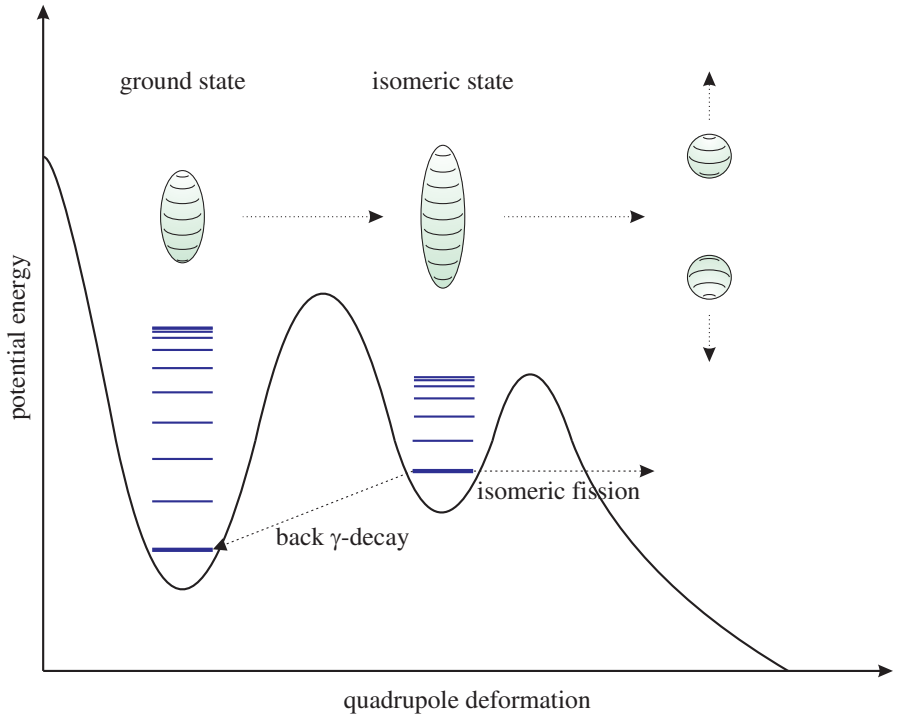

Figure 2.12: Double-humped fission barrier and origin of shape isomeric state.

2.7.2 K-forbidden transitions

K-isomers are strongly related to the phenomena of K-forbidden transitions. Selection rule for electromagnetic transitions requires that the multipolarity of emitted radiation λ must be at least as large as the change of K quantum number (projection of angular momentum onto nucleus symmetry axis) and hence

$$\lambda \geq \Delta K. \tag{2.65}$$

This formula is known as a K-selection rule. Transitions violating it are called K-forbidden and are hindered (therefore they are called also K-hindered) rather than strictly forbidden due to the very small admixtures of nondominant K-values in wave functions of initial and/or final state. Typically these transitions feed higher-spin members of the rotational bands (see Fig.2.13 for illustrative example).

Degree of forbidenness ν is the difference between K-change and multipolarity of emitted radiation

$$\nu = \Delta K - \lambda. \tag{2.66}$$

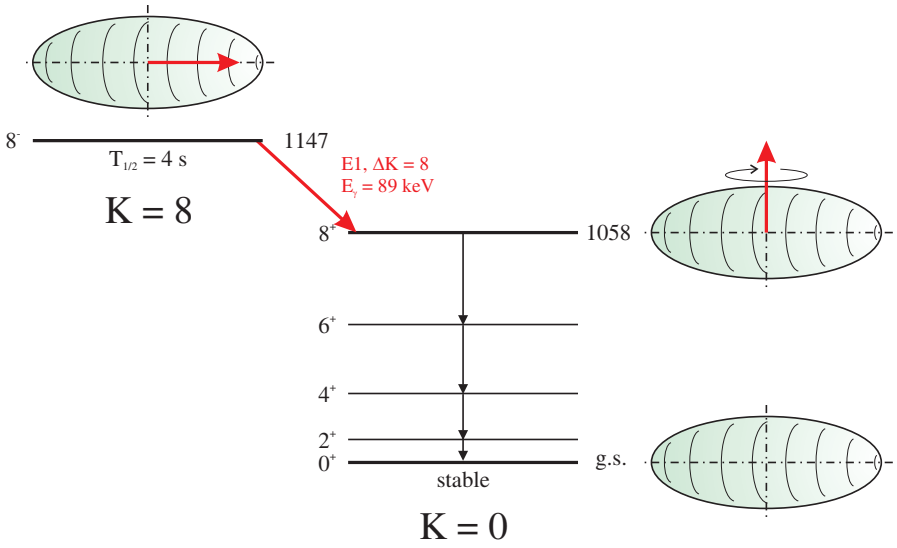

Figure 2.13: Illustrative example of K-isomer in ^{178}Hf. The K,J$^\pi$ = 8,8$^-$ isomeric state decays with the half-life of 4 s into the rotational ground-state band (the state K,J$^\pi$ = 0,8$^+$). Partial scheme is adapted from [Mul97].

Radiation hindrance factor F_W is defined as

$$F_W = \frac{T^\gamma_{1/2}}{T^W_{1/2}}, \tag{2.67}$$

where $T^\gamma_{1/2}$ is the measured partial γ-ray half-life and $T^W_{1/2}$ is the Weisskopf single-particle estimate. Reduced hindrance may be then defined as

$$f_\nu = \left(\frac{T^\gamma_{1/2}}{T^W_{1/2}}\right)^{1/\nu} = F_W^{1/\nu}. \tag{2.68}$$

Value of $f_\nu = 1$ represents unhindered single-particle transition. Theoretical description of F_W was published by Rusinov [Rus61]. He proposed that typically $f_\nu \sim 100$. Systematic experimental study of K-forbidden transitions by Löbner [Loe68] showed that the hindrance factor depends also on the multipolarity of transition and are larger than was predicted by Rusinov (see Fig. 2.14).

There are know also isomeric decays with abnormally low hindrance. These variations indicate with admixtures of other K-values in decaying states. Three possible mechanisms being used for description of K-mixing:

- **Coriolis mixing**

  Occurs if states to which isomer decays are affected by Coriolis mixing [Ste75], e. g. K = 35/2 isomer in ^{179}W [Wal94] or K = 14 isomer in ^{174}Hf [Gjo95].

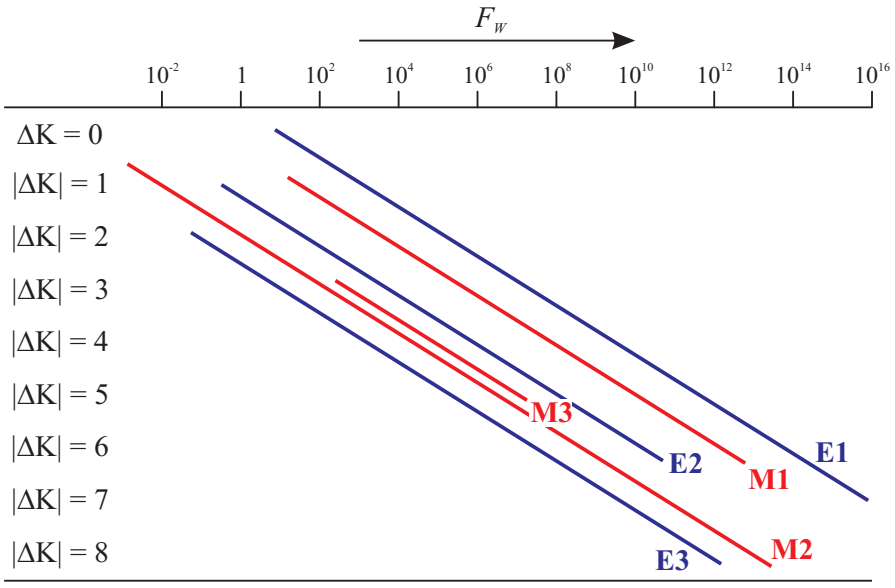

Figure 2.14: Systematics of hindrance factors of K-hindered transition for some multipolarities [Loe68].

- **γ-tunnelling**

  This approach has been suggested to explain very low values of the reduced hindance for K = 25 isomer in ^{182}Os [Cho88, Ben89], or K = 14 isomer in ^{176}W [Cro96]. In this case both initial and final states are axially symmetric but decay proceeds via tunnelling through asymmetric state.

- **Level density effects**

  Arises in the case of close lying levels with the same spin and parity but with different value of K. Then K is not more a "good" quantum number.

Chapter 3

Experimental devices and techniques

3.1 Heavy nuclei production - fusion-evaporation reaction

In the present work ^{254}No nuclei were produced via heavy-ion induced fusion-evaporation reaction, when a stationary target is bombarded with a heavy ions beam. Following the hypothesis of N. Bohr this kind of nuclear reaction can by studied as a two-step process: the formation of highly excited compound nucleus and its decay.

Projectile and target nucleus can fuse together if the bombarding energy exceeds repulsive Coulomb barrier between them. The height of the Coulomb barrier can be described as

$$B_C = \frac{e^2}{4\pi\epsilon_0}\frac{Z_P Z_T}{R_T + R_P}, \tag{3.1}$$

where Z is the proton number and R is the radius of the projectile (P) and of the target (T) respectively. At the energy corresponding to the Coulomb barrier, both nuclei come into contact but do not fuse together. An additional energy is required - this energy is often called as the extra push. To model the Coulomb barrier the Bass barrier [Bas74] is widely used.

After the fusion of both nuclei, the compound nucleus is created. It is in highly excited (it is "hot") high-spin state. First stage of the cooling process proceeds via particle emission - in the region of interest of this work channels with evaporation of charged particle (proton, deuteron, α particle...) are improbable due to the presence of high Coulomb barrier. For a given compound nucleus, the average excitation energy carried away by the evaporation neutron is constant with respect to variations in the excitation energy and in the number of evaporated nucleons [Neu73]. The nucleus after neutrons evaporation is called as evaporation residue (ER).

Below particle evaporation threshold the deexcitation continues by emission of

γ-rays, at first by statistical E1 transitions. Because of a high density of the levels these γ-rays are observable only as a continuum. When the yrast line is reached the yrast cascade towards the ground-state is emitted. These γ-rays are discrete and detectable by the in-beam spectrometers.

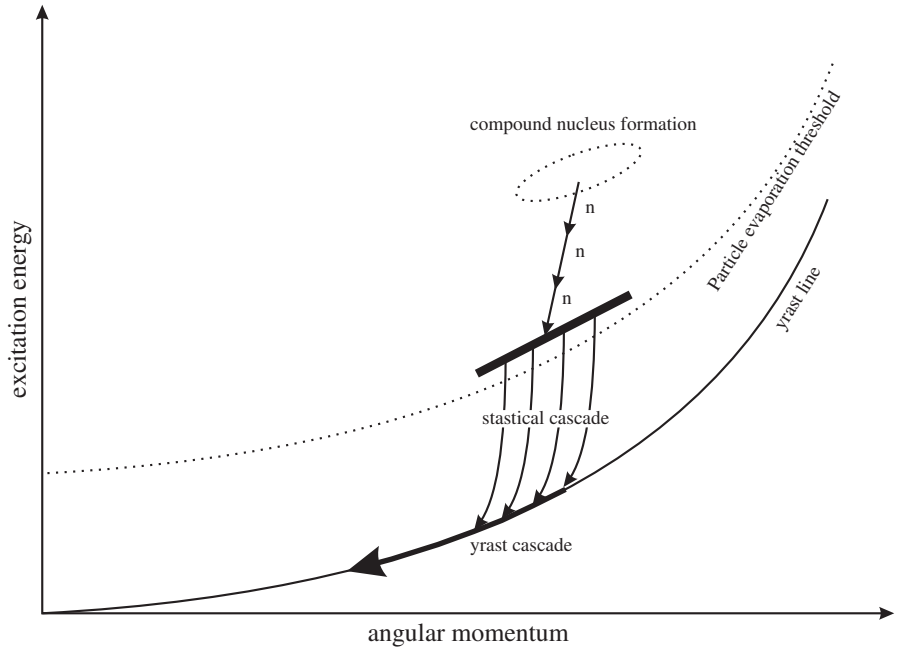

Figure 3.1: Schematic drawing of the compound nucleus cooling process.

3.2 The RITU gas-filled separator

The RITU gas-filled separator [Lei95] has been constructed in years 1992-1993 and it is installed on a beam line of K130 cyclotron at JYFL. Its ion optical configuration is $Q_V DQ_H Q_V$ (first strongly vertically focusing quadrapole was placed in front of the dipole chamber in order to attain higher angular acceptance) and as a working medium diluted helium gas is used. For some technical parameters of the RITU see Tab. 3.1

Working principle of the RITU is based on a collisions between the reaction products and the He gas atoms. These collisions lead to a charge focusing around the average ionic charge state (when leaving the target, the recoils are in the different charge states due to the collisions in the target). Ions then follow the trajectory determined by the average ionic state. Important quantity for the trajectory description is the magnetic rigidity which is defined as a product $B\rho$. The magnetic rigidity in the dipole magnetic field is given by the formula

$$B\rho = \frac{mv_{\perp}}{eq_{ave}}, \tag{3.2}$$

Table 3.1: The RITU gas-filled separator parameters.

Maximum beam rigidity	2.2 Tm
Bending radius	1.85 m
Maximum dipole magnetic field	1.2 T
Typical helium gas pressure	0.5 - 1.0 mbar
Acceptance	10 msr
Dipole bending angle	25°
Bending radius	1.85 m
Total weight	17 500 kg
Total length	4.8 m

where B is the magnetic field flux, ρ is the curvature radius, $mv_\perp$ is the perpendicular momentum of the reaction product with respect to the magnetic field and q_{ave} is the average charge state of the ion. The average charge state q_{ave} is given by the Fermi-Thomas model of atom [Boh41]

$$q_{ave} = \frac{v}{v_0} Z^{1/3}, \tag{3.3}$$

where $v_0 = 2.19 \times 10^6$ m/s is the Bohr velocity. In accordance to the formulas 3.2 and 3.3 we finally obtain

$$B\rho = 0.0227 \frac{A}{Z^{1/3}} \text{ Tm}, \tag{3.4}$$

where Z and A (is given in atomic mass units) are the proton and the mass number of the recoiling ion. The magnetic rigidity depends mainly on the mass number. Thus RITU can be employed as a mass filter in the experiments where only low mass resolving power is needed (in heavy elements experiments values of 20 - 25 amu are typical for RITU [Lei03]).

Only the rough estimation of the magnetic rigidity can be obtained following formula 3.4. For real experimental setting several empirical formulae have been determined - see [Ghi88, Oga91, Sch01] for more detailed discussion.

3.3 The GREAT spectrometer

The GREAT spectrometer [Pag03] has been placed into the focal plane of the RITU in year 2002. It has been designed for coincidence measurements of the protons, the α-particles, the fission fragments, the γ-rays, the X-rays and the conversion electrons emitted by the reaction products. It can be employed as a powerfull stand-alone device for the focal plane measurements, or as a tagging unit for target position detectors. GREAT spectrometer consists of several types of detectors:

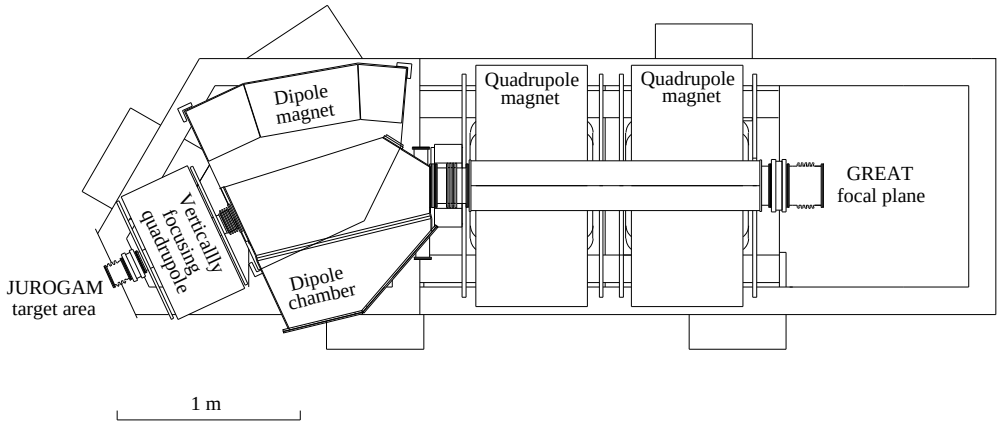

Figure 3.2: Schematic drawing of RITU gas-filled separator.

- Multiwire proportional counter (MWPC)
- Two double sided silicon strip detectors (DSSSD)
- Conversion electron detectors array (PIN diodes)
- Planar HPGe strip detector (PLANAR)
- Four-segmented clover HPGe detector (CLOVER)

A transmission MWPC is placed at the entrance of the GREAT. It is of 131 mm × 50 mm in size and the working medium is 2-Methylpropane. Volume of the MWPC is separated from the helium gas of RITU and from a vacuum chamber of the GREAT by thin Mylar foils. MWPC measures the energy loses in gas and of the time-of-flight (ToF). During tagging experiments its principal function is to distinguish between evaporation residues and products of their radioactive decays.

Recoils transported to the focal plane of the RITU are implanted into the DSSSD (typical implantation depth is of 1 - 10 μm, depends on the reaction). The DSSSDS measure energy of the implanted ions, of the protons, of the α-particles or of the electrons they subsequently emit. Each DSSSD is of 60 mm × 40 mm in size, 300 μm thick and consists of 60 strips in x-direction (horizontal) and 40 strips in y-direction (vertical). Both detectors are mounted side-by-side and their temperature is reduced to -20 °C by an alcohol cooling system.

In the backward hemisphere (relative to the beam direction) of the DSSSDS is mounted an array of 28 silicon PIN diodes. Each PIN diode is of 500 μm thick and

28 mm × 28 mm in size. The array is used for the conversion electrons or for the α-particles that escaped from the implantation detectors.

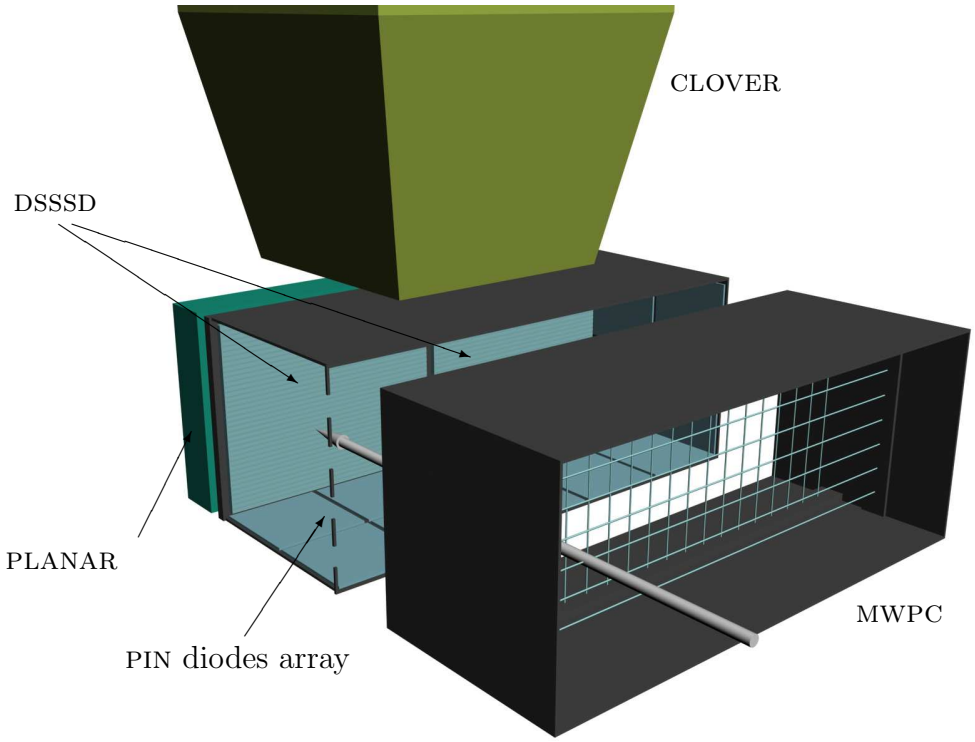

Figure 3.3: Schematic drawing of the GREAT spectrometer.

The PLANAR has been developed especially for GREAT spectrometer for the low energy X-rays and γ-rays measurement. The detector is placed behind the DSSSDS in the same vacuum chamber. It is mounted in its own cryostat behind a thin beryllium entrance window. The rectangular crystal has an active area of 120 mm × 60 mm and a thickness of 15 mm. High segmentation of the PLANAR detector (it consists of 24 horizontal and of 12 vertical strips) increases the $\gamma\gamma$-coincidence efficiency. The PLANAR is more efficient on the front side. It is because that is the side the photon passed through and therefore it definitely registers a hit. There is a chance that the charge from the front hit passes to the rear side and hits the dead area between the strips and is therefore shared between two strips or is lost. This reduces the rear side efficiency. This is magnificent mainly for lower energy γ-rays. This is related to the chance of a Compton scattering in relation to a photo electric absorption. The resolution is worse on the front side due to it being DC coupled and therefore more sensitive and also incomplete charge collection. It is also related to bad vacuum and therefore build up on the crystals surface.

The CLOVER is mounted on the supporting frame outside the vacuum chamber and positioned above the DSSSDS. It measures the high-energy γ-rays. Each crystal is of 105 mm long and has diameter of 70 mm before shaping (the first 30 mm of

its length is tapered at an angle of 15 degrees on the outside surfaces). A BGO shields (with length of 185 mm) in order to improve peak-to-total ratio are used. The CLOVER supporting frame has position for three additional detectors so it is possible to handle simultaneously four large high-energy γ-detectors at the focal plane of the RITU.

For simulated photopeak efficiency curve of both γ-detectors is in Fig. 3.4.

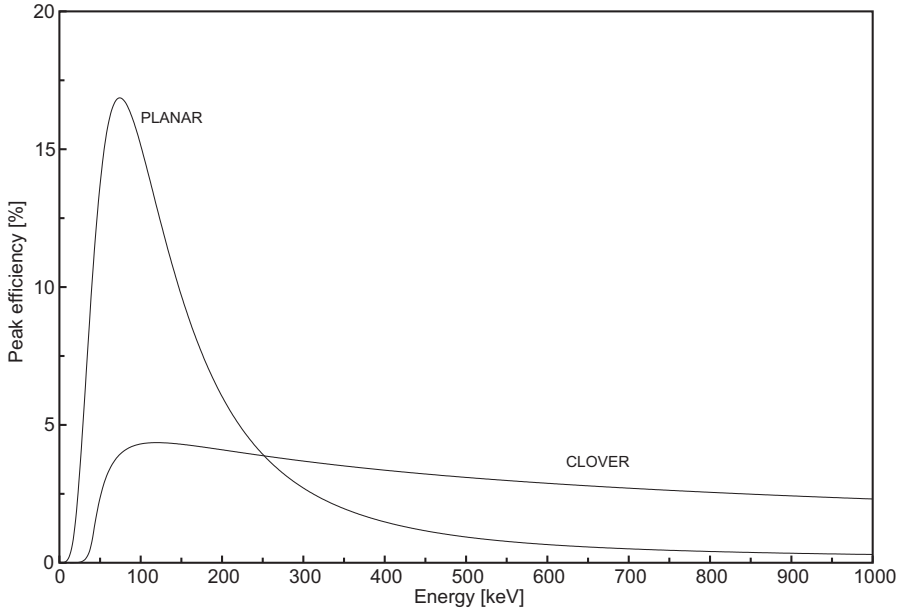

Figure 3.4: Planar and Clover germanium detector peak efficiency simulated using the GEANT code [And04].

3.4 The JUROGAM array

The JUROGAM is a modern target position array consisting of 43 HPGe detectors designed for tagging experiments in conjunction with the RITU gas-filled separator at JYFL. The detectors are placed on a self-supporting frame which can be opened in the direction perpendicular to the beam line. This allows simple access to the target chamber and also use of high-intensity beams for the decay studies without dismounting of whole array. The detectors are placed in rings around the target chamber (see Tab. 3.2). The total absolute photopeak efficiency of whole array is of 4.1 % at an energy of 1.332 MeV and typical FWHM is about 2.8 keV.

Each detector is equipped with the BGO anticompton shield to improve the peak-to-total ratio. In front of each detector 1 mm thick copper plate is placed in order to reduce the counting rate from low-energy X-rays and to inhibit damage of crystals by fission products. The array is implemented into the automatic liquid nitrogen filling system and all detectors are filled three times per day.

Table 3.2: Angles of the JUROGAM rings.

Angle	Number of the detectors
72.05°	8
85.84°	5
94.16°	5
107.94°	10
133.57°	10
157.60°	5

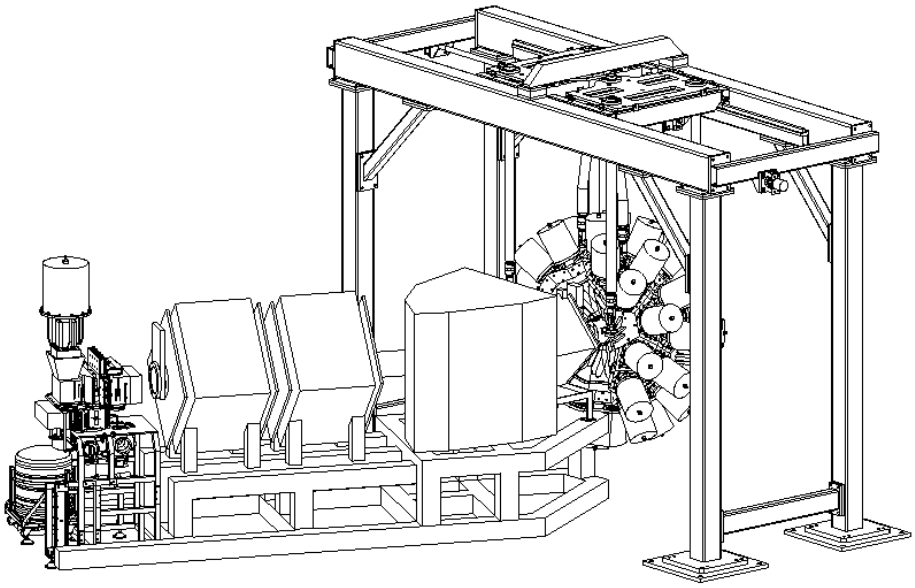

Figure 3.5: Schematic drawing of the RITU gas-filled separator and the GREAT spectrometer combined with the JUROGAM target position array.

During in-beam measurements the source of radiation is moving with respect to the detector. The Doppler effect therefore occurs. The observed γ-ray energy is proportional to the recoil speed as

$$E_\gamma = E_0\big(1 + \frac{v}{c}\cos\Theta\big), \tag{3.5}$$

where E_0 is the initial γ-ray energy, c is the speed of light in the vacuum and Θ is the detector angle with respect to the velocity of the recoil. Using the known ground-state band transitions [Eec05a] a recoil speed was determined to be of 1.78 % of the speed of light.

Another Doppler effect is the broadening of the peaks. It arises from the

opening angle of a single detector and can be expressed as

$$\Delta E = E_0 \sin\Theta \Delta\Theta, \tag{3.6}$$

where $\Delta\Theta$ is the opening angle of the detector.

3.5 The total data readout acquisition system

The conventional data acquisition systems for tagging experiments use a signal from one of the focal plane detectors (in principle from any of those) as a trigger. The time gate width is related to the half-lives of studied processes. During the gate period signals from all detectors are collected into the single event with the timestamp relative to the triggering signal. If the target position detectors are active, signal from them is collected in a delayed coincidence (due to the time-of-flight through the separator). This method leeds to some problems with the dead-time. If long time gate is needed (e. g. in the case of the long-lived isomers studies) the consequential dead time is rather long. Another problem, related to the dead-time is the blind period at the end of the gate. During the experiments with low statistics (typically heavy nuclei studies) the data losing is unacceptable.

To avoid the problems with dead time the Total data readout (TDR) acquisition system has been developed [Laz01]. Typical for this system is the absence of the hardware triggers. All the data are read, timestamped and written into continuous data stream. Events are reconstructed during the analysis proces by software.

Fig. 3.6 shows the block scheme of the TDR electronics. The front-end electronics is based on commercial NIM/CAMAC units. The data are then led into the timestamping ADC. ADC cards are in VXI-D format containing 32 channels.

For the data analysis the GRAIN programm has been developed [Rah07]. It is based on JAVA language with AIDA analytical package and emulates old electronic triggered system for event building. The coincidence window size is chosen by a user with respect of the conditions of a concrete experiment. Any of the detectors can in this system carry out the obligation of trigger. The GRAIN allows full data analysis using histograms, graphs or ntuples.

3.6 Spectroscopy of long-lived K-isomers

If the half-life of a γ-decaying isomer is too long, the conventional recoil-electron or recoil-γ correlation method becomes useless due to the strong amount of observed random correlations. Therefore the method of triple position correlations has been suggested by Jones [Jon02]. It is expected that the high-K isomeric-states decay via cascade of very fast electromagnetic transition. Many of these undergo to the internal conversion with high probability (typically collective low-energy M1/E2 and E2 transitions). Emitted conversion electrons, Augere electrons and low-energy X-rays can create a summed signal in the DSSSD. This can be correlated

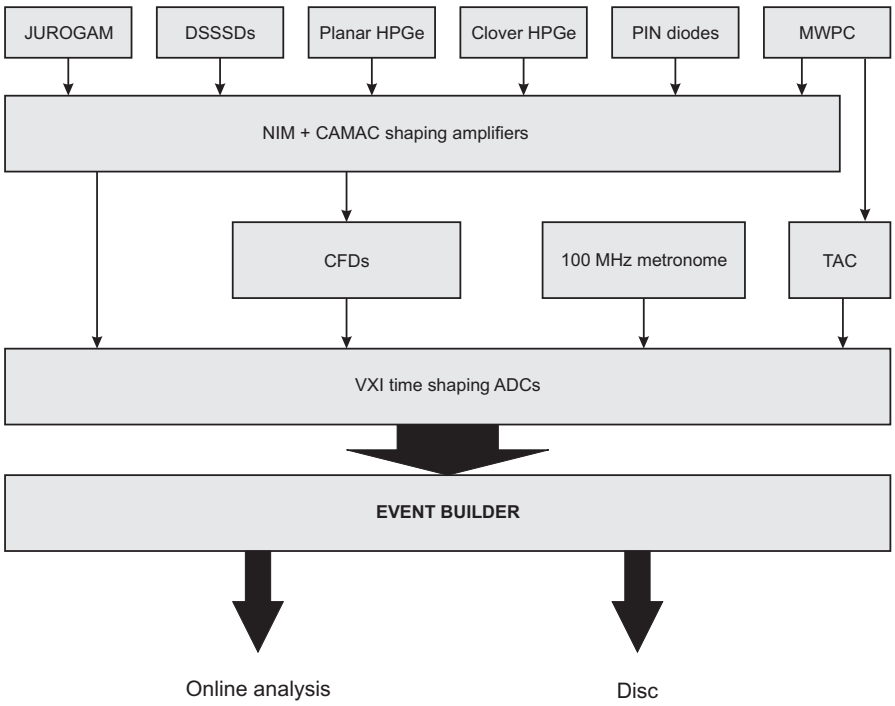

Figure 3.6: Schematic diagram of the TDR data acquisition electronics.

with implantation of the evaporation residue and α decay of the ground state sequentially. Only γ-rays in prompt coincidence with these electrons are measured and this leads to a strong reduction of the random background.

For application of this method, the DSSSD needs to operate in non-standard mode when the X-side (horizontal strips) is tuned for measurement of conversion electrons with extremely low thresholds (below 100 keV). The Y-side (vertical strips) for evaporation residues and α particles is set.

The triple position correlation method allows also the measurement of the bands lying above the isomeric states. In this case standard RDT method is employed with the triple correlations as a tag for target position detectors.

3.7 The recoil-decay tagging method

For the in-beam γ-rays experiments it is crucial to distinguish between γ-rays of interest and the background γ-rays. A source of the background is for example fission (as a dominant decay mode of the compound nucleus), the Coulomb de-excitation and the transfer reaction products. Therefore the recoil-decay-tagging method (RDT) has been developed [Sim86, Pau95].

Prompt γ-rays emitted by evaporation residue within the target or immediately behind it are detected by the JUROGAM. Recoiling evaporation residue passes then through the RITU before being implanted into the DSSSD. For the identification

of the recoil, the MWPC placed in front of DSSSD is in use. The matrix of time of flight vs. energy losses is shown in Fig. 3.7. The recoils of the interest are selected with a displayed two-dimensional gate. Only those evaporation residues that passed this gate (about 50 % of all implantations) are correlated to the decay signals.

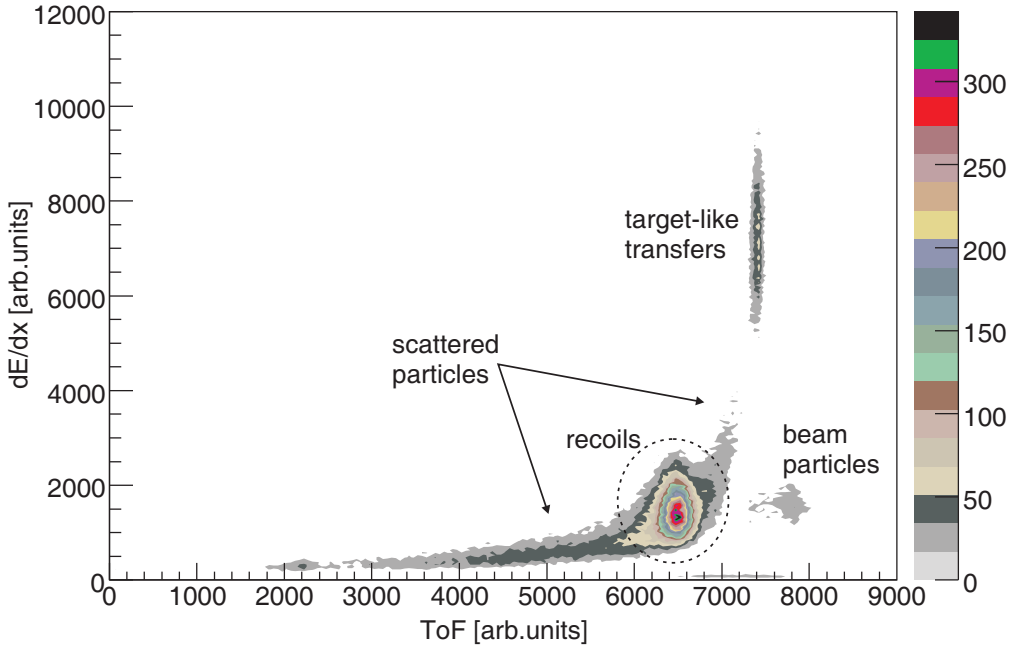

Figure 3.7: Time-of-flight vs. energy loses in the MWPC. Reversed arbitrary units for the time-of-flight are used - large value in spectrum means lower real time-of-flight.

Sequentially the characteristic decay occurs and is detected within the same pixel of the DSSSD and is correlated with initial recoil implantation. γ-rays measured by JUROGAM are associated to the recoils (correlated to characteristic decay) in a delayed coincidence with respect of the time-of-flight through the RITU (typically ~ 1 μs). In Fig 3.8 is shown the time difference between the emission of the γ-rays and implantation to the DSSSD. The displayed spectrum is the sum of all JUROGAM detectors. In analysis the selection gates were set to the dominant peak in the spectrum individualy for each crystal to attain the maximal selectivity of prompt γ-rays. Small baseline peaks correspond to the cyclotron frequency which has been determined to be of 10.3 MHz.

The RDT method allows to establish a link between radioactive decays observed at the focal plane of the RITU and prompt γ-rays native from structures feeding the decaying states.

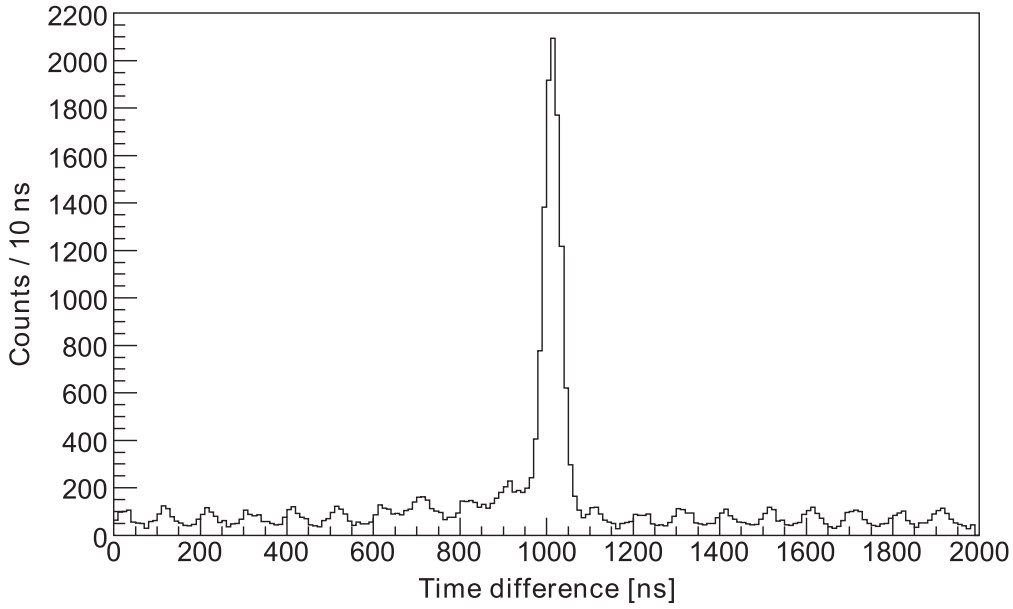

Figure 3.8: Time difference between γ-rays emission at target position and implantation of evaporation residue into the DSSSD at the focal plane of the RITU. Dominant peak corresponds to the typical time-of-flight through the separator.

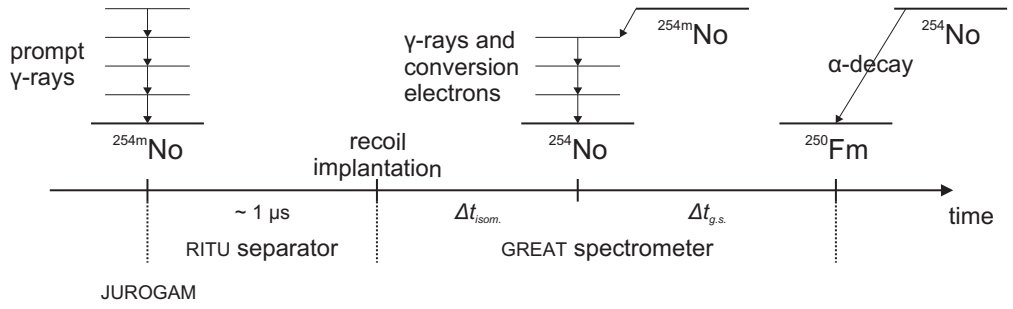

Figure 3.9: Illustration of RDT method in conjuction with recoil-electron tagging. Yrast state above the isomer is populated within the target. This state decays via emission of fast γ-rays towards the isomer. Target is circumscribed by the JUROGAM detectors which detects this radiation. The evaporation residue then passes the RITU separator, makes signal in the MWPC and is implanted into the DSSSD. Recoil implantation together with signals from the gas detector and target position array are collected into single event. In TDR acquisition system this is done by software. Decay of the isomeric state creates summed signal within the same pixel (indigenous from emitted low energy X-rays, conversion and Augere electrons). The subsequent α decay could be correlated as well. The time scale in the figure is only illustrative.

Chapter 4

Experimental results

4.1 Previous studies of ^{254}No

Element with Z = 102 was for the first time identified by Ghiorso *et al.* [Ghi58]. Today, the isotopes with the mass numbers from 250 to 262 are known. The real breakthrough of the spectroscopic studies of nobelium nuclei came at the end of nineties with the application of tagging techniques. Relatively high production cross-section makes ^{254}No one of the most often studied nuclei in this region of the table of isotopes.

The ground-state rotational band was observed by Reiter *et al.* [Rei99] employing the GAMMASPHERE array at ANL and by Leino *et al.* [Lei99] on the SARI array at JYFL. Both laboratories reported the equivalent results, the ground-state rotational band was identified up to spin of $16\hbar$. These results were later improved by an experiment performed at JYFL utilizing new target position γ-spectrometer JUROGAM. The rotational band was extended up to spin of $22\hbar$ [Eec05a] and in addition two high-energy non-yrast transitions were observed [Eec05b]. For deduced level scheme see Fig. 4.1. The properties of the rotational band confirmed strongly prolate deformed shape of the ground-state of ^{254}No. Obtained value of the quadrupole deformation β_2 of 0.27(2) [Her04] is in a good agreement with the theoretical calculations [Cwi96, Pat91].

Sensitivity of the γ-spectroscopy is in heavy nuclei reduced by strong internal conversion. Therefore complementary to the γ-rays experiments, the prompt conversion electrons were studied using the SACRED spectrometer at JYFL [Hum04]. The E2 character of the ground-state band transitions was confirmed. Excepts of discrete peaks corresponding to the ground-state band transitions, also the a huge electron continuum [But02] was observed. It was determined to be of nuclear origin and to arise from low-energy, strongly converted transitions within the bands based on the high-K two-quasiparticle excited states.

Observation of the isomeric state in ^{254}No has been reported by Ghiorso *et al.* [Ghi73]. This was an indirect identification and only the half-life could be determined to be of 0.28(4) s. Other nuclear properties remained unclear. It was expected that the isomer is formed by excited high-K state with two-quasiparticle

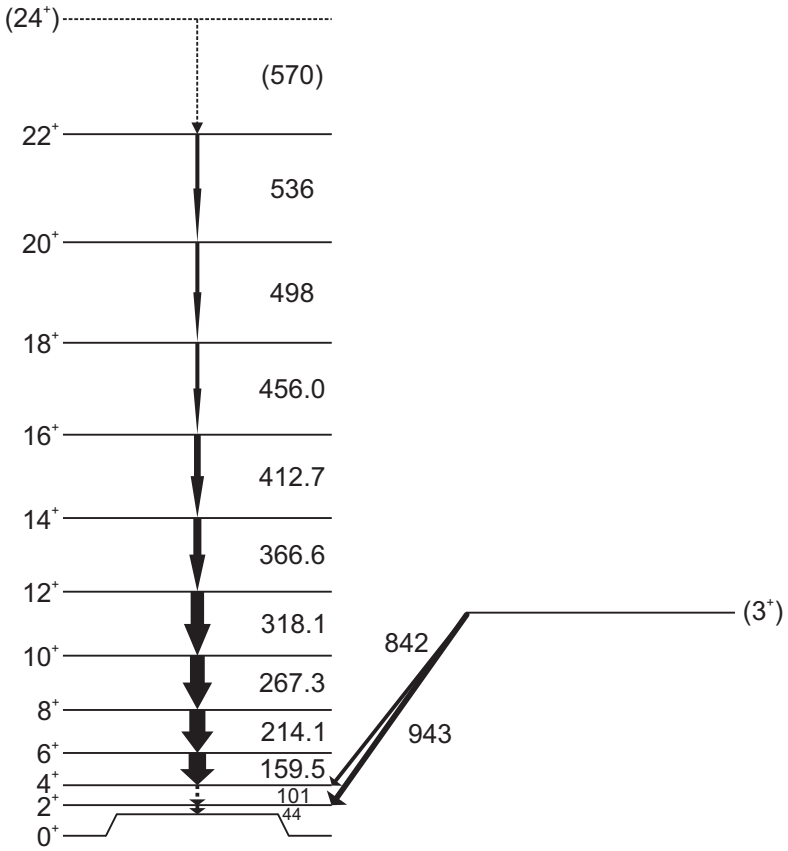

Figure 4.1: The ground-state band of ^{254}No and two non-yrast transitions [Eec05a].

structure. Existence of $K^{\pi} = 8^{-}$ has been predicted by theoretical calculations [Laz89, Sol91] already long time ago (see Tab. 4.1). These states are good candidates to form the observed isomer. Several unsuccessful attempts to establish the properties of the isomer have been performed [Muk05, But02] in past years.

Table 4.1: Predicted $K^{\pi} = 8^{-}$ two-quasiparticle high-spin configurations in ^{254}No

Nilsson configuration	**Excitation energy [MeV]**	
	[Sol91]	**[Laz89]**
$9/2^{-}[734]_{\nu} 7/2^{+}[613]_{\nu}$	1.40	1.20
$9/2^{-}[734]_{\nu} 7/2^{+}[624]_{\nu}$	1.70	-
$9/2^{+}[624]_{\pi} 7/2^{-}[514]_{\pi}$	1.44	1.10

4.2 The details of experiments

This work deals with the analysis of the data obtained during two experiments carried out during 2005 and 2006 at JYFL. Experiments marked as R35 (2005) and JR48 (2006) employed the RITU separator, the GREAT spectrometer and the JUROGAM array (JR48 only). For the experiment JR48 the GREAT was equipped with two additional VEGA clover detectors in order to increase the efficiency for high energy γ-rays. For detailed information about both experiments see Tab. 4.2

During both experiments ^{254}No ions were produced via ^{208}Pb(^{48}Ca,2n)^{254}No reaction. The bombarding energy was of 219 MeV (in laboratory system). The production cross-section is about 2 μbarn at this energy [Gag89]. The beam was produced by the 14 GHz ECRIS ion source [Koi01] and accelerated by the K-130 cyclotron [Hei95]. The rotating targets were provided by GSI. Rotating targets allowed higher beam intensity to be used in comparison with the static ones. During the JR48 experiment the JUROGAM counting rate was limiting the beam current. The limit is of 10 kHz per each detector as a highest rate that can be accepted by the TDR data acquisition system.

For calibration of all detectors in both experiments standard sources were used (see the Tab. 4.3 for list).

Table 4.2: The Details of Experiments.

	R35	**JR48**
Date	2. 5. - 8. 5. 2005	3. 4. - 10. 4. 2006
Employed spectrometers	GREAT	JUROGAM GREAT 2 VEGA clovers
Total time of irradiation	148 hours	110 hours
Total dose	2.0×10^{17} part.	4.6×10^{16} part.
Projectile	$^{48}Ca^{10+}$	$^{48}Ca^{10+}$
Beam energy	219 MeV	219 MeV
Average beam intensity	61 pnA	19 pnA
Target	^{208}PbS	^{208}Pb (metallic)
Target thickness	416 μg/cm^2	446 μg/cm^2

4.3 The α decay of the ground-state of ^{254}No

Fig. 4.3 shows the spectrum of the α decays (vetoed by the MWPC) correlated with recoil implantation within the time gate of 180 s. The strongest peak corresponds

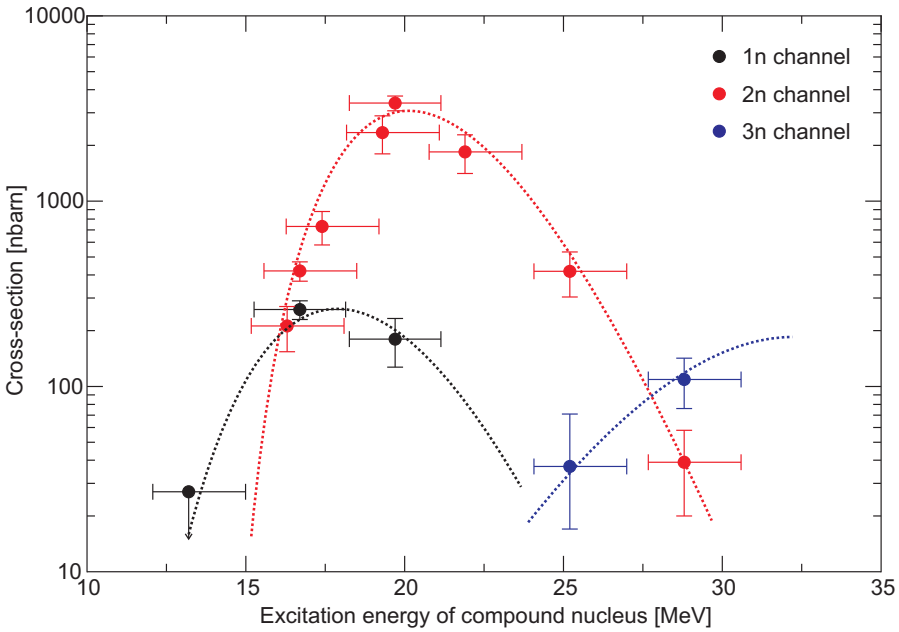

Figure 4.2: The excitation function of the reaction for different energies and neutron evaporation channels [Gag89]. Dotted lines are for guide eyes.

to the decay of the ground-state of ^{254}No. The measured energy of 8.155 MeV is not consistent with the value that was found in the literature (8.093 MeV [Fir96]). It is due to the used calibration with external source which differs from that obtained from the decay of implanted nuclei (effect of dead layer of the detector and of the motion of nucleus after alpha particle emission). As our experiment was oriented mainly to the γ-spectroscopy of isomeric states, precise calibration of the DSSSD was not necessary.

To study the half-life of the ground state of ^{254}No the energy selection gate of 7900 - 8300 keV and the time gate of 2000 s (to fit the random background) was chosen. The inset of Fig. 4.3 displays the measured decay curve with the random background. The expansion of the early part of the curve is in Fig. 4.4. The decay curve shows the characteristic growing activity in first couple of bins. This can be explained by the feeding of the ground-state by a decay of the isomeric states. To extract the half-lives of both states, the curve was fitted by

$$N(\Delta t) = a\left(e^{-(\lambda_2+r)\Delta t)} - e^{-(\lambda_1+r)\Delta t)}\right) + be^{-(\lambda_2+r)\Delta t)} + ce^{-r\Delta t}, \qquad (4.1)$$

where λ_1 and λ_2 are the decay constants of the isomer and of the ground-state respectively. The quantity r arises due to the random correlations [Cha06].

For the ground-state the half-life of 49.2*(3)* s was obtained which is in rough agreement with previously reported values. It needs to be pointed out that fitting of the decay curve is strongly sensitive to the bining of the histogram. Because of the large difference between the half-life of the ground-state and of the isomeric

Table 4.3: List of energy calibration sources. Both sources for DSSSD calibration (3-line α-source and ^{133}Ba) are placed inside the vacuum chamber of the GREAT spectrometer and can be inserted in and out automatically.

Detector	**Source**	**Used lines** [keV]
DSSSD X-side	^{133}Ba	75.3, 240.4,
PIN diodes		266.9, 320.0,
(conversion electrons)		350.5 [Trz90]
DSSSD Y-side	^{239}Pu	5155 [Fir96]
(α-particles)	^{241}Am	5486 [Fir96]
	^{244}Cm	5805 [Fir96]
PLANAR	^{133}Ba (BDR1122, 42.4 kBq, 1.4.2003)	81.0,121.8
	^{152}Eu (EFR1122, 40.1 kBq, 1.4.2003)	244.7, 276.4
		302.9, 344.3
		356.0 [Fir96]
CLOVER	dtto as PLANAR	81.0, 121.8
VEGA		244.7, 276.4
JUROGAM		302.9, 344.3
		356.0, 383.9
		411.1, 444.0
		778.9, 867.4
		964.1, 1112.1 [Fir96]

state, the growing part only in the first couple of bins is evident. This leads to the large error in the case of the half-life of the isomer. Anyway obtained value of 376.5*(2669)* ms is in good agreement with that published by Ghiorso *et al.* and also with the value obtained from the recoil-electron correlations as it will be discussed later.

4.4 Analysis of observed correlation chains

The analysis of the correlation chains has been performed using only data from experiment R35. Dataset from this run contains enough statistics for this analysis and a small additional statistics from the in-beam experiment cannot bring any new information on the half-lives and the isomeric ratios.

To investigate the properties of the K-isomers the recoil-electron position cor-

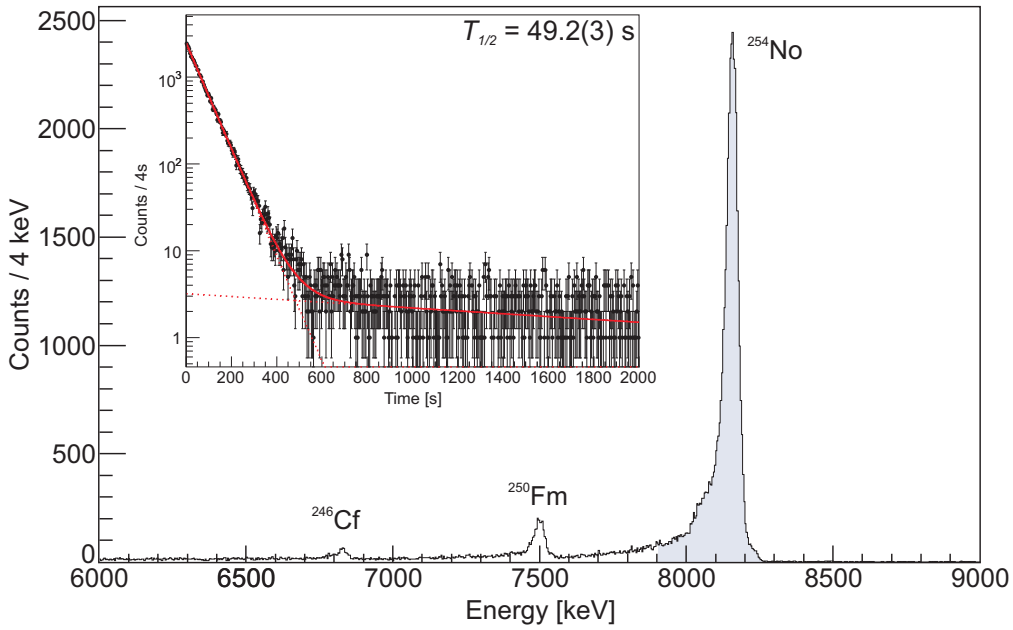

Figure 4.3: Correlated alpha spectrum vetoed by the MWPC. The inset shows the decay curve of ground-state of ^{254}No .

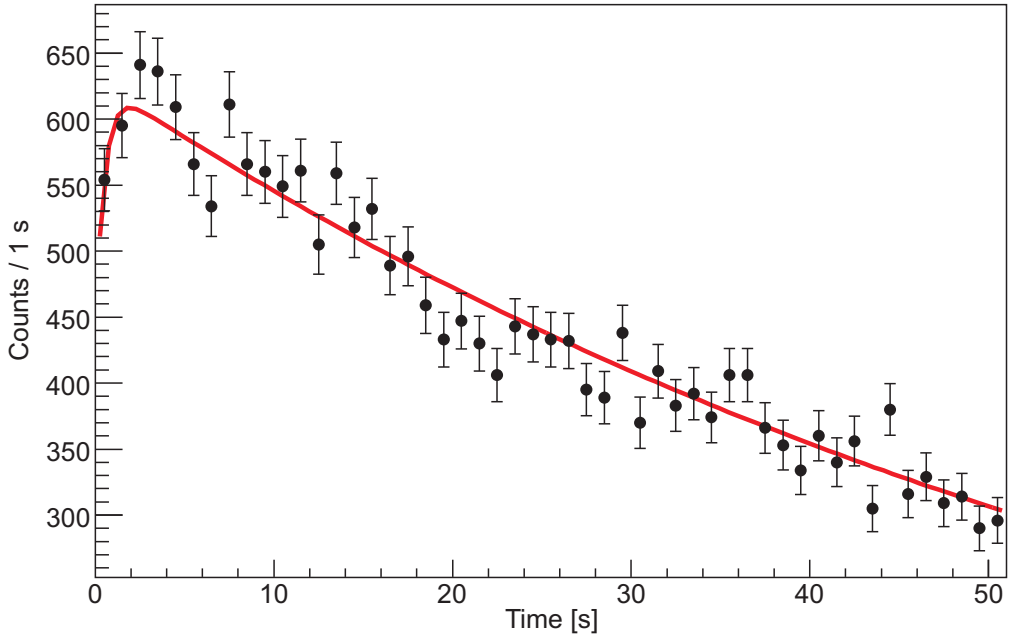

Figure 4.4: Early part of ^{254}No ground-state decay curve with growing activity corresponding to the feeding from the isomeric states.

relation chains with time window of 10 s were analyzed. A long time window compared to expected half-life of the isomeric state was chosen for the random

background substraction. The time difference between the recoil implantation and the electron emission is shown in Fig. 4.5. There are two components of the exponential decay evident there, the expansion of first two bins of the decay curve is displayed in the inset. To extract the values of half-lives, the decay curves have been fitted with the function

$$N(\Delta t) = ae^{-(\lambda+r)\Delta t} + be^{-r\Delta t}, \tag{4.2}$$

where λ is the decay constant of the isomer and r arises from the random correlations [Lei86].

Using the decay curves, the isomeric ratios for both isomers could be obtained. The isomeric ratio is a ratio between observed decays of the isomer and decays of the ground-state and it represents the probability of a population of the isomeric state in the complete fusion reaction. For summary of obtained half-lives and isomeric ratios see Tab. 4.4. The α branch of ^{254}No ground-state is of 0.9 [Fir96] and the efficiency for ^{254}No α particles was estimated to be of 55 %. Due to low thresholds of the DSSSD, the efficiency for the electrons was nearly 100 %.

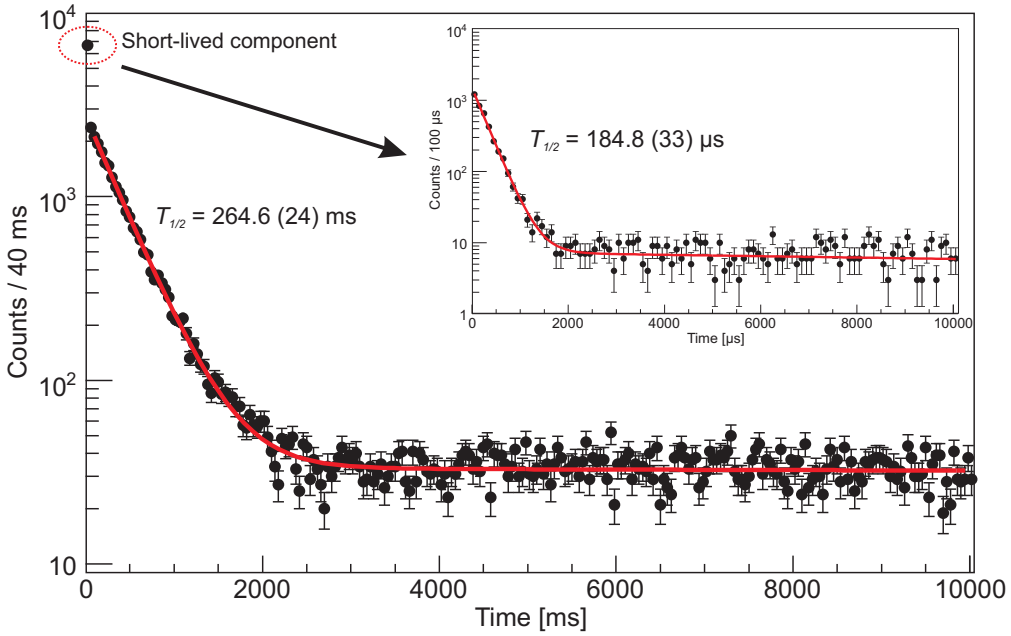

Figure 4.5: The recoil-electron correlations time distribution. Two decay components of the exponential decay are evident. The inset displays the expansion of the short-lived component corresponding to the decay of previously unknown isomeric state.

Obtained half-life of 264.6(24) ms of the long-lived isomeric state is in a good agreement with that reported by Ghiorso *et al.*. The short-lived component with the half-life of 184.8(33) μs corresponds to the decay of a previously unknown isomeric state. Indication of the existence of this isomer was already observed in

Table 4.4: Half-lives and isomeric ratios of observed isomers summary.

State	Half-life	Number of decays	Isomeric ratio
m1	264.6*(24)* ms	26 192*(171)*	29.5*(2)* %
m2	184.8*(33)* μs	4 139*(69)*	4.7*(1)* %
g.s.	50.7*(4)* s	43 884*(229)*	-

one of the previous experiments at JYFL [But03] and now it was unambiguosly confirmed.

To verify that observed isomers are really populated in ^{254}No, triple correlations of the type of recoil-electron-α were studied. This analysis fully confirmed it, as the same half-lives of both isomers were observed. But the statistics is lowered in this case mainly due to the low efficiency for detection of the α particle and relatively long half-life of the ground-state. According to this, the statistics when the triple correlations were used represents only 43 % compared to the recoil-electron tagging. But in this type of reaction typically the main output channel dominates. Therefore in the next analysis only recoil-electron correlations were used.

In more detailed analysis it was found that short-lived isomer decay is always adjacent to evaporation residue implantation, while the long-lived one is partially preceded by another electron. It was found that the half-life and isomeric ratio of this component corresponds to the short-lived isomer. The 264.6 ms isomer state is thus populated directly and also by a decay of the 184.8 μs isomer. No direct decay branch from short-lived isomeric state to the ground-state was observed. Schematic drawing of isomeric states decay sequence is shown in Fig. 4.6.

4.5 Decay properties of the 264.6 ms isomer

In order to study the properties of the 264.6 ms isomer, the time gate of 2 - 1700 ms was used. Larger lower limit for the time gate was chosen of 2 ms instead of 0 ms to avoid the contibution of the 184.8 μs isomer. The energy of correlated electrons within this time gate is shown in Fig. 4.7.

4.5.1 The γ-rays and electrons from decay of isomer

Signals from correlated electrons were used as a tag for γ-detectors. Fig. 4.8 shows the γ-spectrum measured by CLOVER and VEGA detectors in prompt coincidence with electrons. Dominant are transitions of 943.4 keV and 841.8 keV. These lines

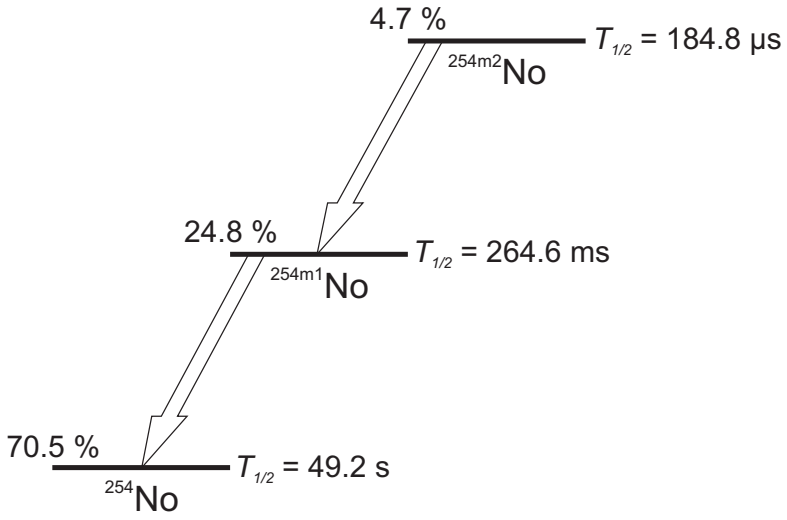

Figure 4.6: Isomeric states in ^{254}No. Half-life and the probability of direct population is given for each state. The long-lived isomer is produced directly and partly also by a decay of short-lived one.

Table 4.5: Number of observed correlation chains within 2 - 1700 ms time gate .

Experiment	**Number of observed correlations**
R35	27 195
JR48	8 725

were for the first time observed by Eeckhaudt *et al.* [Eec05a] in the in-beam experiment as a prompt radiation at the target position. Their energy difference is equal to energy of the $4^+ \rightarrow 2^+$ ground-state band transition. Therefore they were awarded to be a transitions from the $K^\pi = 3^+$ two-quasiparticle level into the ground-state band. This assignment was only tentative. Matrix of the energy of the correlated electrons vs. the coincident γ-rays energy is shown in Fig. 4.9. Its evident that the calorimetric footprint of electrons coincident to 841.8 keV is shifted towards the higher energy. This supports the scheme proposed by Eeckhaudt *et al.* because the additional electron energy originates from the $4^+ \rightarrow 2^+$ ground-state band transition. This is in coincidence with the 841.8 keV but not with the 943.4 keV transition.

Only E1, E2 or M1 multipolarity is possible for the 841.8 keV and the 943.4 keV transitions (because they were observed as a prompt radiation at the target position and this limits the life time of $K^\pi = 3^+$ state up to couple of ns). To determine the multipolarity, the α_K of both transitions were calculated. The relative intensities of 0.80(7) and 0.20(3) were taken into account. These are the relative

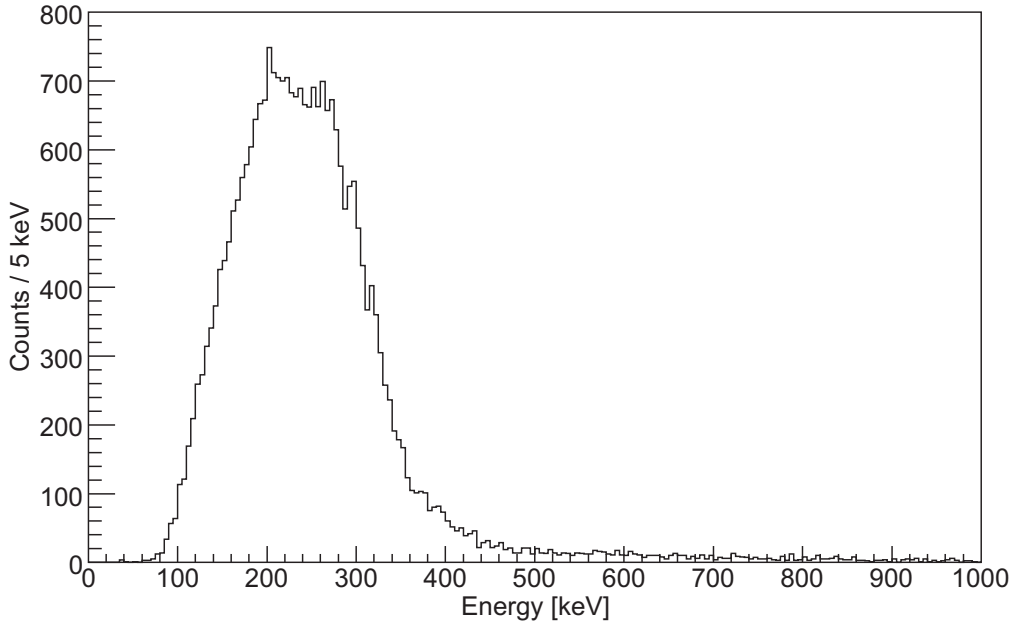

Figure 4.7: Spectrum of electrons correlated to recoils within 1700 ms time gate.

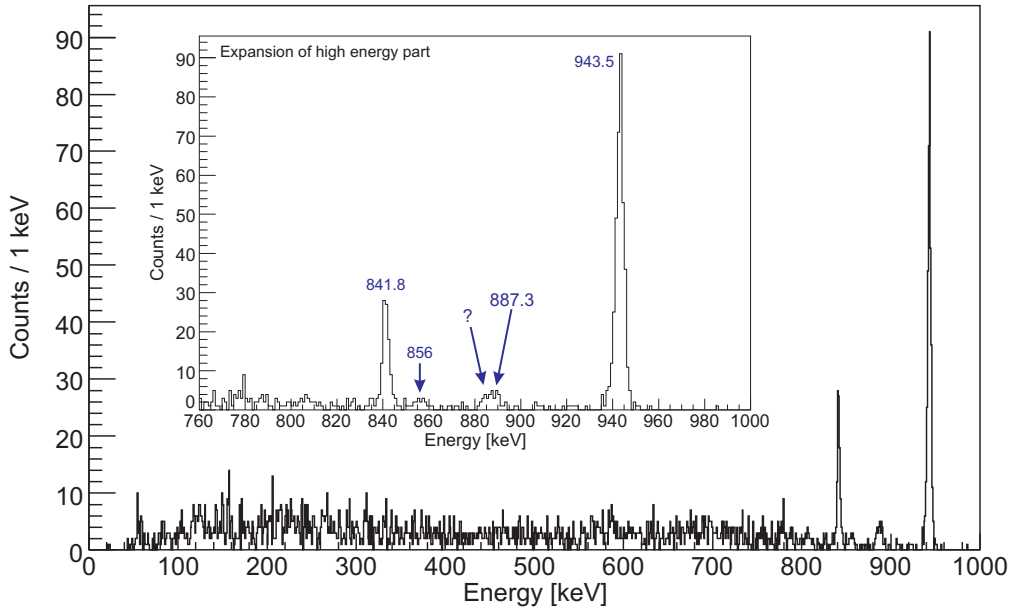

Figure 4.8: Spectrum of high-energy γ-rays (measured by the CLOVER and the VEGA detectors) tagged with the decay of the 264.6 ms isomeric state. Relevant part of the spectrum is expanded in the inset.

intensities of γ-lines, as the internal conversion is weak at this energy and does not affect too much the strength of γ-rays emission. As all other transitions above the

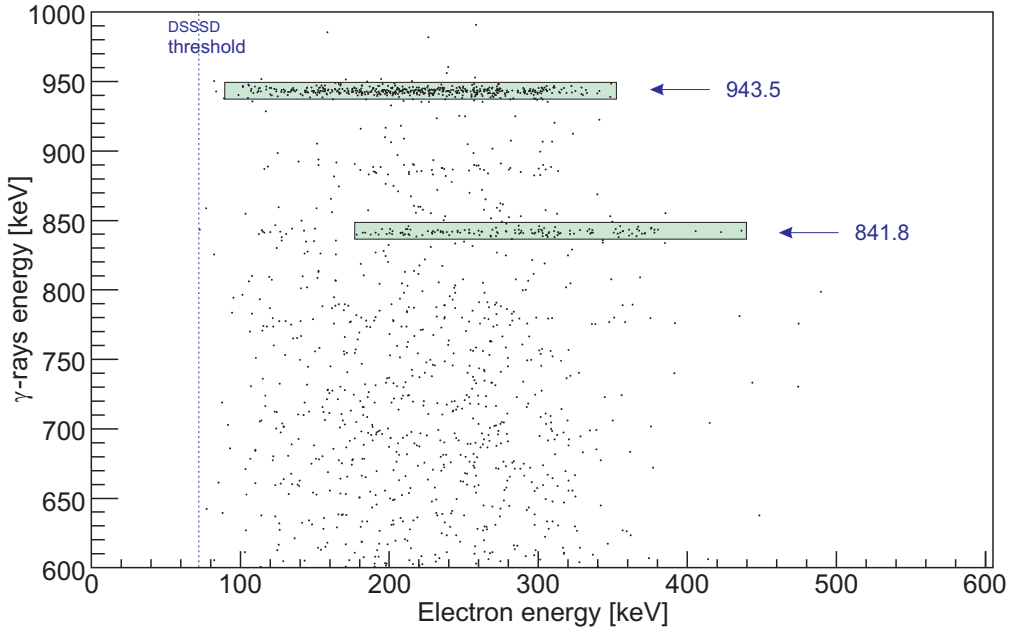

Figure 4.9: The energy of the electrons correlated with the recoil implantation vs. the coincident γ-rays energy.

K-electron binding energy ($E_B^K = 149.21$ keV [Fir96]) are weak, the α_K could be obtained (according to the intensities of the transitions) using the strongest $K_{\alpha 1}$ line (127.4 keV, $I = 0.44$ [Fir96]) - see the PLANAR spectrum if Fig. 4.10. Obtained values could by compared with those calculated with BRICC software [Kib05]. For comparison of calculated and experimentally measured values see Tab. 4.6. Obtained results are in good agreement with M1 multipolarity. Thus the observed two-quasiparticle state has been unambiguously determined as a $K^\pi = 3^+$ state with an excitation energy of 987.5 keV.

Table 4.6: Experimental and theoretical values [Kib05] of α_K for inter-band transitions between the $K^\pi = 3^+$ band and the ground-state band.

Energy [keV]	**Experimental** α_K	**Theoretical** α_K		
		E1	**E2**	**M1**
943.4	0.09*(2)*	0.01	0.02	0.12
841.8	0.10*(3)*	0.01	0.03	0.15

There was observed a broad continuum originating from a high-multiplicity conversion electron cascades in the in-beam experiment performed at the SACRED spectrometer [Hum04]. It was speculated that it was arising from strongly converted low-energy transitions within the bands based on high-K states. These

in-band transitions should dominate against K-forbidden high-energy inter-band transitions into the ground-state band. There are some weak high-energy transitions evident in the CLOVER spectrum. The strongest of these is located at energy of 887.3 keV (it is too broad compared to others in this energy region, the most probably it is a doublet with another peak of 884 keV). According to the structure of known non-yrast two-quasiparticle bands in heavy-region (e. g. in ^{256}Fm [Hal89] or ^{250}Cf [Fre77]) and in homologous rare-earths region (e. g. ^{170}Yb [Arc98] or ^{172}Yb [Kay67]) the 887.3 keV could be placed into the scheme as a decay of first excited state of the $K^{\pi} = 3^{+}$ rotational band ($K,J^{\pi} = 3,4^{+} \rightarrow K,J^{\pi} = 0,4^{+}$ transition). This allows to locate 4^{+} rotational state of 45.5 keV above the band-head. Strongly converted 45.5 keV mixed M1/E2 transition was not observed in the γ-spectrum.

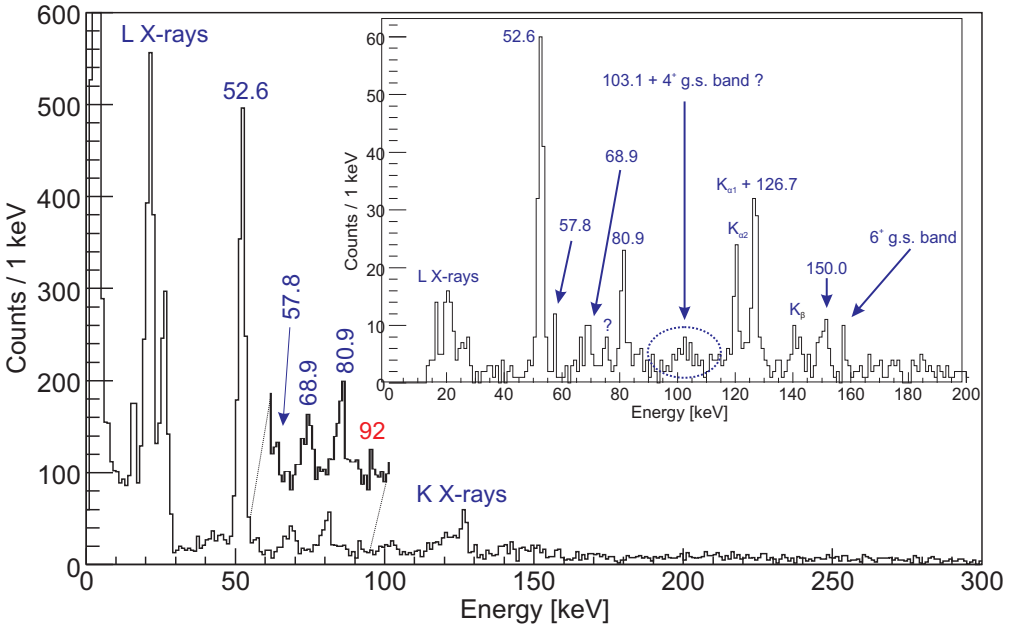

Figure 4.10: Spectrum of low-energy γ-rays (measured by the PLANAR - strips on front side) tagged with the decay of the long-lived isomer. Smaller inset shows magnification of energy range from 54 to 95 keV to show presence of 92 keV which is indication of existence of third isomeric state in ^{254}No. Larger inset displays the PLANAR spectrum when only events with same energy measured simultaneously on both sides of crystal are taken. Statistics here is much less (due to the lowered efficiency of rear side of the PLANAR detector) but the spectrum is cleaner and several peaks became observable. Both spectra are shown in order to present the power of the method of cleaning spectrum using both sides of the PLANAR.

When the excitation energy of first rotational level is known, the static moment of inertia could be estimated, the rotational formula 2.27 applied and the excitation energy of higher states calculated (see Tab. 4.7). In Fig. 4.10 is shown the PLANAR spectrum. Excepts dominating peak at 52.6 keV there are also some weak transitions evident. Energies of 57.6, 68.9 and 80.9 keV are in good agreement

with rotational formula prediction. Thus these transitions were interpreted as mixed M1/E2 in-band transitions. Presence of the 92 keV peak, corresponding to predicted in-band transition $8^+ \rightarrow 7^+$ in the spectrum will be discussed later. Also a 150.0 keV stretched E2 transition in evident (see larger inset of Fig. 4.10). Properties of the band and their influence on the band-head structure will be discussed in more details later.

Table 4.7: Comparison of measured energy of transitions within the $K^\pi = 3^+$ band with the prediction by the rotational formula.

$\mathbf{J}_i^\pi \rightarrow \mathbf{J}_f^\pi$	**Measured energy [keV]**	**Rotational formula [keV]**
$4^+ \rightarrow 3^+$	45.5 - not observed	45.5
$5^+ \rightarrow 4^+$	57.6	56.9
$6^+ \rightarrow 5^+$	68.9	68.3
$7^+ \rightarrow 6^+$	80.9	79.6
$8^+ \rightarrow 7^+$	92	91.0

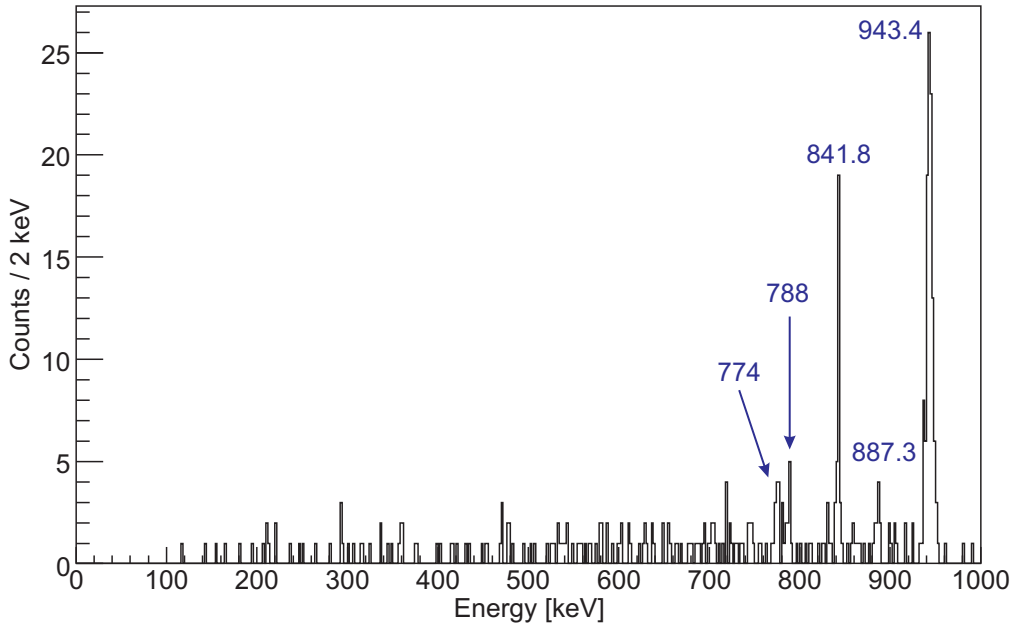

Figure 4.11: Spectrum of summed coincidence signals from crystals of the CLOVER and VEGA detectors.

The strongest peak in the PLANAR spectrum is already mentioned 52.6 keV transition. Intensity of the γ-line excludes any other multipolarity than the E1

(see Tab. 4.9 for ICC summary). To determine the character of this transition, the $\gamma\gamma$-coincidences analysis was performed (see Fig. 4.12). The 52.6 keV transition is clearly in coincidence with high-energy γ-rays corresponding to the decay of the low-lying states of the $K^\pi = 3^+$ band and with the 80.9 keV in-band transition.

Due to the lack of the statistics, only indications of coincidence with another in-band transitions were observed. The 52.6 keV peak is also in strong coincidence with L X-rays corresponding to converted low-energy in-band M1 transitions. Thus the 52.6 keV transition connects the $K^\pi = 3^+$ band at the $K,J^\pi = 3,7^+$ state. According to this and to the properties of known K-isomers in the hafnium region, the 52.6 transition was identified as a K-forbidden decay of the isomeric state. This clearly identifies isomer as the $K^\pi = 8^-$ state. The selection rules for E1 transitions allow also the $K^\pi = 7^-$ scenario, but in this case there should exist also another K-forbidden E1 transition feeding the $K,J^\pi = 3,6^+$ state. The energy of this transition would be of 133.5 keV, but such a transition was not observed. The full decay scheme could be build up (see Fig. 4.13). The excitation energy of the isomeric state is of 1293.0(15) keV. A weak peak of 856 keV fits well into the scheme as a $K,J^\pi = 3,6^+ \rightarrow K,J^\pi = 0,6^+$ transition and its presence is an additional argument for support of proposed decay pattern.

To increase the statistics for high-energy γ-rays, Compton scattered signals were also taken into account. When two crystals of the CLOVER or of the same VEGA detector give signal in prompt coincidence, sum of both energies is taken. For the spectrum of these summed energies see Fig. 4.11. Excepts of already discussed transitions, a weak peaks appeared at 774 and 787 keV. These can be tentatively placed into the scheme as a direct decay of isomeric state into the ground-state band and and as another inter-band transition between the $K^\pi = 3^+$ band and the ground-state band. The summary of all transitions associated to the decay of the 264.6 ms isomeric state is in Tab. 4.8.

4.5.2 Indication of the existence of the third isomer

As it was already mentioned above, there is peak corresponding to the $8^+ \rightarrow 7^+$ (the energy of 92 keV) in-band transition of the $K^\pi = 3^+$ band visible in the PLANAR. If it is really an in-band transition it cannot be fed from the $K^\pi = 8^-$ isomeric state, because the excitation energy of the 8^+ rotational state is higher. Its intensity, which is much less than that of the 80.9 keV transition also excludes the $K^\pi = 9^-$ structure of the isomer.

To clarify the origin of the 92 keV transition, the individual half-life and $\gamma\gamma$-coincidence were studied. The time distribution of recoil-electrons in prompt coincidence with the 92 keV transition was fitted by the universal curve [Sch00] (see the inset in Fig. 4.14). The half-life of $302.5^{+42.2}_{-31.8}$ ms was obtained. Since only 1 sigma error is given obtained, the value of the half-life cannot unambiguously identify new isomer. But it differs from that of the $K^\pi = 8^-$ isomer and thus it supports the idea of the existence of the third isomeric state.

To confirm the scenario with continuation of the $K^\pi = 3^+$ band, fed from the

Table 4.8: The γ-ray transitions associated to decay of the 264.6 ms isomeric state. The intensity of γ-lines is given relative to the 52.6 keV transition and it was corrected to the total photo-peak efficiency [And04] of the PLANAR and of the CLOVER. ^{A} The energy of the ground-state band transitions was taken from [Eec05a] because these lines are very weak in the decay of the $K^{\pi} = 8^{-}$ isomeric state. ^{B} In-band transition is dominated by the strong $K_{\alpha 1}$ peak and the intensity was extracted using the ratio of intensity with the $K_{\alpha 2}$ peak. This ratio was taken from [Fir96]. ^{C} Only indication of these transition was observed and their placement into the scheme is very tentative. They were observed in the Compton coincidence spectrum (see Fig. 4.11), therefore the efficiency is very questionable and the intensity could not be given.

E_γ [keV]	**Multipolarity**	**K,J_i^π**	**K,J_f^π**	**Relative intensity**
52.6*(4)*	E1	$8,8^-$	$3,7^+$	1.00
57.6*(5)*	M1/E2	$3,5^+$	$3,4^+$	0.04*(2)*
68.9*(3)*	M1/E2	$3,6^+$	$3,5^+$	0.08*(1)*
80.9*(2)*	M1/E2	$3,7^+$	$3,6^+$	0.12*(2)*
126.5*(6)*^{B}	E2	$3,6^+$	$3,4^+$	0.05*(3)*
150.0*(3)*	E2	$3,7^+$	$3,5^+$	0.11*(1)*
159.5*(10)*^{A}	E2	$0,6^+$	$0,4^+$	< 0.04
214.1*(10)*^{A}	E2	$0,8^+$	$0,6^+$	< 0.04
774*(2)*^{C}	E1	$8,8^-$	$0,8^-$	-
787*(2)*^{C}	M1	$3,5^+$	$0,6^+$	-
841.8*(2)*	M1	$3,3^+$	$0,4^+$	0.31*(8)*
856*(1)*	M1(E0)	$3,6^+$	$0,6^+$	< 0.04
887.3*(9)*	M1(E0)	$3,4^+$	$0,4^+$	< 0.07
943.5*(2)*	M1	$3,3^+$	$0,2^+$	1.25*(11)*

Table 4.9: Total ICCs for 52.6 keV transition for various multipolarities [Kib05].

E1	**E2**	**M1**	**M2**
0.84	652.80	84.56	3 259.00

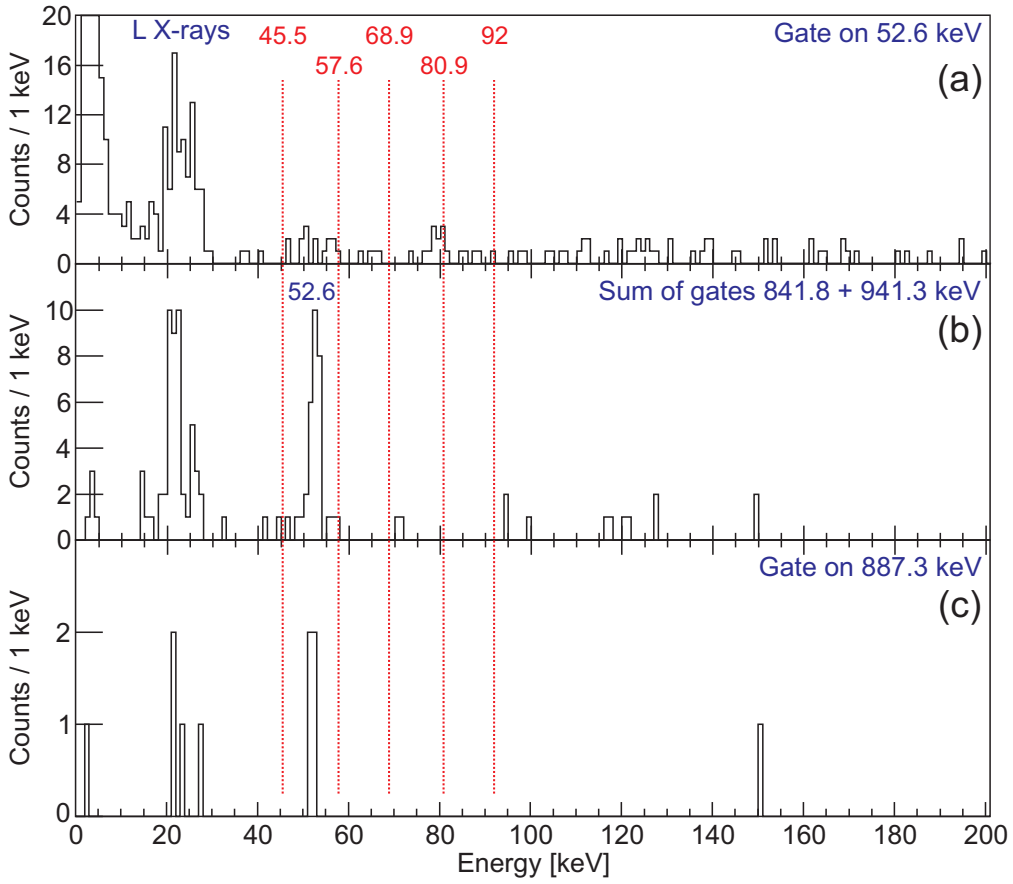

Figure 4.12: $\gamma\gamma$-coincidence PLANAR spectra tagged with the decay of the 264.6 ms isomer with gate on the (a) 52.6 keV transition, (b) sum of the gates on the 841.8 and 943.5 keV transitions and (c) 887.3 keV transition. Red lines indicate the energy of in-band mixed M1/E2 transitions within $K^{\pi} = 3^{+}$ band.

third isomeric state, the $\gamma\gamma$-coincidences analysis has been performed. The gate was put on the strongest well separated in-band transitions (see Fig. 4.14). The spectrum contains three counts corresponding to the 92 keV transition, but unfortunately the background is presented as well. But these coincidence signals together with a different half-life of the 92 keV transition and the rotational formula prediction form strong arguments for the existence of the third isomer. An improved statistics might help to solve this puzzle.

4.5.3 In-beam spectroscopy of states on the top of the $K^{\pi} = 8^{-}$ isomer

The recoil-electron tagging method has been employed in order to study the band structure above the $K^{\pi} = 8^{-}$ isomeric state. When the structure of the decoupled band is known, the crossover-to-total ratios could be extracted and thus unambigu-

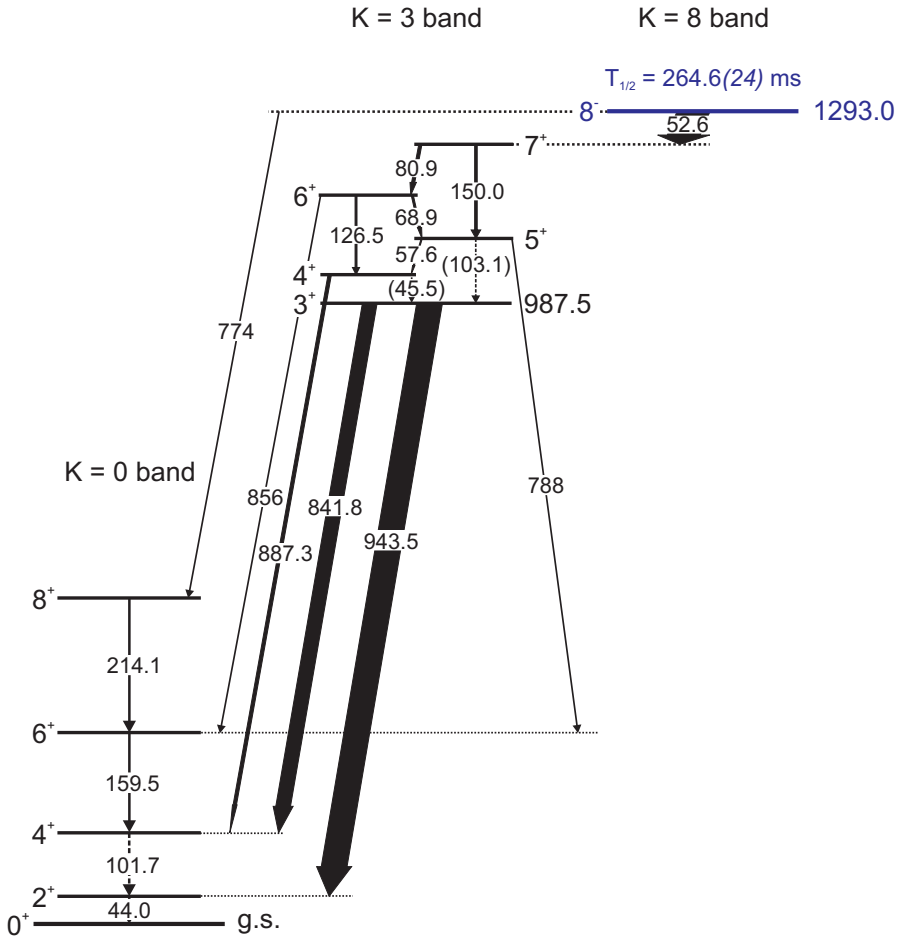

Figure 4.13: Decay scheme of the 264.6 ms isomeric state in ^{254}No. The ground-state band ($K^{\pi} = 0^{+}$) was previously observed up to a spin of $22\hbar$ [Eec05a]. Some low energy transitions are marked with dashed lines for clarity though they were not observed.

ously assign the nucleonic structure to the band-head. Previous analysis showed that the decay of the 184.8 µs isomer directly feeds the $K^{\pi} = 8^{-}$ state. Some of the observed transitions must be therefore the same in both decay patterns (in-beam and decay of the short-lived isomer). Both datasets therefore needs to be discussed together.

Fig. 4.15 displays the JUROGAM spectrum tagged by the decay of the 264.6 ms isomer. The region around the K X-rays is expanded in the inset. Excepts of the strong K X-rays only weak peaks at 111 and 134 keV are evident. Indications of peaks are also in the region above the K_{β} X-rays, but none of them exceeds the background by a factor at least of 3. But some of them are observed in the decay of short-lived isomer.

Peak at energy close to 600 keV (in Fig. 4.15 marked with red ellipse) can be interpreted as a singlet or as a doublet. This transition is incidental with the decay

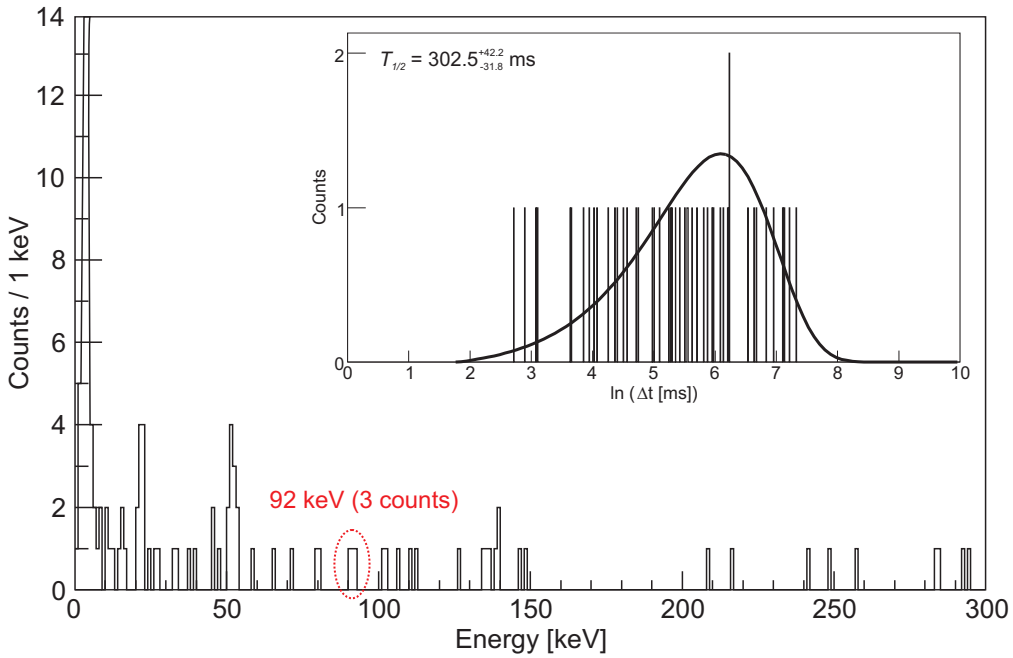

Figure 4.14: $\gamma\gamma$-coincidence PLANAR spectrum with sum of the gates on 68.9, 80.9 and 150.0 keV transitions. Coincidence between these in-band transitions and 92 keV peak is indicated as 3 counts are evident. The inset shows distribution of recoil-electron time differences when only events with electrons coincident to 92 keV transition are taken. Spectrum was fitted by universal curve and half-life of $302.5^{+42.2}_{-31.8}$ was obtained.

of the short-lived isomer (there is similar energy observed at the focal plane) and therefore it will be analysed later.

Only $\gamma\gamma$-coincidences analysis with gates on the K X-rays could be performed due to the lack of statistics. Fig. 4.16 shows the spectrum of the γ-rays coincident to the K X-rays. It is evident that the K X-rays are in coincidence with the K X-rays and are coming from the strongly converted cascade. Evident is also the transition of 134 keV.

4.6 Decay properties of the 184.8 μs isomeric state

Analysis of the properties of the 184.8 µs isomer was more difficult, because the gained statistics was much lower in this case. Only tentative decay scheme based on speculations and theory could be deduced.

To investigate the properties of the short-lived isomeric state the time gate of 0 - 1130 µs for recoil-electron correlations was applied. A contribution of the 264.6

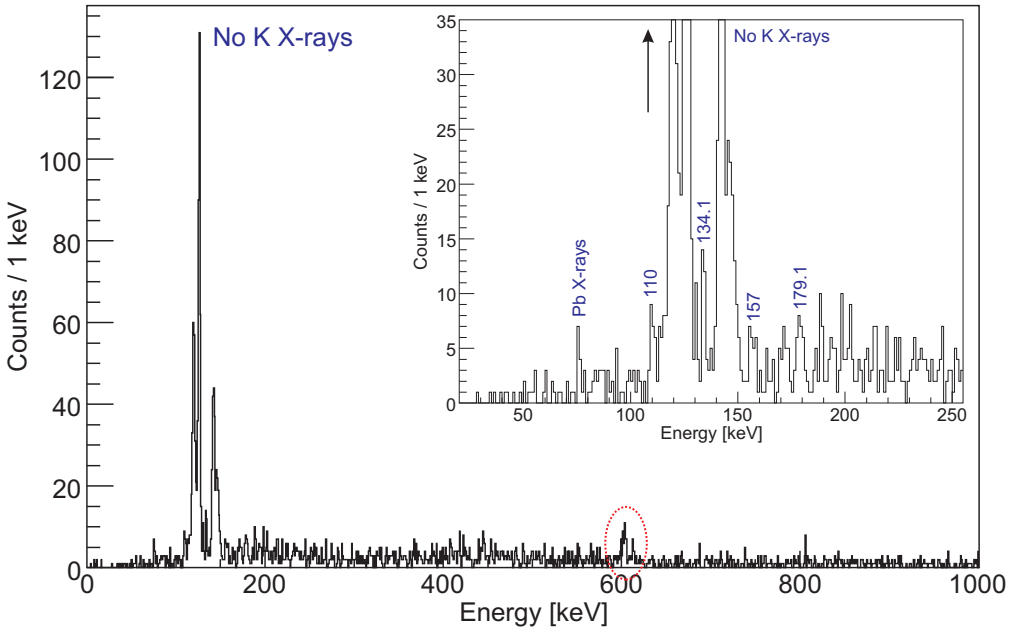

Figure 4.15: Spectrum of prompt γ-rays tagged by the decay of the $K^{\pi} = 8^{-}$ isomeric state measured by the JUROGAM. Because of low statistics the band structure could not be clearly observed. Here only peaks incidental with the decay of the short-lived isomer are marked. These will be discussed later.

ms isomer is neglictible (only 0.3 % decays occurs within this short time gate). The summary of observed correlation chains is in Tab. 5.6. The energy spectrum of correlated electrons is in Fig. 4.17. The calorimetric footprint of the electrons is in this case distinct compared with the long-lived isomer. More high-energy signals are presented here.

Table 4.10: Number of observed correlation chains within 2 - 1700 ms time gate .

Experiment	**Number of observed correlations**
R35	3 969
JR48	1 544

The decay of short-lived isomer connects directly the $K^{\pi} = 8^{-}$ isomeric state. It is expected that this feeding proceeds via the $K^{\pi} = 8^{-}$ rotational band (as in known K-isomers in hafnium region - e.g. ^{178}Hf [Smi03]). Spectrum of γ-rays associated to the decay of the 184.8 μs isomer is displayed in Fig. 4.18. The high-energy part is in the inset.

The high-energy part of the spectrum contains only single 605.9 keV transition.

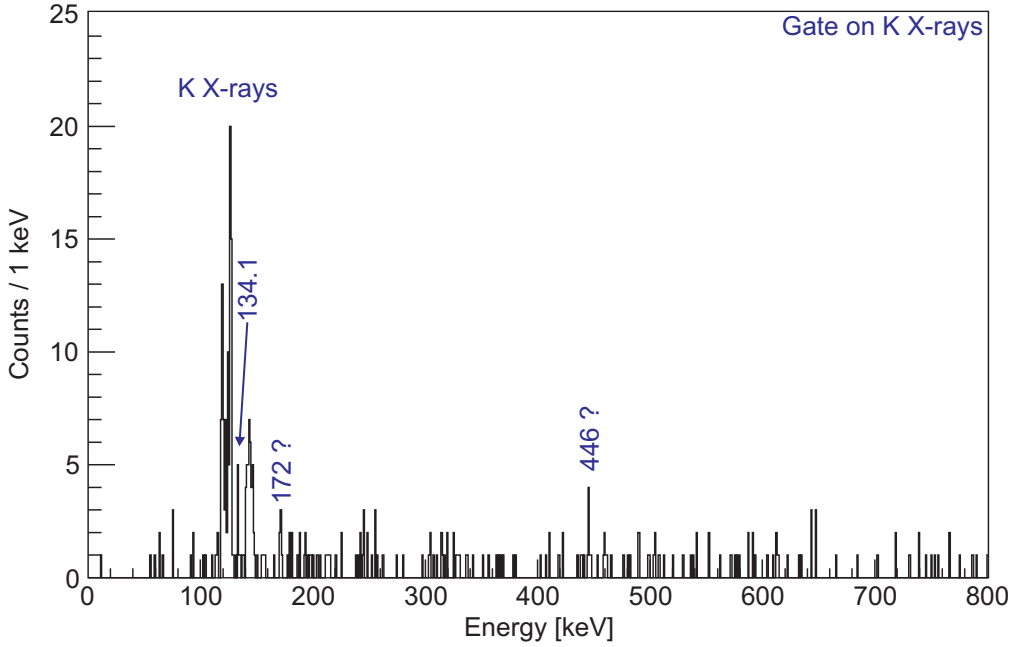

Figure 4.16: $\gamma\gamma$-coincidence JUROGAM spectrum with the gate on the K X-rays.

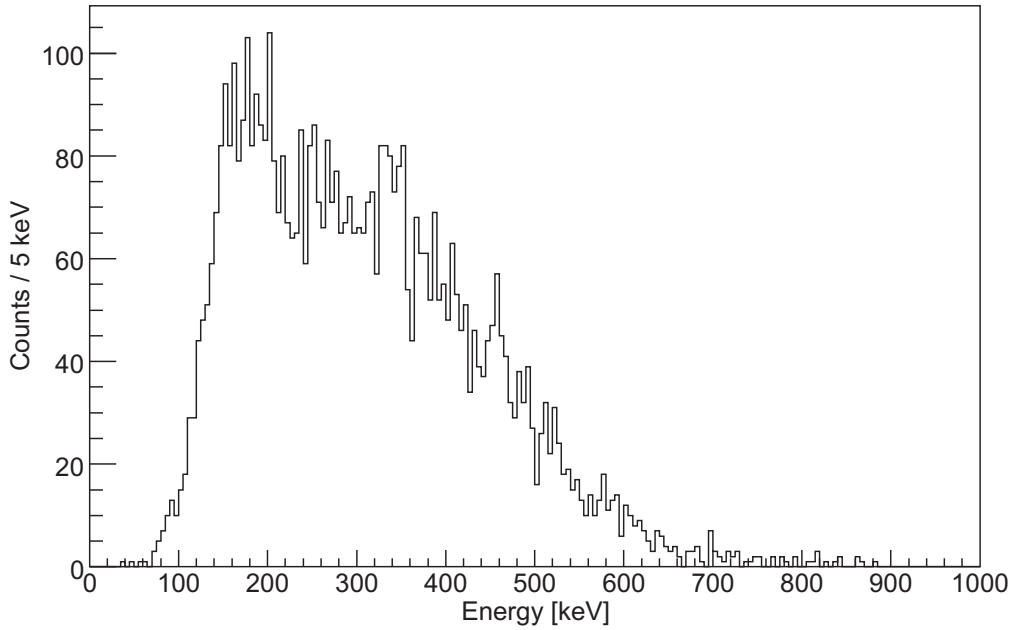

Figure 4.17: Spectrum of correlated electrons within 0 - 1130 μs time gate.

Peak at similar energy was observed in the JUROGAM on the top of the long-lived isomer. But the peak observed in the JUROGAM is too broad to be a single tran-

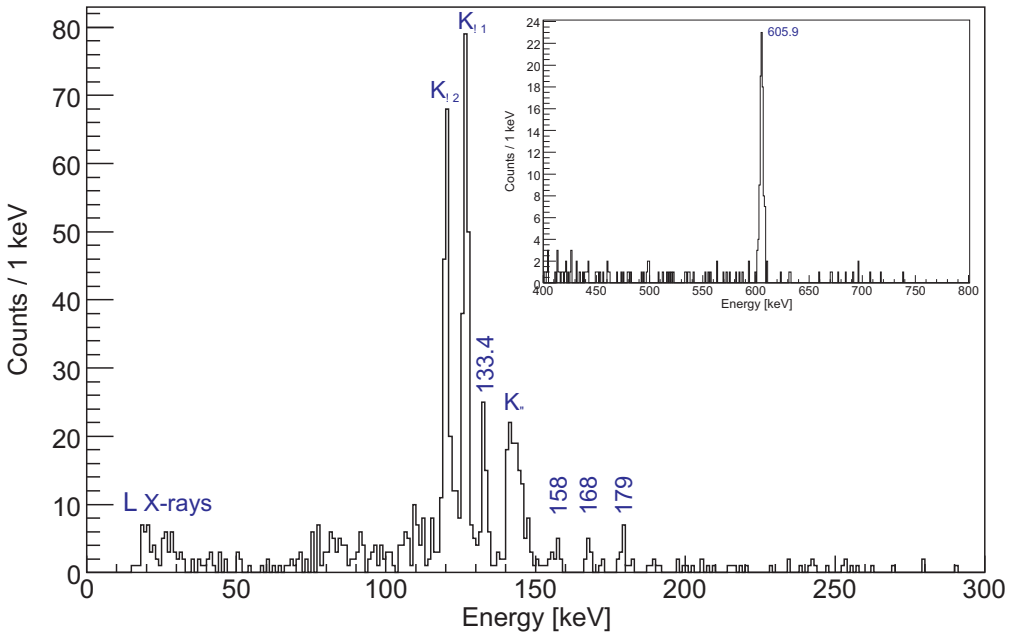

Figure 4.18: Spectrum of γ-rays assigned to the decay of the short-lived isomer. Low-energy part (large spectrum) was measured by the PLANAR and only events with the same energy on both sides were collected. High-energy part was obtained by the CLOVER and the VEGA detectors and is displayed in the inset.

sition - it looks to be a doublet. Both, single and double peak fit was performed. The energy was found to be of 602.5 keV in the case of one peak fit and of 601.9 and 604.4 keV with double peak fit. The energy differences against the focal plane appeared too large - of 3.4 keV or 1.5 keV respectively. To check the energy calibration, careful analysis of γ-rays from the standard sources ^{133}Ba and ^{152}Eu was done. No inconsistence with literature values was found. This means that the 605.9 keV transition is not observed in the in-beam spectrum and thus it arises directly from depopulation of the isomeric state. It is not immediately evident what might be the source of mentioned line (or two lines) which are observed in the JUROGAM data. One possibility is that it could be a decay from an intrinsic state with the half-life $\sim$ 1 ns or less into the $K^\pi = 8^-$ band.

In the low-energy part of the spectrum there are dominating L and K X-rays. As they come in cascade (see Fig. 4.20 (b)), the decay must pass over a converted band structure. This can be built up directly on the $K^\pi = 8^-$ isomeric state or on another two-quasiparticle excited state.

There are also weak transitions of 158, 168 and 179 keV evident in the PLANAR. These are good candidates for in-band mixed M1/E2 transitions of the $K^\pi = 8^-$ band. To investigate the properties of these states, $\gamma\gamma$-coincidences analysis was performed. Spectrum in Fig. 4.19 (a) shows that these in-band transitions are in coincidence with the 605.9 keV line. Coincidences between different strips of

the PLANAR (see Fig. 4.20 (b)) indicates also feeding of the 111 keV line by in-band transitions. Evidence for this transition is presented in the PLANAR singles spectrum and was observed also in the JUROGAM. Therefore it was assigned to be the decay of first rotational level of the $K^{\pi} = 8^{-}$ band. When energies of some in-band transitions are known the rotational formula could be applied. Energies of collective in-band transitions follow very well those calculated (see Tab. 4.11). Some of mixed M1/E2 transitions were not observed because they are dominated by strong K X-rays. Unfortunately no stretched E2 transitions were visible at this level of statistics.

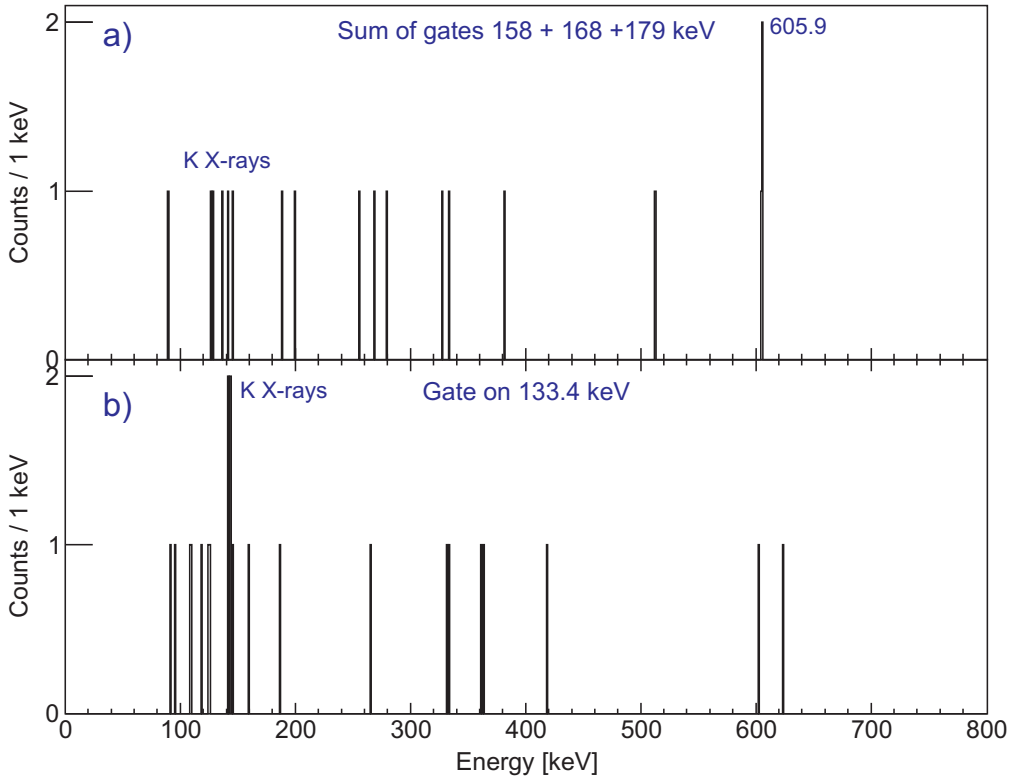

Figure 4.19: $\gamma\gamma$-coincidence CLOVER spectra tagged with the decay of the 184.8 μs isomer with gate on the (a) sum of the gates on the 158, 168 and 179 keV transition, (b) on the 133.4 keV transition. Evident is coincidence between in-band transitions and the 605.9 keV transition.

Rough identification of the rotational band up to state $K,J^{\pi} = 8,15^{-}$ and strong transition feeding it directly from the isomer allow to speculate about the character of the isomeric state. The excitation energy is roughly of 2 917 keV. This energy is too high for two-quasiparticle state, thus the isomeric level must have a four-quasiparticle structure. Possible nucleonic structures will be discussed later. The multipolarity of the 605.9 keV transition cannot be assigned unambigously because there are too many K-converted transitions in the decay scheme. Limit for α_K is in this case useless, because it would allow any multipolarity as the K X-rays are

comming mainly from other transitions. Anyway, tentatively the E1 character could be suggested. In the case of the quadrupole transition (E2, M2) there would exist more preferable E1 or M1 transition feeding the K,$J^\pi = 8,16^-$ state. Higher order of multipole is excluded by the short half-life of the isomer. Positive parity of the isomer was taken from theoretical calculations, which predicts only positive parity four-quasiparticle states around this excitation energy [Tan06, Her06a] and spin. According to all these arguments we have tentatively determined the short-lived isomer as the $K^\pi = 16^+$ state.

Table 4.11: Comparison of observed transition energies and those calculated using the rotational formula.

$\mathbf{J}_i^\pi \rightarrow \mathbf{J}_f^\pi$	**Measured energy [keV]**	**Rotational formula [keV]**
$9^- \rightarrow 8^-$	111	111.1
$10^- \rightarrow 9^-$	-	122.5
$11^- \rightarrow 10^-$	134	134.0
$12^- \rightarrow 11^-$	-	145.5
$13^- \rightarrow 12^-$	156	157.0
$14^- \rightarrow 13^-$	168	168.4
$15^- \rightarrow 14^-$	179	179.9

There is also the strong transition of 133.4 keV evident in the PLANAR spectrum. Similar energy (134 keV) was observed also in the JUROGAM. This energy corresponds to the $11^- \rightarrow 10^-$ mixed M1/E2 transition within the $K^\pi = 8^-$ band predicted by the rotational formula. But according to the PLANAR efficiency [And04] and to the ICCs [Kib05], the 134 keV in-band γ-line should be stronger only by a factor of 1.4 than the 179 keV transition ($15^- \rightarrow 14^-$). In our case the ratio of observed γ-rays intensity is of $3.9^{+1.4}_{-1.0}$. Thus the line observed in the PLANAR is most probably a doublet combined from the in-band transition and from the transition adherent to the second decay branch of the isomer. To probe this, the $\gamma\gamma$-coincidences were studied. The CLOVER spectrum in coincidence with the PLANAR and gate on the 133.4 transition is shown in Fig. 4.19 (b). The is one count at 606 keV. This is not significant as there is also some background presented. With this level of the statistics it is impossible to confirm or to fully exclude the coincidence between two strongest peaks, especially when there should be the contribution of the in-band transition in the 133.4 keV line, which is in coincidence with the 605.9 keV transition.

To exclude that the 133.4 keV transition originates from an another isomeric state with the half-life within used time gate, the individual half-lives of both strongest lines were extracted. Because of the lack of the statistics the maximum

likelihood method [Sch84] was used. The half-lives of $183^{+17.2}_{-14.5}$ μs (133.4 keV) and $200.2^{+23.4}_{-19.0}$ μs were obtained. Within the frame of error bars (here only 1 σ error is given) both half-lives correspond to the 184.8 μs isomer.

Second decay branch of the 184.8 μs isomer, containing the 133.4 keV transition was tentatively identified. We expect that this decay pattern proceeds via the $K^\pi = 7^-$ rotational band and the 133.4 keV line could be the K-hindered transition feeding it or be a decay of of the non-isomeric band-head. The intensity of the 134 keV peak in the JUROGAM is comparable with that of 111 keV (which was determined to be the $9^- \rightarrow 8^-$ in-band transition). This indicates that the most of the intensity of the delayed 133.4 keV transition is not seen in-beam. According to this, the 133.4 keV transition observed in the PLANAR could be assigned as the K-hindered decay of the 184.8 μs isomeric state.

The deduced decay scheme is in the Fig. 4.21. It needs to be pointed out again that this scheme is due to the lack of statistics only tentative. Improved statistics (from both in-beam and decay experiment) could enlighten the structure and the decay properties of the short-lived isomeric state more satisfactorily.

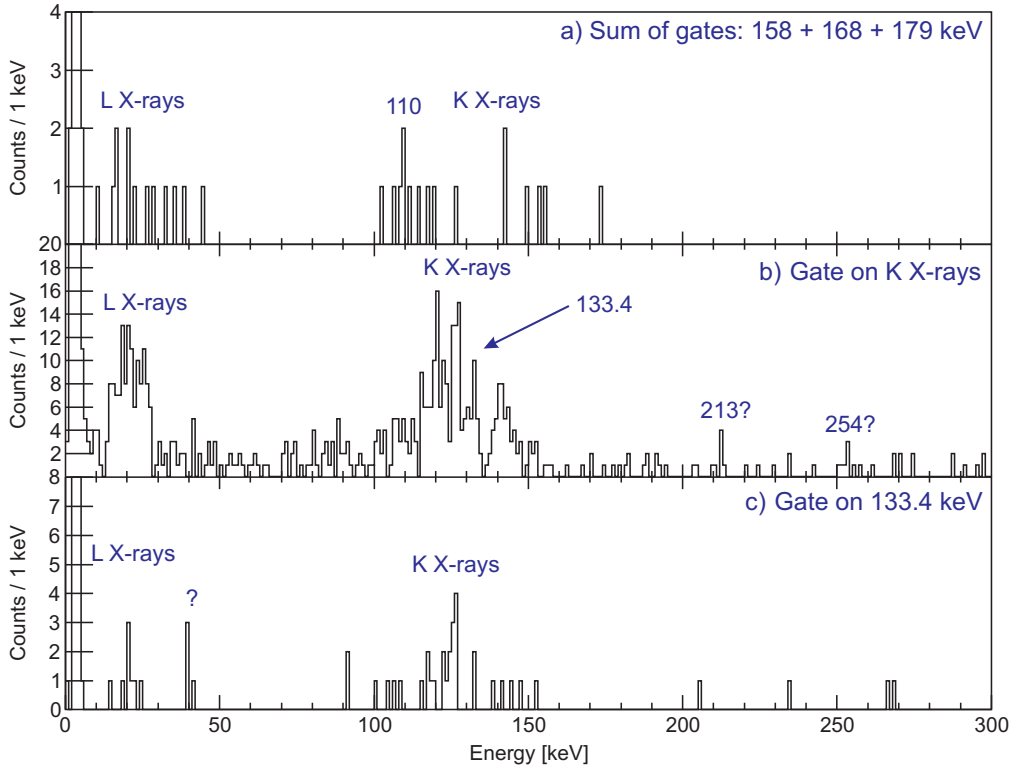

Figure 4.20: $\gamma\gamma$-coincidence PLANAR spectra tagged with decay of the 184.8 μs isomer with gate on the (a) sum of the gates on the 158, 168 and 179 keV transition, (b) on the K X-rays and (c) on the 133.4 keV transition.

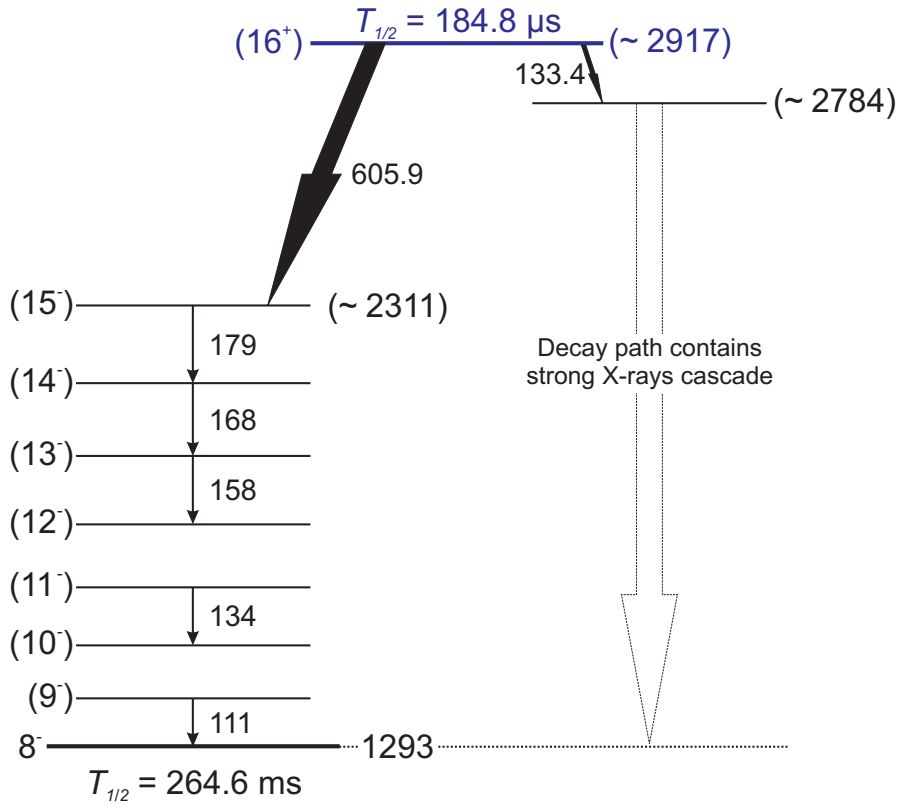

Figure 4.21: Proposed decay scheme of the 184.8 μs isomeric state.

Chapter 5

Discussion

5.1 Structure of the $K^\pi = 3^+$ two-quasiparticle state

The strongest decay branch of the $K^\pi = 8^-$ isomeric state proceeds via the underlying $K^\pi = 3^+$ rotational band. Several mixed M1/E2 and stretched E2 in-band γ-transitions were clearly identified. According to this we were able to extract the crossover-to-total ratio for decay of K,$J^\pi = 3{,}6^+$ and K,$J^\pi = 3{,}7^+$ state respectively. For the summary of all other obtained parameters like the quadrupole mixing ratio and the total ICC (calculated with [Kib05] according to quadrupole mixing) for the mixed transitions, the energies of the transitions and the g_K factor for both rotational states see Tab. 5.1. Finally we determined the value of the g_K factor of the band-head (as an average of individual g_K factors) to be of $0.89^{+0.14}_{-0.13}$.

Table 5.1: Decay properties of some of rotational states of the $K^\pi = 3^+$ band.

$\mathbf{J}^\pi_{init.}$	$\mathbf{E}_1$ [keV]	$\mathbf{E}_2$ [keV]	λ_γ	δ	α_t **(M1/E2)**	$\mathbf{g}_K$
7^-	80.9*(2)*	150.0*(3)*	0.92*(15)*	0.22*(9)*	$26.82^{+2.51}_{-1.79}$	$1.01^{+0.05}_{-0.06}$
6^-	68.9*(3)*	126.5*(6)*	0.61*(39)*	0.24*(19)*	$46.10^{+14.42}_{-7.38}$	$0.76^{+0.24}_{-0.18}$

Both, two-quasineutron and two-quasiproton singlet states with $K^\pi = 3^+$ could be formed in ^{254}No (see Tab. 5.2. The value of the g_K factor extracted from present data is in excellent agreement with that expected for two-quasiproton configuration, providing an unambiguous assignment of the $1/2^-[521]_\pi \otimes 7/2^-[514]_\pi$ configuration to the $K^\pi = 3^+$ state. The excitation energy of the $K^\pi = 3^+$ is exceptionally low for a two-quasiparticle state. This can occur only when accountable orbitals lie very close to Fermi surface. This confirms the theoretical prediction [Ahm77, Ahm78] that there is no deformed shell gap at Z = 102.

Table 5.2: Predicted $J^\pi = 3^+$ two-quasiparticle singlet states in ^{254}No.

Structure of the state	**Single-particle g_K factors**	**Two-quasiparticle g_K factor**
$1/2^-[521]_\pi 7/2^-[514]_\pi$	-0.92 ($1/2^-[521]$) 0.63 ($7/2^-[514]$)	0.82
$7/2^+[624]_\nu 1/2^+[620]_\nu$	-1.72 ($1/2^+[620]$) 0.28 ($7/2^+[624]$)	0.53

5.2 Structure of the $K^\pi = 8^-$ isomeric state

The 264.6 ms isomeric state was definitely identified as the $K^\pi = 8^-$ state with the excitation energy of 1293.0(20) keV. Theoretical calculations predicting the excitation energy of a $K^\pi = 8^-$ two-quasiparticle triplet states in ^{254}No were performed by many authors [Her06a, Xu04, Sol91, Laz89, Tan06] - see Fig 5.1. Two-quasiproton $7/2^-[514]_\pi \otimes 9/2^+[624]_\pi$ and two-quasineutron $7/2^+[613]_\nu \otimes 9/2^-[734]_\nu$ structures are found in all calculations. Ref. [Laz89] predicts also two-quasineutron state $7/2^+[624]_\nu \otimes 9/2^-[734]_\nu$ to lie higher in energy that previous mentioned two-quasineutron state.

From the data obtained in the present work it is not possible to determine unambiguously the structure of the $K^\pi = 8^-$ isomer. We tentatively prefer two-quasiproton scenario due to presence of the strong 52.6 keV E1 transition connecting the isomeric state with the lower-lying $K^\pi = 3^+$ two-quasiproton state. In the case of two-quasiproton structure of the isomer it represents a single-proton transition rather than transition of two protons and two neutrons as it would be in the case of two-quasineutron character of the isomeric state. This indicates two-quasiproton structure $7/2^-[514]_\pi \otimes 9/2^+[624]_\pi$ of the $K^- = 8^-$ isomer. Two-quasineutron structure of course cannot be fully excluded and the 52.6 keV transition could be partially hindered due to such complicated transition.

Table 5.3: Calculated g_K factors for predicted $K^\pi = 8^-$ two-quaparticle states.

Nucleonic structure of the state	**g_K factor**
$7/2^-[514]_\pi \otimes 9/2^+[624]_\pi$	1.006
$7/2^+[613]_\nu \otimes 9/2^-[734]_\nu$	-0.017
$7/2^+[624]_\nu \otimes 9/2^-[734]_\nu$	-0.270

For unambiguous determination of the structure of the $K^\pi = 8^-$ isomer γ-rays intensities of transitions within band on the top of it must be studied. Summary of possible $K^\pi = 8^-$ two-quasiparticle states together with calculated g_K factors is

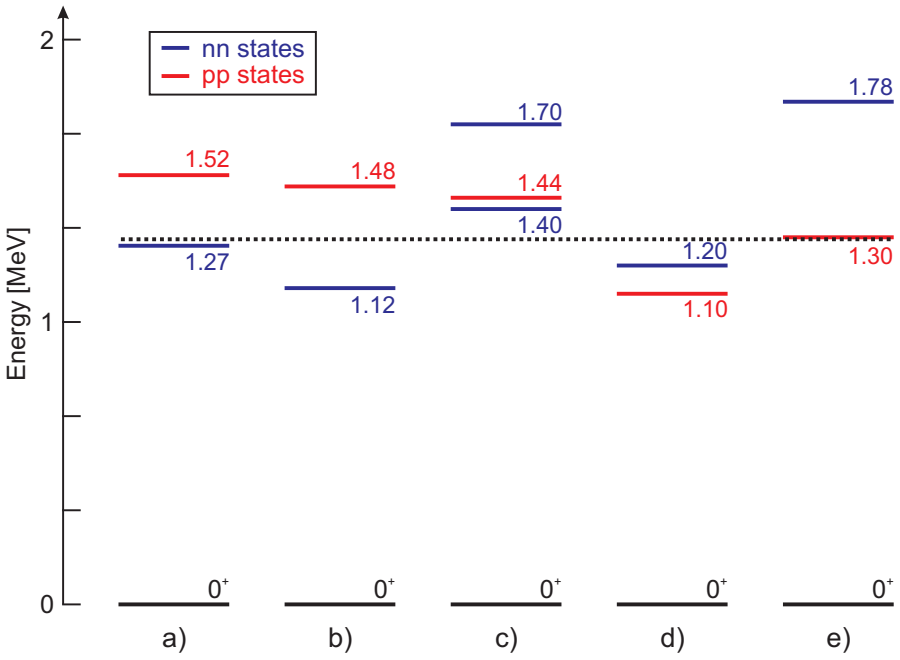

Figure 5.1: Excitation energy of a $K^{\pi} = 8^{-}$ two-quasiparticle states predicted in ^{254}No. by a) [Her06a], b) [Xu04], c) [Laz89], d) [Sol91] and e) [Tan06, Kho06]. The experimental value of 1293.0 keV obtained in the present work is marked with a dashed line.

in Tab. 5.3. The band structure based on $K^{\pi} = 8^{-}$ state was tentatively identified by interconnection of the in-beam data and of the decay of the 184.8 μs isomer (see Fig. 4.21). The γ-ray strengths of the in band transitions was calculated for different band-head structures. The calculation was based on the Bohr-Mottelson rotational model with the $Q_0 = 13.28$ ebarn and the $g_R = 0.4$. For calculated ratios of intensity of M1/E2 and E2 transitions see Tab. 5.4. Unfortunately only weak mixed M1/E2 in-band transitions were identified. Thus it is not possible to extract experimental branching ratios of γ-rays and compare them with calculated values. We calculated γ-rays intensities ratio between $15^{-} \rightarrow 14^{-}$ and $14^{-} \rightarrow 13^{-}$ mixed M1/E2 (see last line of Tab.5.4). This is also sensitive to the band-head configuration. Experimentally we obtained the ratio of $1.44^{+0.56}_{-0.39}$. This excludes the $7/2^{+}[613]_{\nu} \otimes 9/2^{-}[734]_{\nu}$ two-quasineutron structure. Remaining two-quasineutron structure is found only in one quite old calculation [Laz89]. This gives an additional argument for proposed level scheme and for the two-quasiproton structure of the $K^{\pi} = 8^{-}$ isomeric state.

The obtained hindrance factor of the 52.6 keV transition was 2.28×10^{11}. This corresponds to the reduced hindrance of 691 which is in a good agreement with the Löbner systematics. For a direct E1 transition from the isomer into the ground-state band ($8^{-} \rightarrow 8^{+}$ transition) for which only indication was observed is the reduced hindrance of > 133. Large values of the reduced hindrance indicates

Table 5.4: Calculated ratios of the intensity of mixed M1/E2 and stretched E2 in-band transitions of $K^\pi = 8^-$ band.

	g_K = **-0.017**	g_K = **-0.27**	g_K = **1.006**
$\frac{I_\gamma(15\to14)}{I_\gamma(15\to13)}$	0.71	1.63	1.36
$\frac{I_\gamma(14\to13)}{I_\gamma(14\to12)}$	0.87	2.00	1.67
$\frac{I_\gamma(13\to12)}{I_\gamma(13\to11)}$	1.17	2.69	2.25
$\frac{I_\gamma(12\to11)}{I_\gamma(12\to10)}$	1.62	3.73	3.11
$\frac{I_\gamma(11\to10)}{I_\gamma(11\to9)}$	2.58	5.94	4.96
$\frac{I_\gamma(10\to9)}{I_\gamma(10\to8)}$	5.38	12.38	10.34
$\frac{I_\gamma(15\to14)}{I_\gamma(14\to13)}$	2.41	1.61	1.73

that the K quantum number is "good" for all observed states and its "goodness" is conserved to high value of excitation energy and spin. This is in agreement with the self-consistent mean-field theories [Afa03, Dug01] which predict the axial symmetry for ground-state of the ^{254}No. Our results show that the axial symmetry remains conserved also at high-spin two-quasiparticle excitation.

The right part of Fig. 5.2 shows the Woods-Saxon single-proton orbitals lying close to the Fermi surface. The energies of the single-particle orbitals were calculated using Woods-Saxon potential with "Universal" parameters [Cwi87, Naz85]. Occupation of the single-particle orbitals by protons in the case of the $K^\pi = 3^-$ and the $K^\pi = 8^-$ excitation is marked. The decay of the isomeric state can be explained as a single-particle transition from $9/2^+[624]$ to $1/2^-[521]$ orbital. The single occupied $7/2^-[514]$ state plays in this transition the role of the spectator. Clear identification of presence of the $1/2^-[521]$ in the $K^\pi = 3^+$ excited state is one of the most important results of the experiment discussed in present work. The $1/2^-[521]$ orbital arises from the $2f_{5/2}$ spherical orbital (see left part of Fig. 5.2). This encloses the spherical gap at Z = 114 and thus localisation of the excitation energy of the $1/2^-[521]$ orbital is a valuable input for models predicting position of next closed proton magic number for which the theory still has not consensus yet.

The excitation energy and unambiguous identification of the nucleonic structure of observed two-quasiproton states allowed to calculate the value of the pair gap - see Tab. 5.5. The theoretically calculated ground-state pair gap value (unaffected by the orbital blocking) is of 0.638 MeV [Mol97]. Reduction due to the orbital blocking effect is thus about 70 %.

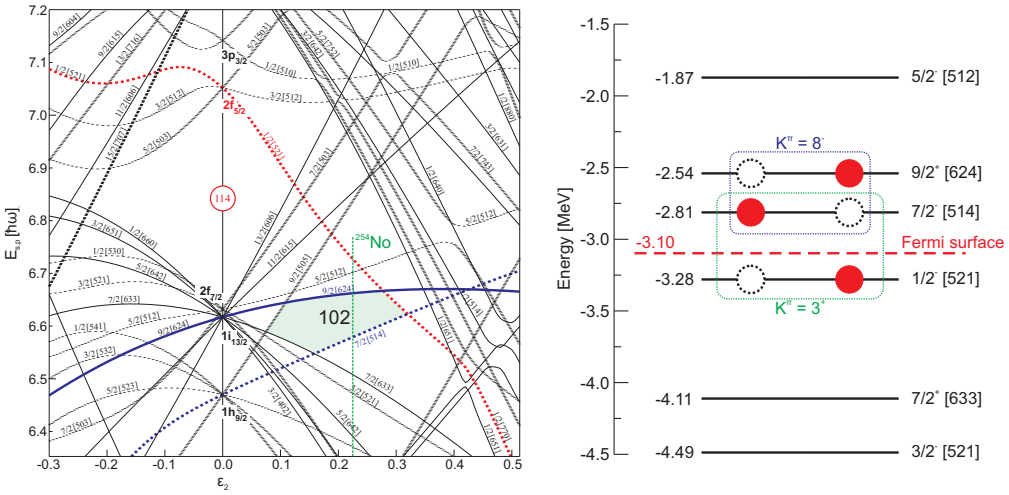

Figure 5.2: Woods-Saxon single-proton orbitals in ^{254}No close to the Fermi surface (right side) and Nillson diagram for protons in studied region of proton number[Fir96]. The diagram is only illustrative, the excitation energies and ordering of the orbitals for given deformation could differ compared to the values obtained by Woods-Saxon calculation. The deformation of ^{254}No is marked with a green line.

Table 5.5: Observed two-quasiparticle levels and calculated pair gap values.

K^{π}	Half-life	Excitation energy [keV]	Nucleonic structure	Pair gap [MeV]
3^+	<10 ns	987.5*(10)*	$1/2^-[521]_{\pi}\otimes 7/2^-[514]_{\pi}$	0.433
8^-	264.6*(24)* ms	1293.0*(15)*	$7/2^-[514]_{\pi}\otimes 9/2^+[624]_{\pi}$	0.480

5.3 Properties of the $K^{\pi} = 16^+$ isomeric state

The statistics gained in both experiments in not sufficient and only ambiguous results can be given. The isomeric state with the half-life of 184.8 μs was tentatively determined to be the $K^{\pi} = 16^+$ with excitation energy of 2 917 keV. According to high excitation energy only four-quasiparticle excitation could be considered. In the contrast to two-quasiparticle states, there are not many theoretical works on four-quasiparticle states found in the literature. Some calculations can be found in [Her06a, Tan06].

There is a good two-quasineutron-two-quasiproton candidate with nucleonic structure $7/2^+[613]_{\nu}\otimes 9/2^-[734]_{\nu}\otimes 7/2^-[514]_{\pi}\otimes 9/2^+[624]_{\pi}$ predicted in both publication. The predicted excitation energy of 2.75 MeV is in rough agreement with our experimental data.

We have identified two decay branches of the $K^{\pi} = 16^{+}$ isomeric state. We expect that the weak decay path containing the 133.4 keV transition proceeds via the band on the top of the non-isomeric two-quasiparticle state. There is predicted [Tan06] the two-quasiproton $K^{\pi} = 7^{-}$ state with $7/2^{-}[514]_{\pi} \otimes 7/2^{+}[633]_{\pi}$ structure. The E1 multipolarity could be therefore suggested for the 133.4 keV transition.

Table 5.6: Transitions associated to the decay of $K^{\pi} = 16^{+}$ isomeric state .

Energy [keV]	**Branching ratio**	**Multipolarity**	**Δ K**	**Partial half-life**	**Reduced hindrance**
605.9*(2)*	0.86*(2)*	E1	8	215.1*(167)* μs	43.3*(5)*
134.4*(4)*	0.14*(8)*	E1	9	1311.7*(7292)* μs	19.2*(13)*

The summary of both speculated E1 K-hindered transitions is in Tab. 5.6. The reduced hindrances (calculated according to the E1 character of both transitions and to the ratio of intensity of observed γ-lines) are too small. This could indicate the admixture of another value of K in the state or some deviations from axial symmetry at very high-spin and excitation energy. Due to the lack of the statistics it is not excluded that our spin assumption for the isomer is wrong. Another high-spin four-quasiparticle state with a $K^{\pi} = 14^{+}$ is predicted to lie lower in the energy than $K^{\pi} = 16^{+}$ [Tan06]. The nucleonic structure of this state is $3/2^{+}[622]_{\nu} \otimes 9/2^{-}[734]_{\nu} \otimes 7/2^{-}[514]_{\pi} \otimes 9/2^{+}[624]_{\pi}$. It is not excluded that the short-lived isomer is formed by this state. Only way how to answer this question is to gain much higher statistics and build unambiguous decay scheme.

5.4 K-isomers studies experiments in nobelium region

The successful experiments R35 and JR48 have generated a whole research programme now pursued by several groups around the globe. In this section only experiments which were carried out within the program of K-isomers studies at JYFL and GSI during year 2005 - 2008. The production cross-section of employed reactions is lower than in the case of ^{254}No but still remains on the level when it is possible to produce enough statistics within short period of beam-time.

Results of experiments on ^{254}No from the present work were confirmed utilising the FMA in ANL [Tan06] and the velocity filter SHIP in GSI [Sul07a]. Both groups fully confirmed our results on the long-lived isomer but obtained different results on the short-lived one. At SHIP due to the possibility of intensive ^{48}Ca beam ($\sim$ 1 pμA) much higher statistics was obtained. Analysis of the data together with additional statistics obtained during digital electronics test at the JUROGAM is in the progress and will be published elsewhere [Her08].

As a continuation of K-isomers programme at JYFL, K-isomer in ^{250}Fm was studied. First identification was referred by Ghiorso *et al.* [Ghi73]. But as in the case of ^{254}No, only the half-life of the isomeric state could be indirectly obtained. The experiment at JYFL utilised the ^{204}HgS(^{48}Ca,2n)^{250}Fm reaction. The projectile energy was of 209 MeV in the middle of the target. The DSSSD operated in the same mode as during experiments discussed in this work (i. e. the X-side tuned for calorimetric signals from electrons while Y-side for recoil implantation and α particles). The focal plane and the in-beam measurements were performed simultaneously. Due to the JUROGAM employment and to the chemical properties of the target material, the beam intensity had to be reduced to 8 pnA. The half-life of 1.92(5) s, which is in excellent agreement with findings of Ghiorso *et al.*, was acquired. Plenty of new γ-transitions were identified and full decay scheme builded. The isomeric state was determined to be the $K^\pi = 8^-$ state with the excitation energy of 1199.5 keV. The band structure above the isomer was observed and the ratios B(M1)/B(E2) could be extracted. These allowed the unambiguous assignment of the orbital structure $9/2^-[734]_\nu \otimes 7/2^+[624]_\nu$ to the isomer. The low-lying $K^\pi = 2^-$ state was identified in the decay path of the isomeric state. The wave function of this state is mixed from the octupole and the two-quasineutron configuration $9/2^-[734]_\nu \otimes 5/2^+[622]_\nu$. The measured g_K factor indicates that the two-quasineutron configuration dominates the structure. For more detailed discussion see [Gre07].

Heavier isotone of ^{250}Fm - ^{252}No was under investigation at SHIP. ^{252}No nuclei were produced via ^{206}PbS(^{48}Ca,2n)^{252}No reaction. This reaction was employed as a spontaneous fission calibration during an attempt to confirm the Dubna data for the element Z = 112 [Hof07]. As a by-product, previously unknown K-isomer was identified. New experiment was therefore performed and a sufficient statistics was gained [Sul07a, Sul07b]. The decay pattern very similar to that observed in ^{250}Fm was discovered. Also in this case K-isomer is the $K^\pi = 8^-$ state and the excitation energy is of 1254 keV. The $9/2^-[734]_\nu \otimes 7/2^+[624]_\nu$ orbital configuration could be assigned only tentatively to the isomer. For unambiguous determination of the structure of the isomeric state, the band properties above it have to be studied. No four-quasiparticle isomer which decay would populate the band above the $K^\pi = 8^-$ isomeric state was observed. Therefore the in-beam experiment has been proposed [Sul07c]. The proposal has been accepted at JYFL and will be carried out in April 2008. The JUROGAM array, the RITU separator and the GREAT spectrometer will be employed.

In a similar experiment, more neutron-deficient fermium isotope, ^{248}Fm was studied at JYFL. The reaction was ^{48}Ca(^{202}HgS,2n)^{248}Fm. The main goal was to study the ground-state rotational band. In addition, the decay of new isomeric state was observed. Unfortunately, due to the problems with the ECR ion source, the gained statistics was only about a half of that expected. Half-life of isomeric state is about 8 ms [Her07]. The data analysis is in the progress and new experiment is scheduled in April 2008 (back-to-back with the ^{252}No in-beam experiment).

The summary of basic properties of known K-isomers in even-even nuclei in heavy and superheavy region is in the Tab. 5.7.

Table 5.7: Properties of known two-quasiparticle K-isomers in even-even isotopes in region of heavy and superheavy nuclei. In many cases assignments of K^π and orbital configurations are only tentative - see references for more detailed discussion.

Isotope	$\mathbf{T}_{1/2}$	$\mathbf{K}^\pi$	$\mathbf{E}_X$ **[MeV]**	**Decay mode**	**Configuration**	**Ref.**
^{244}Cm	34 ms	6^+	1.040	γ	$5/2^+[622]_\nu \otimes 7/2^+[624]_\nu$	[Hof84]
^{246}Cm	-	8^-	1.179	γ	$7/2^+[624]_\nu \otimes 9/2^-[734]_\nu$	[Mul76]
^{248}Fm	$\simeq$ 8 ms	-	-	γ	-	[Her07]
^{250}Fm	1.92 s	8^-	1.195	γ	$9/2^-[734]_\nu \otimes 7/2^+[624]_\nu$	[Gre07]
^{256}Fm	70 ns	7^-	1.425	γ,SF	$7/2^+[633]_\pi \otimes 7/2^-[514]_\pi$	[Hal89]
^{250}No	42 μs	6^+	-	SF, γ?	$5/2^+[622]_\nu \otimes 7/2^+[624]_\nu$	[Pet06]
^{252}No	110 ms	8^-	1.425	γ	$9/2^-[734]_\nu \otimes 7/2^+[624]_\nu$	[Sul07a]
^{254}No	264 ms	8^-	1.293	γ	$7/2^-[514]_\pi \otimes 9/2^+[624]_\pi$	p.w. [Her06a]
^{270}Ds	6 ms	9^- 10^-?	$\simeq$ 1.13	α	$11/2^-[725]_\nu \otimes 7/2^+[613]_\nu$ $11/2^-[725]_\nu \otimes 9/2^+[615]_\nu$	[Hof01]

5.5 Systematics of two-quasiparticle levels - influence of shell-gaps in nobelium region

Experiments mentioned in the previous section along with older data yield limited systematics of two-quasiparticle levels in even-even isotones in the region of deformed shell-gaps Z = 100 and N = 152 - see Tab. 5.8.

Two two-quasiproton states were observed in ^{254}No. Two-quasineutron states must lie higher in energy due to the presence of the gap enclosing single-neutron orbitals $9/2^-[734]_\nu$ and $1/2^+[620]_\nu$. As we go to N = 150 isotone, the Fermi level moves under the closed shell. Consequent of this, the excitation energy of two-quasineutron states is lowered below the two-quasiproton ones - as it is observed in ^{252}No. The excitation energy of two-quasiproton excitations should remain more or less constant within all even-even nobelium isotopes. There were two-quasineutron excited states observed with the same structure, similar decay pattern and similar excitation energy in ^{250}Fm. In this nucleus two-quasiproton states are expected to

go up in the excitation energy as a result of the existence of shell-gap located at Z = 100.

Two-quasiparticle levels were described by calculations [Tan06, Gre07] based on Woods-Saxon calculations with "Universal" parameters (for comparison of with experimental data see Fig.5.3). While experimental results for ^{254}No are well represented by calculations, in N = 150 isotones the excitation of the $K^{\pi} = 8^{-}$ states is underestimated by used model. This could be explained by higher separation of $7/2^{+}[624]$ and $9/2^{-}[734]_{\nu}$ single-neutron orbitals. But the energy difference between this orbitals is not so significant as in the case of N = 152 gap because otherwise we would observe two-quasiproton states in ^{252}No (due to almost degeneration of single-proton orbitals $1/2^{-}[521]_{\pi}$ and $7/2^{-}[514]_{\pi}$).

Table 5.8: Summary of two-quasiparticle levels in nuclei around Z = 100 and Z = 152 deformed gaps.

Isotope	**K^{π}**	**Excitation energy [keV]**	**Nucleonic structure**	**Reference**
^{254}No	3^{+}	987.5	$1/2^{-}[521]_{\pi}\otimes 7/2^{-}[514]_{\pi}$	p.w., [Her06a]
	8^{-}	1293.0	$7/2^{-}[514]_{\pi}\otimes 9/2^{+}[624]_{\pi}$	
^{252}No	2^{-}	929.0	$9/2^{-}[734]_{\nu}\otimes 5/2^{+}[622]_{\nu}$	[Sul07a]
	8^{-}	1254.0	$9/2^{-}[734]_{\nu}\otimes 7/2^{+}[624]_{\nu}$	
^{250}Fm	2^{-}	881.0	$9/2^{-}[734]_{\nu}\otimes 5/2^{+}[622]_{\nu}$	[Gre07]
	8^{-}	1199.2	$9/2^{-}[734]_{\nu}\otimes 7/2^{+}[624]_{\nu}$	

5.6 Future projects

Development of the recoil-electron correlation method opens new possibilities in heavy elements nuclear structure studies. It is possible to investigate the states that are not populated (or their population is very rare) by the α decay or via the fusion-evaporation reaction or their half-life is too long for conventional recoil-γ tagging method. As a natural way how to proceed in research of even-even N = 152 isotones is to study heavier elements (^{256}Rf, ^{258}Sg). Moving up of the Fermi surface would allow to "scan" the gaps between the single-particle states (via low lying two-quasiparticle states) and thus test predictive power nuclear models. For single-particle orbital scheme see Fig. 5.4.

^{256}Rf could be produced via ^{208}Pb(^{50}Ti,2n)^{256}Rf reaction. This reaction was studied by Heßberger *et al.*[Hes97]. Main decay mode of ^{256}Rf is spontaneous fission (α branch is < 0.5 %), the half-life is of 6.2 ms and the production cross-section is of 12 nb. No second component of the fission half-life was identified

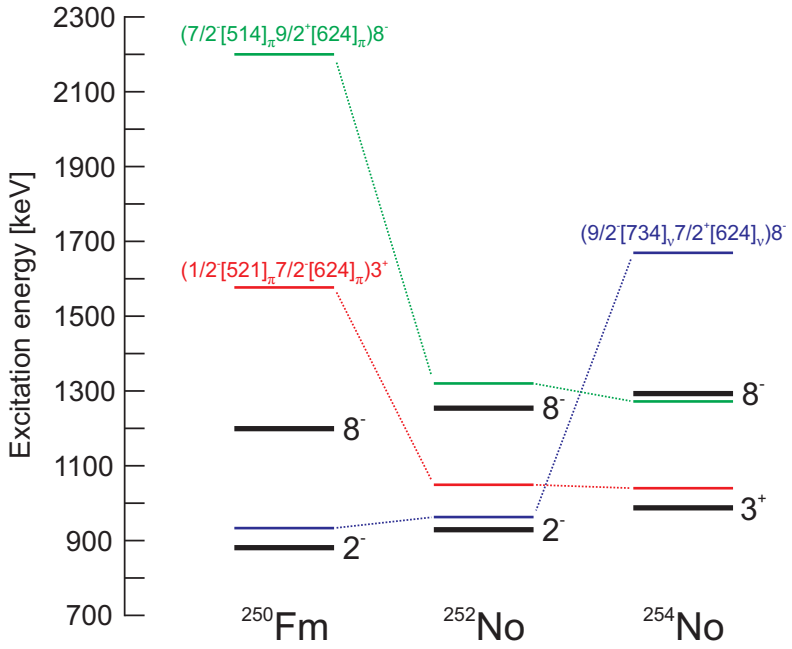

Figure 5.3: Comparison of experimentally observed two-quasiparticle levels with theoretical predictions using Woods-Saxon potential. Theoretical values were taken from [Gre07].

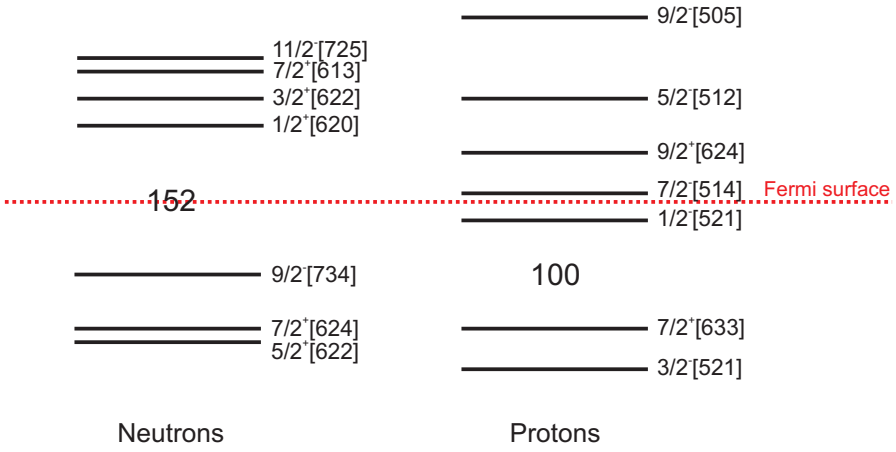

Figure 5.4: Single-particle orbitals in region of interest calculated by using of Woods-Saxon potential with "Universal" parameters.

[Hes07]. This indicates that if there exist high-K isomeric state (if there exist any) must be much shorter-lived than the ground-state. The recoil-electron-SF tagging experiment was performed in October 2007 in ANL [Kho07]. No results have been published yet. Studies of ^{258}Sg would be much more complicated. The cross-section of reactions leading to this nucleus is expected to be of several tens of

picobarns. This is not enough for detailed γ-spectroscopical studies with presently existing experimental facilities. The same problem exists also in the case of N = 150 isotones.

Less neutron deficient nuclei are reachable only via hot fusion reactions. The reaction ^{238}U(^{22}Ne,4n)^{256}No was tested at SHIP. Unfortunately these very asymetric reaction are very difficult with common kinematic separators because usually the transmission is very low. Another problem resulting from very low velocity of evaporation residue. This makes usage of transit detectors, which is crucial for recoil-electon tagging method. This makes hot fusion reaction useless for high-K isomers studies. Thus without radioactive target or beams less neutron deficient nuclei than ^{254}No are inaccesible for this kind of studies.

The recoil-electron tagging method can be applied also in studies of odd-mass nuclei. This would allow to observe the decays of highly excited high-spin three-quasiparticle K-isomers populating bands on low-lying single-particle states. These bands could be populated with much higher statistics than in the case of in-beam studies - in focal plane experiment it is possible to use much higher beam current. Limitation is that three-quasiparticle states lie high in excitation energy thus are produced with less probability. As a first step nuclei ^{255}Lr and ^{253}No were studied in GSI [Ant08]. Several reactions leading to odd-A nuclei in the region around Z = 100 are possible with doubly magic ^{48}Ca beam (cross-section is less than in the case of ^{254}No but still on reachable level).

The main limitation of heavy and superheavy nuclei decay studies is the beam intensity. Therefore S^3 (Super Separator Spectrometer) project has been proposed. S^3 will be a unique device designed for experiments with high intensive beams up to 1 pmA. S^3 will be set-up on a beamline of linear accelerator LINAG at GANIL. In the present time S^3 project is in the preliminary design phase. Different technical aspects of the device needs to be solved. For example the target must be able to withstand to very high power dissipation (possible are large rotating cooled targets, gas or liquid targets...). Reaction products must be separated from primary ions beam. This can be done in two steps, first separator should be a powerful beam stopper and the second one high purification spectrometer. Between these two steps the secondary target could be placed (also possible equiped with target position detectors). Very intensive beams will open possibility for detailed spectroscopical studies of nuclei with Z = 104 - 108 and for syntesis of elements above Z = 112 via cold-fusion reactions.

One of the major problems of in-beam γ-spectroscopy of heavy elements is presence of strong internal conversion especially for low-energy transitions. To overcome this problem new target position spectrometer SAGE will be constructed at JYFL. The SAGE heralds combination of JUROGAM2 array and conversion electron silicon spectrometer centered around magnetic solenoid. The JUROGAM2 array will consist of 24 Clover detectors and up to 15 Phase-I type detectors. All channels (from both germanium and silicon detectors) will be equiped with digital electronics which allows usage of higher counting rates and thus higher beam intensity that could be used for in-beam experiments. Also development of highly-efficient

γ-tracking spectrometers AGATA and GRETA will allow to reach lower production cross-sections than in present time. It is possible to expect that in couple of years the in-beam experiments on nanobarn level will be possible.

Chapter 6

Conclusion

The target position γ-array JUROGAM and the focal plane spectrometer GREAT in conjunction with the RITU gas-filled separator are in the present time active at JYFL. This setup is an unique experimental facility with large degree of versatility. This is documented by numerous performed experiments during which different physical cases were studied (experiments from rare-earths region up to transfermium nuclei).

In the present work results of two experiment are summarized. Experimental setup has been used for detailed spectroscopic studies of K-isomers in ^{254}No. Isomeric state in this nucleus was indirectly discovered by Ghiorso *et al.* [Ghi73]. They were able to give only the half-life of 280(40) ms for the isomeric state. Now, more than 30 years later we were able to study the decay of the K-isomer in more details. ^{254}No nuclei were produced via ^{208}Pb(^{48}Ca,2n)^{254}No reaction. For K-isomers studies the recoil-electron tagging method [Jon02] has been succesfully employed for the first time in super-heavy region. Two isomeric decays with the half-lives of 264.6 ms and 184.8 μs were clearly identified. While the value of 264.6 ms is in excellent agreement with that observed by *Ghiorso et al.*, the additional half-life of 184.8 μs corresponds to the decay of previously unknown isomeric state. It was found that the short-lived isomer feeds directly the long-lived one.

Obtained statistics allowed to assign two-quasiproton structure to the 264.6 ms isomeric state. It was identified as the $K^\pi = 8^-$ state and it decays via K-hindered E1 transition into rotational band based on the lower-lying non-isomeric $K^\pi = 3^+$ state. The band upon this state was observed and the g_K was extracted. This allowed unambiguos assumption of two-quasiproton configuration $1/2^-[521]_\pi 7/2^-[514]_\pi$ to the band-head. Exceptionally low excitation energy fully confirms nearly degeneration of single-proton orbitals forming the $K^\pi = 3^+$ state. Orbital $1/2^-[521]_\pi$ arises from spherical $2f_{5/2}$ which is crucial for the prediction of position of next proton magic number. This is one of the central questions of existence of shell-stabilized superheavy nuclei. The data from present work therefore provides valuable input for improving of model predictions.

The decay scheme of new short-lived isomer is more complex and only tentative conclusion based on low statistics speculations and nuclear theory could be done.

High excitation energy bespeaks on the four-quasiparticle structure. In the decay path a part of the band tentatively assigned to be based on the top of the long-lived isomer was observed. Its structure is in tentative agreement with two-quasiproton assignment to the 264.6 ms isomeric state. Improved statistics could help to find answer to several puzzles in the decay of the short-lived isomer.

Success of presented experiments has generated a whole research program now pursued by several experimental groups around the world. Obtained results were confirmed at GSI [Hes07, Sul07b] and ANL [Tan06]. In close connection to ^{254}No studies successfull γ-spectroscopical studies ^{248,250}Fm were performed at JYFL. ^{252}No has been under investigation at GSI [Sul07a] and ANL [Kho06]. Obtained results allowed to build the limited systematics of two-quasiparticle levels. Relative position of some single-particle orbitals has been fixed experimentaly and thus theoretical predictions in this region can be adjusted.

List of refereed publications

1. R.-D. Herzberg, P. T. Greenlees, P. A. Butler, G. D. Jones, M. Venhart, I. G. Darby, S. Eeckhaudt, K. Eskola, T. Grahn, C. Gray-Jones, F. P. Heßberger, P. Jones, R. Julin, S. Juutinen, S. Ketelhut, W. Korten, M. Leino, A. - P. Leppänen, S. Moon, M. Nyman, R. D. Page, J. Pakarinen, A. Pritchard, P. Rahkila, J. Sarén, C. Scholey, A. Steer, Y. Sun, Ch. Theisen and J. Uusitalo
Nuclear isomers in superheavy elements as stepping stones towards the island of stability
Nature (London) **442** (2006) 896

2. R.-D. Herzberg, P. T. Greenlees, P. A. Butler, G. D. Jones, I. G. Darby, S. Eeckhaudt, T. Grahn, C. Gray-Jones, F. P. Heßberger, P. Jones, R. Julin, S. Juutinen, S. Ketelhut, M. Leino, A.-P. Leppänen, S. Moon, M. Nyman, R. D. Page, J. Pakarinen, A. Pritchard, P. Rahkila, M. Sandzelius, J. Sarén, C. Scholey, J. Uusitalo and M. Venhart
Isomer spectroscopy in ^{254}No
Phys. Scr. **T125** (2006) 73

3. P. T. Greenlees, R.-D. Herzberg, S. Ketelhut, P. A. Butler, T. Grahn, C. Gray-Jones, G. D. Jones, P. Jones, R. Julin, S. Juutinen, T.-L. Khoo, M. Leino, S. Moon, M. Nyman, J. Pakarinen, P. Rahkila, D. Rostron, J. Sarén, C. Scholey, J. Sorri, S. Tandel, J. Uusitalo and M. Venhart
High-K structure in ^{250}Fm and the influence of the deformed shell gaps at N = 152 and Z = 100
submitted to Phys. Rev. Lett.

4. B. Sulignano, S. Heinz, F. P. Heßberger, S. Hofmann, D. Ackermann, S. Antalic, B. Kindler, I. Kojouharov, P. Kuusiniemi, B. Lommel, R. Mann, K. Nishio, A. G. Popeko, Š. Šáro, B. Streicher, M. Venhart and A. V. Yeremin
Identification of a K-isomer in ^{252}No
Eur. Phys. J. A **33** (2007) 327

5. S. Hofmann, D. Ackermann, S. Antalic, H. G. Burkhard, V. F. Comas, R. Dressler, Z. Gan, S. Heinz, J. A. Heredia, F. P. Heßberger, J. Khuyagbaatar, B. Kindler, I. Kojouharov, P. Kuusiniemi, M. Leino, B. Lommel, R. Mann, G. Münzenberg, K. Nishio, A. G. Popeko, Š. Šáro, H. J. Schött, B. Streicher, B. Sulignano, J. Uusitalo, M. Venhart and A. V. Yeremin
The reaction ^{48}Ca + ^{238}U $\rightarrow^{286}$112* studied at the GSI-SHIP
Eur. Phys. J. A **32** (2007) 251

6. F. P. Heßberger, S. Hofmann, D. Ackermann, S. Antalic, B. Kindler, I. Kojouharov, P. Kuusiniemi, M. Leino, B. Lommel, R. Mann, K. Nishio, A. G. Popeko, B. Sulignano, Š. Šáro, B. Streicher, M. Venhart and A. V. Yeremin
Alpha-gamma decay studies of ^{255}No
Eur. Phys. J. A **29** (2006) 165

7. F. P. Heßberger, S. Hofmann, D. Ackermann, S. Antalic, B. Kindler, I. Kojouharov, P. Kuusiniemi, M. Leino, B. Lommel, R. Mann, K. Nishio, A. G. Popeko, B. Sulignano, Š. Šáro, B. Streicher, M. Venhart and A. V. Yeremin
Alpha-gamma decay studies of ^{255}Rf, ^{251}No and ^{247}Fm
Eur. Phys. J. A **30** (2006) 561

8. S. Antalic, A. N. Andreyev, D. Ackermann, L. Bianco, D. Cullen, I. G. Darby, S. Franchoo, S. Heinz, F. P. Heßberger, S. Hofmann, M. Huyse, B. Kindler, I. Kojouharov, A.-P. Leppänen, S. R. Lesher, B. Lommel, R. Mann, G. Münzenberg, K. Nishio, R. D. Page, J. Pakarinen, J. J. Ressler, Š. Šáro, B. Streicher, B. Sulignano, J. Thomson, P. van Duppen, M. Venhart, D. Wiseman and R. Wyss
The isotopes in Po-Rn region
Acta Phys. Pol. **38** (2007) 1557

9. B. Streicher, F. P. Heßberger, D. Ackermann, S. Antalic, B. Kindler, I. Kojouharov, P. Kuusiniemi, B. Lommel, R. Mann, B. Sulignano, Š. Šáro and M. Venhart
Alpha-gamma decay studies of ^{261}Sg
Acta Phys. Pol. **38** (2007) 1561

10. D. T. Joss, I. G. Darby, R. D. Page, J. Uusitalo, S. Eeckhaudt, T. Grahn, P. T. Greenlees, P. M. Jones, R. Julin, S. Juutinen, S. Kettelhut, M. Leino, A. - P. Leppänen, M. Nyman, J. Pakarinen, P. Rahkila, J. Sarén, C. Scholey, A. Steer, A. J. Cannon, P. D. Stevenson, J. S. Al-Khalili, S. Ertürk, M. Venhart, B. Gall, B. Hadinia and J. Simpson
Probing the limit of nuclear existence: Proton emission from ^{159}Re
Phys. Lett. B **641** (2006) 34

11. R. D. Page, L. Bianco, I. G. Darby, J. Uusitalo, D. T. Joss, T. Grahn, R.-D. Herzberg, J. Pakarinen, J. Thomson, S. Eeckhaudt, P. T. Greenlees, P. M. Jones, R. Julin, S. Juutinen, S. Ketelhut, M. Leino, A.-P. Leppänen, M. Nyman, P. Rahkila, J. Sarén, C. Scholey, A. Steer, M. B. Gómez Hornillos, J. S. Al-Khalili, A. J. Cannon, P. D. Stevenson, S. Ertürk, B. Gall, B. Hadinia, M. Venhart, and J. Simpson
α decay of ^{159}Re and proton emission from ^{155}Ta
Phys. Rev. C **75** (2007) 061302

List of other publications

1. B. Sulignano, F. P. Heßberger, S. Hofmann, D. Ackermann, S. Antalic, I. Kojouharov, P. Kuusiniemi, R. Mann, K. Nishio, Š. Šáro, B. Štreicher and M. Venhart
   Evidence for an isomeric state in ^{251}No
   GSI Scientific Report, Vol. 2005-1 (2005) 75

2. F. P. Heßberger, S. Hofmann, D. Ackermann, S. Antalic, I. Kojouharov, P. Kuusiniemi, R. Mann, K. Nishio, Š. Šáro, B. Štreicher, B. Sulignano and M. Venhart
   Decay spectroscopy of ^{255}No
   GSI Scientific Report, Vol. 2005-1 (2005) 73

3. F. P. Heßberger, S. Hofmann, D. Ackermann, S. Antalic, I. Kojouharov, P. Kuusiniemi, R. Mann, K. Nishio, Š. Šáro, B. Štreicher, B. Sulignano and M. Venhart
   Nillson levels in odd-mass odd-Z nuclei in the region Z=(99-105)
   GSI Scientific Report, Vol. 2005-1 (2005) 74

4. D. T. Joss, I. G. Darby, R. D. Page, J. Uusitalo, S. Eeckhaudt, T. Grahn, P. T. Greenlees, P. M. Jones, R. Julin, S. Juutinen, S. Ketelhut, M. Leino, A.-P. Leppänen, M. Nyman, J. Pakarinen, P. Rahkila, J. Sarén, C. Scholey, A. N. Steer, J. S. Al-Khalili, A. J. Cannon, P. D. Stevenson, S. Ertürk, B. Gall, B. Hadinia, M. Venhart, and J. Simpson
   Discovery of the proton emitting nucleus ^{159}Re
   AIP Conf. Proc. **961** (2007) 28

5. C. Dossat, Ch. Theisen, A. Bürger, E. Clément, A. Görgen, W. Korten, S. Eeckhaudt, P. Jones, T. Grahn, P. T. Greenlees, R. Julin, S. Juutinen, M. Leino, A.-P. Leppänen, M. Nyman, J. Pakarinen, P. Rahkila, J. Sarén, C. Scholey, J. Sorri, J. Uusitalo, and M. Venhart
   Spectroscopy of the very-neutron deficient ^{189}Bi
   AIP Conf. Proc. **961** (2007) 196

6. R. D. Page, L. Bianco, I. G. Darby, D. T. Joss, T. Grahn, R.-D. Herzberg, J. Pakarinen, J. Thomson, J. Uusitalo, S. Eeckhaudt, P. T. Greenlees, P. M. Jones, R. Julin, S. Juutinen, S. Ketelhut, M. Leino, A.-P. Leppänen,

M. Nyman, P. Rahkila, J. Sarén, C. Scholey, A. N. Steer, M. Venhart, J. Simpson, J. S. Al-Khalili, A. J. Cannon, P. D. Stevenson, S. Ertürk, B. Gall, and B. Hadinia
Probing single-particle structures beyond the proton drip line
AIP Conf. Proc. **961** (2007) 137

7. A. V. Yeremin, A. V. Belozerov, M. L. Chelnokov, V. I. Chepigin, V. A. Gorshkov, A. P. Kabachenko, O. N. Malyshev, Yu. Ts. Oganessian, A. G. Popeko, A. V. Shutov, A. I. Svirikhin, A. Lopez-Martens, K. Hauschild, Ch. Briancon, A. Korichi, D. Curien, O. Dorvaux, B. Gall, F. Khalfallah, M. Rousseau, N. Rowley, M. Guttormsen, S. Siem, A.-C. Sunde, N. Syed, F. Hanappe, A. Minkova, Š. Šáro, M. Venhart, and Ch. Theisen
Gamma and electron spectroscopy of heavy nuclei at FLNR JINR
AIP Conf. Proc. **912** (2007) 119

Zhrnutie

Vlastnosti a štruktúra ťažkých (Z > 100) atómových jadier je pomerne málo prebádaná a nedostatočne pochopená. Je to tak v dôsledku viacerých faktorov a tými sú: komplexnosť problematiky, vysoká náročnosť experimentálneho štúdia vlastností týchto jadier, najmä veľmi nízky účinný prierez reakcií úplnej syntézy. Fyzika ťažkých jadier potrebuje pre svoje zdokonalenie ďalšie systematické experimentálne skúmanie vlastností týchto jadier. Najefektívnejším spôsobom sa javí pokračovanie vštúdiu rôznych typov jadrových reakcií úplnej syntézy pri vytvorení podmienok pre experimentálnu prácu s vyššou štatistikou nameraných údajov. Medzi najväčšie svetové centrá spektroskopického výskumu ťažkých jadier patria Univerzita v Jyväskylä - JYFL (Fínsko), GSI Darmstadt (Nemecko), Argonne National Laboratory (USA) a GANIL (Francúzsko).

Významným nástrojom na štúdium štruktúry atómových jadier je jadrová spektroskopia. Jadrá sú produkované v reakciách úplnej syntézy, produkty reakcií separované pomocou rýchlostných alebo hmotnostných separátorov a následne analyzované poliami detektorov rôzneho typu. Na spektroskopiu promptných prechodov, prebiehajúcich bezprostredne po reakcii sa využívajú spektrometre gama žiarenia alebo konverzných elektrónov vokolí terčovej komory (in-beam).

V súčasnosti spektroskopický výskum ťažkých jadier sleduje viaceré smery:

- In-beam spektroskopia rotačných stavov v párno-párnych jadrách poskytuje informáciu o parametroch ako sú momenty hybnosti jadra, stabilita voči štiepeniu adeformácia. V uplných rokoch prebehlo v JYFL viacero experimentov tohto druhu na za použitia spektrometrov ako napríklad SACRED alebo JUROGAM. Boli získané dáta o jadrách ^{250}Fm [Gre07] a ^{252,254}No [Lep06, Her06a]. V budúcnosti je planované štúdium ^{256}Rf.

- In-beam spektroskopia nepárnych jadier umožňuje stanovenie kvázičasticovej štruktúry základného a izomérických stavov. Toto je veľmi dôležité z hľadiska overenia a spresnenia existujúcich teoretických modelov jednočasticových orbitálov v ťažkých jadrách.V JYFL boli experimentálne študované izotopy ^{251}Md [Cha07], ^{253}No [Eec06] a ^{255}Lr [Gre05].

- Rozpadová koincidenčná alfa-gama spektroskopia študuje rozloženie nízkoležiacich orbitálov v nepárnych jadrách. Najvýznamnejším svetovým centrom tohto typu výskumu je GSI Darmstadt, kde boli v minulých rokoch študované viaceré jadrá. Z najvýznamnejších výsledkov možno spomenúť

systematiku Nillsonovych hladín v nepárnych izotopoch einsteinia [Hes05], štúdium ^{251,253,255}No (viď napr. [Hes06] a referencie tam uvedené) a iné.

- Spektroskopia K-izomérov v párno-párnych jadrách v súčasnosti prekonáva výrazný boom. Dôkazom toho sú úspešné experimenty vJYFL (experimenty prezentované v tejto práci), GSI a Argonne. K-izoméria je spojená s fenoménom K-zakázaných prechodov, t. j. elektromagnetických prechodov jednoznačne narušujúcich výberové pravidlo, podľa ktorého zmena projekcie spinu na os jadra (kvantové číslo K) nesmie byť väčšia než je rád multipólu. Vďaka prímesiam vlnových funkcií s vyšším K, tieto prechody nie sú úplne zakázané, ale výrazne potlačené. K-zakázané prechody sú pozorované pri rozpade vysokospinových stavov na vyššie členy rotačných pásov. Preto nutnou podmienkou formovania K-izoméru je deformácia jadra (je podmienkou generovania rotačných stavov) a existencia vysokospinových orbitálov v blízkosti Fermiho energie. V prípade párno-párnych jadier sú potom izomérické hladiny tvorené narušením valenčného páru nukleónov (narušených párov môže byť aj viac). Obe podmienky sú splnené v oblasti jadier so Z = 100 a N = 152.

Predkladaná práca je postavená na analýze dvoch experimentov zameraných na štúdium K-izomérov v jadre ^{254}No. Experimenty prebehli v rámci dlhodobého programu výskumu K-izomérov v JYFL. Využitý bol plynom plnený separátor RITU a spektrometre JUROGAM a GREAT. Jadrá ^{254}No boli produkované v reakcií ^{208}Pb(^{48}Ca,2n)^{254}No . Detaily oboch experimentov sú zhrnuté v tabuľke 6.1.

Table 6.1: Zhrutie analyzovaných experimentov.

	R35	**JR48**
Dátum	2. 5. - 8. 5. 2005	3. 4. - 10. 4. 2006
Použité spektrometre	GREAT	JUROGAM GREAT 2 VEGA detektory
Doba ožarovania	148 hod.	110 hod.
Celková dávka	2.0×10^{17} část.	4.6×10^{16} část.
Projektil	$^{48}Ca^{10+}$	$^{48}Ca^{10+}$
Energia zväzku	219 MeV	219 MeV
Priemerná intenzita zväzku	61 pnA	19 pnA
Terč	^{208}PbS	^{208}Pb (metallic)
Hrúbka terča	416 μg/cm^2	446 μg/cm^2

K-izoméry sa rozpadajú kaskádou rýchlych gama prechodov. Tieto podliehajú v zvýšenej miere vnútornej konverzii. Emisia elektrónov vytvára sumačný signál, ktorý môže byť pozične a časovo korelovaný s implantáciou evaporačného rezídua. To umožňuje presné meranie doby polpremeny študovaných izomérov a zároveň

získanie čistých gama spektier zodpovedajúcich rozpadu ich rozpadu (len gama kvantá v koincidencii s korelovanými elektrónami sú zaznamenané čo vedie k výraznej redukcii pozadia).

K-izomér v ^{254}No bol po prvý krát pozorovaný Ghiorsom a kol. [Ghi73] v nepriamej identifikácii. Cieľom prezentovaných experimentov bolo stanoviť rozpadovú schému a spektroskopické vlastnosti. Boli pozorované rozpady dvoch izomérických stavov s dobami polpremeny 264.6 ms a 184.8 μs. Dlhožijúci izomér zodpovedá tomu, ktorý bol pred rokmi pozorovaný Ghiorsom. Krátkožijúci izomér bol doteraz neznámy. Detailnou analýzou bolo zistené, že izomér s dobou polpremeny 184.8 μs sa rozpadá na dlhožijúci izomér. Zo získanej štatistiky bola zostavená rozpadová schéma dlhožijúceho izoméru. Tento bol jednoznačne identifikovaný ako stav $K^\pi = 8^-$ s excitačnou energiou 1293.0 keV. Ten sa rozpadá silným K-zakázaným E1 prechodom do rotačného pásu nad dvojkvázičasticovým stavom $K^\pi = 3^+$. Existencia tohoto stavu bola týmto experimentom definitívne potvrdená, navyše mu bolo možné na základe štruktúry pásu jednoznačne priradiť štruktúru $1/2^-[521]_\pi 7/2^-[514]_\pi$. Extrémne nízka excitačná energia (987.5 keV) svedčí o takmer degenerácii jednočasticových orbitálov. Veľmi dôležitá je prítomnosť orbitálu $1/2^-[521]$. Ten pochádza zo sférického protónového orbitálu $2f_{5/2}$ ktorý je veľmi dôležitý z hľadiska predpovede lokalizácie alšieho protónového magického čísla pre ktorý teória zatiaľ stále nemá konsenzus. túdium orbitálu $1/2^-[521]$ je možné v jadrách nobelia z dôvodu ich veľkej kvadrupólovej deformácie.

Z rozpadových vlastností nie je možné jednoznačne určiť nukleónovú štruktúru izomérického stavu $K^\pi = 8^-$. Preto bolo realizované meranie rotačného pásu nad izomérickou hladinou. Bohužiaľ získaná štatistika neumožnila jednoznačnú identifikáciu gama čiar (v spektre je pozorované veľmi silné charakteristické röntgenovské žiarenie svedčiace o prítomnosti silne konvertovaných prechodov) a teda prisúdená štruktúra $7/2^-[514]_\pi \otimes 9/2^+[624]_\pi$ je len predbežná a čaká na definitívne potvrdenie.

Krátkožijúci izomér je populovaný výrazne slabšie než izomér $K^\pi = 8^-$. Získaná štatistika umožnila len špekulácie o jeho spine a parite. Na základe pozorovaných prechodov bola uvažovaná štvorkvázičasticová štruktúra s $K^\pi = 16^+$. Získanie výraznejšej štatistiky by mohlo napomôcť k vyriešeniu uvedených problémov.

Okrem už spomenutých výsledkov bola pozorovaná indikácia existencie tretieho izomérického stavu. Bohužiaľ nie je možné zatiaľ jeho existenciu jednoznačne potvrdiť, nakoľko je (pokiaľ existuje) populovaný veľmi slabo.

Na spomínané experimenty nadviazali úspešné štúdie K-izomérov v susedných párno-párnych jadrách ako ^{248,250}Fm (JYFL) a ^{252}No (GSI). Systematický výskum bude pokračovať aj v budúcnosti v súvislosti s vývojom nových experimentálnych zariadení.

Výsledky boli porovnané s teoretickými modelmi založenými na WS potenciáli.

Bibliography

[Afa03] A. V. Afanasjev, T. L. Khoo, S. Frauendorf, G. A. Lalazissis and I. Ahmad, Phys. Rev. C **67** (2003) 024309

[Ahm77] I. Ahmad, A. M. Friedman, R. R. Chasman and S. W. Yates, Phys. Rev. Lett. **39** (1977) 12

[Ahm78] I. Ahmad, R. K. Sjoblom, A. M. Friedman and S. W. Yates, Phys. Rev. C **17** (1978) 2163

[And00] A. N. Andreyev, M. Huyse, P. van Duppen, L. Weissman, D. Ackermann, J. Gerl, F. P. Heßberger, S. Hofmann, A. Kleinböhl, G. Münzenberg, S. Reshitko, C. Schlegel, H. Schaffner, P. Cagarda, M. Matos, Š. Šáro, A. Keenan, C. Moore, C. D. O'Leary, R. D. Page, M. Taylor, H. Kettunen, M. Leino, A. Lavrentiev, R. Wyss, K. Heyde, Nature (London) **405** (2000) 430

[And04] A. N. Andreyev, P. A. Butler, R. D. Page, D. E. Appelbe, G. D. Jones, D. T. Joss, R.-D. Herzberg, P. H. Regan, J. Simpson and R. Wadsworh, Nucl. Instr. and Meth. in Phys. Res. A **533** (2004) 422

[Ant08] S. Antalic *et al.*, draft is ready (2008)

[Arc98] D. E. Archer, M. A. Riley, T. B. Brown, D. J. Hartley, J. Döring, G. D. Johns, J. Pfohl, S. L. Tabor, J. Simpson, Y. Sun and J. L. Egido, Phys. Rev. C **57** (1998) 2924

[Bas74] R. Bass, Nucl. Phys. A **231** (1974) 45

[Bas06] J. E. Bastin, R.-D. Herzberg, P. A. Butler, G. D. Jones, R. D. Page, D. G. Jenkins, N. Amzal, P. M. T. Brew, N. J. Hammond, R. D. Humphreys, P. J. C. Ikin, T. Page, P. T. Greenlees, P .M. Jones, R. Julin, S. Juutinen, H. Kankaanpää, A. Keenan, H. Kettunen, P. Kuusiniemi, M. Leino, A. P. Leppänen, M. Muikku, P. Nieminen, P. Rahkila, C. Scholey, J. Uusitalo, E. Bouchez, A. Chatillon, A. Hürstel, W. Korten, Y. Le Coz, Ch. Theisen, D. Ackermann, J. Gerl, K. Helariutta, F. P. Heßberger, Ch. Schlegel, H. J. Wollersheim, M. Lach, A. Maj, W. Meczynski, J. Styczen, T. L. Khoo, C. J. Lister, A. V. Afanasjev, H. J. Maier, P. Reiter, P. Bednarczyk, K. Eskola and K. Hauschild, Phys. Rev. C **73** 024308 (2006)

[Bel59] S. T. Belyaev, Mat. Fys. Medd. Dan. Vid. Selsk.**31** (1959) 1

[Ben79] R. Bengtsson and S. Frauendorf, Nucl. Phys. **A314** (1979) 27

[Ben89] T. Bengtsson, R. A. Broglia, E. Vigezzi, F. Barranco, F. Dönau and J. Zhang, Phys. Rev. Lett. **62** (1989) 2448

[Ben00] M. Bender, K. Rutz, P.-G. Reinhard and J. A. Maruhn, Eur. Phys. J. A **8** (2000) 59

[Ben03] M. Bender, P. Bonche, T. Duguet and P.-H. Heenen, Nucl. Phys. A **723** (2003) 354

[Boh55] A. Bohr, P. O. Fröman and B. Mottelson, Dan. Mat. Fys. Medd. 29, No. 10 (1955)

[Boh75] A. Bohr and B. R. Mottelson, *Nuclear Structure Volume II: Nuclear Deformations*, W. A. Benjamin Inc., New York (1975)

[Boh58] A. Bohr, B. R. Mottelson and D. Pines, Phys. Rev. **110** (1958) 936

[Boh41] N. Bohr, Phys. Rev. **59** (1941) 270

[But02] P. A. Butler, R. D. Humphreys, P. T. Greenlees, R.-D. Herzberg, D. G. Jenkins, G. D. Jones, H. Kankaanpää, H. Kettunen, P. Rahkila, C. Scholey, J. Uusitalo, N. Amzal, J. E. Bastin, P. M. T. Brew, K. Eskola, J. Gerl, N. J. Hammond, K. Hauschild, K. Helariutta, F.-P. Heßberger, A. Hürstel, P. M. Jones, R. Julin, S. Juutinen, A. Keenan, T.-L. Khoo, W. Korten, P. Kuusiniemi, Y. Le Coz, M. Leino, A.-P. Leppänen, M. Muikku, P. Nieminen, S. W. Ødegård, T. Page, J. Pakarinen, P. Reiter, G. Sletten, Ch. Theisen and H.-J. Wollersheim, Phys. Rev. Lett. **89** (2002) 202501

[But03] P. A. Butler, R. D. Humphreys, P. T. Greenlees, R.-D. Herzberg, D. G. Jenkins, G. D. Jones, H. Kankaanpää, H. Kettunen, P. Rahkila, C. Scholey, J. Uusitalo, M. Amzal, C. Andreoiu, A. N. Andreyev, D. Appelbe, J. E. Bastin, P. M. T. Brew, K. Eskola, S. J. Freeman, J. Gerl, N. J. Hammond, K. Hauschild, K. Helariutta, F. P. Heßberger, A. Hürstel, P. J. C. Ikin, P. M. Jones, D. T. Joss, R. Julin, S. Juutinen, A. Keeman, T. L. Khoo, W. Korten, P. Kuusiniemi, Y. Le Coz, M. Leino, A.-P. Leppänen, M. Muikku, P. Nieminen, S. W. Ødegård, R. D. Page, T. Page, J. Pakarinen, P. Reiter, J. Simpson, G. Sletten, Ch. Theisen, B. J. Varley and H.-J. Wollersheim, Acta Phys. Pol. **34** (2003) 2107

[Con28] E. U. Condon and R. W. Gurney, Nature **122** (1928) 438

[Cro96] B. Crowell, P. Chowdhury, D. J. Blumenthal, S. J. Freeman, C. J. Lister, M. P. Carpenter, R. G. Henry, R. V. F. Janssens, T. L. Khoo, T. Lauritsen, Y. Liang, F. Soramel and I. G. Bearden, Phys. Rev. C **53** (1996) 1173

[Cwi87] S. Ćwiok, J. Dudek, W. Nazarewicz, J. Skalski and T. Werner, Comp. Phys. Comm. **46** (1987) 379

[Cwi94] S. Ć wiok, S. Hofmann and W. Nazarewicz, Nucl. Phys. A **573** (1994) 356

[Cwi96] S. Ćwiok, J. Dobaczewski, P.-H. Heenen, P. Magierski, W. Nazarewicz, Nucl. Phys. A **611** (1996) 211

[Dug01] T. Duguet, P. Bonche, P.-H. Heenen and J. Meyer, Phys. Rev. C **65** (2001) 014311

[Eec05a] S. Eeckhaudt, N. Amzal, J. E. Bastin, E. Bouchez, P. A. Butler, A. Chatillon, K. Eskola, J. Gerl, T. Grahn, A. Görgen, P. T. Greenlees, R.-D. Herzberg, F. P. Heßberger, A. Hürstel, P. J. C. Ikin, G. D. Jones, P. Jones, R. Julin, S. Juutinen, H. Kettunen, T. L. Khoo, W. Korten, P. Kuusiniemi, Y. Le Coz, M. Leino, A. -P. Leppänen, P. Nieminen, J. Pakarinen, J. Perkowski, A. Pritchard, P. Reiter, P. Rahkila, C. Scholey, Ch. Theisen, J. Uusitalo, K. Van de Vel, J. Wilson and H. J. Wollersheim, Eur. Phys. J. A **25** (2005) 605

[Eec05b] S. Eeckhaudt, P. T. Greenlees, N. Amzal, J. E. Bastin, E. Bouchez, P. A. Butler, A. Chatillon, K. Eskola, J. Gerl, T. Grahn, A. Görgen, R.-D. Herzberg, F. P. Heßberger, A. Hürstel, P. J. C. Ikin, G. D. Jones, P. Jones, R. Julin, S. Juutinen, H. Kettunen, T. L. Khoo, W. Korten, P. Kuusiniemi, Y. Le Coz, M. Leino, A.-P. Leppänen, P. Nieminen, J. Pakarinen, J. Perkowski, A. Pritchard, P. Reiter, P. Rahkila, C. Scholey, Ch. Theisen, J. Uusitalo, K. Van de Vel and J. Wilson, Eur. Phys. J. **26** (2005) 227

[Eec06] S. Eeckhaudt, Ph.D. Thesis, University of Jyväskylä (2006)

[Fir96] R. B. Firestone, V. S. Shirley, C. M. Baglin, S. Y. F. Chu and J. Zipkin, *Table of Isotopes* 8^{th} ed. Vol. II, John Wiley and Sons, Inc., New York (1996)

[Fle67] G. N. Flerov, A. A. Pleve, S. M. Polikanov, S. P. Tretyakova, I. Boca, M. Sezon, I. Vilcov and N. Vilcov, Nucl. Phys. A **102** (1967) 443

[Fre77] M. S. Freedman, I. Ahmad, F. T. Porter, R. K. Sjoblom, R. F. Barnes, J. Lerner, and P. R. Fields, Phys. Rev. C **15** (1977) 760

[Fro57] P. O. Fröman, Mat. Fys. Skr. Dan. Vid. Selsk. 1, No. 3 (1957)

[Gal62] C. J. Gallagher, Phys. Rev. 126 (1962) 1525

[Gam28] G. Gamow, Z. Phys. **51** (1928) 204

[Gag89] H. W. Gäggeler, D. T. Jost, A. Türler, P. Armbruster, W. Brüchle, H. Folger, F. P. Heßberger, S. Hofmann, G. Münzenberg, V. Ninov, W. Reisdorf, M. Schädel, K. Sümmerer, J. V. Kratz, U. Scherer and M. Leino, Nucl. Phys. A **502** (1989) 561

[Gei11] H. Geiger and J. M. Nuttall, Phil. Mag. **22** (1911) 613

[Ghi58] A. Ghiorso, T. Sikkeland and J. R. Walton, Phys. Rev. Lett. **1** (1958) 18

[Ghi73] A. Ghiorso, K. Eskola, P. Eskola, M. Nurmia, Phys. Rev. C **7** (1973) 2032

[Ghi88] A. Ghiorso, S. Yashita, M. Leino, L. Frank, J. Kalnins, P. Armbruster, J.-P. Dufour and P. K. Lemmertz, Nucl. Instr. and Meth. A **269** (1988) 192

[Gjo95] N. L. Gjørup, P. M. Walker, G. Sletten, M. A. Bentley, B. Fabricius and J. F. Sharpey-Schafer, Nucl. Phys. A **582** (1995) 369

[Gre05] P. T. Greenlees, private communication (2005)

[Gre07] P. T. Greenlees, R.-D. Herzberg, S. Ketelhut, P. A. Butler, P. Chowdhury, T. Grahn, C. Gray-Jones, G. D. Jones, P. Jones, R. Julin, S. Juutinen, T.-L. Khoo, M. Leino, S. Moon, M. Nyman, J. Pakarinen, P. Rahkila, D. Rostron, J. Sarén, C. Scholey, J. Sorri, S. K. Tandel, J. Uusitalo and M. Venhart, submitted to PRL (2007)

[Hal89] H. L. Hall, K. E. Gregorich, R. A. Henderson, D. M. Lee, D. C. Hoffman, M. E. Bunker, M. M. Fowler, P. Lysaght, J. W. Starner and J. B. Wilhelmy, Phys. Rev. C **39** (1989) 1866

[Hax49] O. Haxel, J. H. D. Jensen and H. E. Suess, Phys. Rev. **75** (1949) 1766

[Hei95] P. Heikkinen and E. Liukkonen, 14^{th} International Conference on Cyclotrons and Their Applications, Cape Town (1995)

[Her02] R.-D. Herzberg, N. Amzal, J. E. Bastin, F. Becker, P. M. T. Brew, P. A. Butler, A. J. C. Chewter, J. F. C. Cocks, O. Dorvaux, K. Eskola, J. Gerl, P. T. Greenlees, N. J. Hammond, K. Hauschild, K. Helariutta, F. Heßberger, M. Houry, A. Hürstel, R. D. Humphreys, G. D. Jones, P. M. Jones, R. Julin, S. Juutinen, H. Kankaanpää, H. Kettunen, T. L. Khoo, W. Korten, P. Kuusiniemi, Y. Le Coz, M. Leino, A.-P. Leppänen, C. J. Lister, R. Lucas, M. Muikku, P. Nieminen, R. D. Page, T. Page, P. Rahkila, P. Reiter, Ch. Schlegel, C. Scholey, G. Sletten, O. Stezowski, Ch. Theisen, W. H. Trzaska, J. Uusitalo and H. J. Wollersheim, Eur. Phys. J. A **15** (2002) 205

[Her04] R.-D. Herzberg, J. Phys. G **30** (2004) R123

[Her06a] R.-D. Herzberg, P. T. Greenlees, P. A. Butler, G. D. Jones, M. Venhart, I. G. Darby, S. Eeckhaudt, K. Eskola, T. Grahn, C. Gray-Jones, F. P. Heßberger, P. Jones, R. Julin, S. Juutinen , S. Kettelhut, W. Korten, M. Leino, A. - P. Leppänen, S. Moon, M. Nyman, R. D. Page, J. Pakarinen, A. Pritchard, P. Rahkila, J. Sarén, C. Scholey, A. Steer, Y. Sun, Ch. Theisen and J. Uusitalo, Nature (London) **442** (2006) 896

[Her06b] R.-D. Herzberg, P. T. Greenlees, P. A. Butler, G. D. Jones, I. G. Darby, S. Eeckhaudt, T. Grahn, C. Gray-Jones, F. P. Heßberger, P. Jones, R. Julin, S. Juutinen, S. Ketelhut, M. Leino, A.-P. Leppänen, S. Moon, M. Nyman, R. D. Page, J. Pakarinen, A. Pritchard, P. Rahkila, M. Sandzelius, J. Sarén, C. Scholey, J. Uusitalo and M. Venhart, Phys. Scr. **T125** (2006) 73

[Her07] R.-D. Herzberg, private communication (2007)

[Her08] R.-D. Herzberg, F. P. Heßberger *et al.*, to be published (2008)

[Hes97] F. P. Heßberger, S. Hofmann, V. Ninov, P. Armbuster, H. Folgen, G. Münzenberg, H. J. Schött, A. G. Popeko, A. V. Yeremin, A. N. Andreyev and Š. Šáro, Z. Phys. A **359** (1997) 415

[Hes05] F. P. Heßberger, S. Antalic, B. Štreicher, S. Hofmann, D. Ackermann, B. Kindler, I. Kojouharov, P. Kuusiniemi, M. Leino, B. Lommel, R. Mann, K.Nishio, Š. Šáro and B.Sulignano, Eur.Phys.J. A **26** (2005) 233

[Hes06] F. P. Heßberger, S. Hofmann, D. Ackermann, S. Antalic, B. Kindler, I. Kojouharov, P. Kuusiniemi, M. Leino, B. Lommel, R. Mann, K. Nishio, A. G. Popeko, B. Sulignano, Š. Šáro, B. Štreicher, M. Venhart and A. V. Yeremin, Eur. Phys. J. A **29** (2006) 165

[Hes07] F. P. Heßberger, private communication (2007)

[Hey04] K. Heyde, *Basic Ideas and Concepts in Nuclear Physics, 3rd Edition*, The Institute of Physics, London (2004)

[Hod97] P. E. Hodgson, E. Gadioli and E. Gadioli Erba, *Introductory Nuclear Physics*, Oxford University Press Inc., New York (1997)

[Hof84] R. W. Hoff, T. von Egidy, R. W. Lougheed, D. H. White, H. G. Börner, K. Schreckenbach, and G. Barreau and D. D. Warner, Phys. Rev. C **29** (1984) 618

[Hof01] S. Hofmann, F.P. Heßberger, D. Ackermann, S. Antalic, P. Cagarda, S. Ćwiok, B. Kindler, J. Kojouharova, B. Lommel, R. Mann, G. Münzenberg, A. G. Popeko, Š. Šáro, H. J. Schött and A. V. Yeremin, Eur. Phys. J. A **10** (2001) 5

[Hof07] S. Hofmann, D. Ackermann, S. Antalic, H. G. Burkhard, V. F. Comas, R. Dressler, Z. Gan, S. Heinz, J. A. Heredia, F. P. Heßberger, J. Khuyagbaatar, B. Kindler, I. Kojouharov, P. Kuusiniemi, M. Leino, B. Lommel, R. Mann, G. Münzenberg, K. Nishio, A. G. Popeko, Š. Šáro, H. J. Schött, B. Streicher, B. Sulignano, J. Uusitalo, M. Venhart and A. V. Yeremin, Eur. Phys. J. A **32** (2007) 251

[Hum04] R. D. Humphreys, P. A. Butler, J. E. Bastin, P. T. Greenlees, N. J. Hammond, R.-D. Herzberg, D. G. Jenkins, G. D. Jones, H. Kankaanpää, A. Keenan, H. Kettunen, T. Page, P. Rahkila, C. Scholey, J. Uusitalo, N. Amzal, P. M. T. Brew, K. Eskola, J. Gerl, K. Hauschild, K. Helariutta, F.-P. Heßberger, A. Hürstel, P. M. Jones, R. Julin, S. Juutinen, T.-L. Khoo, W. Korten, P. Kuusiniemi, Y. Le Coz, M. Leino, A.-P. Leppänen, M. Muikku, P. Nieminen, S. W. Ødegård, J. Pakarinen, P. Reiter, G. Sletten, Ch. Theisen and H.-J. Wollersheim, Phys. Rev. C **69** (2004) 064324

[Cha06] A. Chatillon, Ch. Theisen, P. T. Greenlees, G. Auger, J. E. Bastin, E. Bouchez, B. Bouriquet, J. M. Casandjian, R. Cee, E. Clement, R. Dayras, G. de France, R. de Tourreil, S. Eeckhaudt, A. Görgen, T. Grahn, S. Grevy, K.Hauschild, R.-D. Herzberg, P. J. C. Ikin, G. D. Jones, P. Jones, R. Julin, S. Juutinen, H. Kettunen, A. Korichi, W. Korten, Y. Le Coz, M. Leino, A. Lopez-Martens, S. M. Lukyanov, Yu. E. Penionzhkevich, J. Perkowski, A. Pritchard, P. Rahkila, M. Rejmund, J. Sáren, C. Scholey, S. Siem, M. G. Saint-Laurent, C. Simenel, Yu. G. Sobolev, Ch. Stodel, J. Uusitalo, A. Villari, M. Bender, P. Bonche, P.-H. Heenen, Eur. Phys. J. A **30** (2006) 397

[Cha07] A. Chatillon, C. Theisen, E. Bouchez, P. A. Butler, E. Clement, O. Dorvaux, S. Eeckhaudt, B. J. P. Gall, A. Görgen, T. Grahn, P. T. Greenlees, R.-D. Herzberg, F. P. Heßberger, A. Hürstel, G. D. Jones, P. Jones, R. Julin, S. Juutinen, H. Kettunen, F. Khalfallah, W. Korten, Y. Le Coz, M. Leino, A.-P. Leppänen, P. Nieminen, J. Pakarinen, J. Perkowski, P. Rahkila, M. Rousseau, C. Scholey, J. Uusitalo, J. N. Wilson, P. Bonche and P.-H. Heenen, Phys. Rev. Lett. **98** (2007) 132503

[Cho88] P. Chowdhury, B. Fabricius, C. Christensen, F. Azgui, S. Bjørnholm, J. Borggreen, A. Holm, J. Pedersen, G. Sletten, M. A. Bentley, D. Howe, A. R. Mokhtar, J. D. Morrison, J. F. Sharpey-Schafer, P. M. Walker and R. M. Lieder, Nucl. Phys. A **485** (1988) 136

[Igo58] G. Igo, Phys. Rev. Lett. **1** (1958) 72

[Ing54] D. R. Inglis, Phys. Rev. **96** (1954) 1059

[Jen84] A. S. Jensen, P. G. Hansen and B. Jonson, Nucl. Phys. A **431** (1984) 393

[Jon02] G. D. Jones, Nucl. Instr. and Meth. A **488** (2002) 471

[Kat73] K. Katori , A. M. Friedman and J. R. Erskine, Phys. Rev. C **8** (1973) 2336

[Kay67] G. Kaye, Nucl. Phys. A **108** (1967) 625

[Kib05] T. Kibédi, T. W. Burrows, M. B. Trzhaskovskaya and C. W. Nestor, Jr., AIP Conf. Proc. **769** (2005) 268
URL: http://wwwrsphysse.anu.edu.au/ txk103/bricc/

[Kho75] T. L. Khoo, F. M. Bernthal, R. A. Warner, G. F. Bertsch and G. Hamilton, Phys. Rev. Lett. **35** (1975) 1256

[Kho06] T. L. Khoo, private communication via P. T. Greenlees (2006)

[Kho07] T. L. Khoo, private communication (2007)

[Koi01] H. Koivisto, P. Heikkinen, V. Hänninen, A. Lassila, H. Leinonen, V. Nieminen, J. Pakarinen, K. Ranttila, J. Ärje and E. Liukkonen, Nucl. Instr. and Meth. B **174** (2001) 379

[Kra88] K. S. Krane, *Introductory Nuclear Physics*, John Wiley and Sons, Inc., New York (1988)

[Laz89] Yu. A. Lazarev, Yu. A. Lobanov, R. N. Sagaidak, V. K. Utyonkov, M. Hussonnois, Yu. P. Kharitonov, I. V. Shirokovsky, S. P. Tretyakova and Yu. Ts. Oganessian, Phys. Scr. **39** (1989) 422

[Laz01] I. H. Lazarus, D. E. Appelbe, P. A. Butler, P. J. Coleman-Smith, J. R. Cresswell, S. J. Freeman, R.-D. Herzberg, I. Hibbert, D. T. Joss, S. C. Letts, R. D. Page, V. F. E. Pucknell, P. H. Regan, J. Sampson, J. Simpson, J. Thornhill and R. Wadsworth, IEEE Trans. on Nucl. Sci. **48** (2001) 567

[Lei86] M. Leino, S. Yashita and A. Ghiorso, Phys. Rev. C **24** (1986) 2370

[Lei95] M. Leino, J. Äystö, T. Enquist, P. Heikkinen, A. Jokinen, M. Nurmia, A. Ostrowski, W. H. Trzaska, J. Uusitalo, K. Eskola, P. Armbruster, V. Ninov, Nucl. Instr. and Meth. B **99** (1995) 653

[Lei99] M. Leino, H. Kankaanpää, R.-D. Herzberg, A. J. Chewter, F. P. Heßberger, Y. Le Coz, F. Becker, P. A. Butler, J. F. C. Cocks, O. Dorvaux, K. Eskola, J. Gerl, P. T. Greenlees, K. Helariutta, M. Houry, G. D. Jones, P. Jones, R. Julin, S. Juutinen, H. Kettunen, T. L. Khoo, A. Kleinböhl, W. Korten, P. Kuusiniemi, R. Lucas, M. Muikku, P. Nieminen, R. D. Page, P. Rahkila, P. Reiter and A. Savelius, Ch. Schlegel, Ch. Theisen, W. H. Trzaska, H.-J. Wollersheim, Eur. Phys. J. A **6** (1999) 63

[Lei03] M. Leino, Nucl. Instr. and Meth. B **204** (2003) 129

[Lep06] A.-P. Leppänen, J. Uusitalo, P. T. Greenlees, R.-D. Herzberg, N. Amzal, F. Becker, P. A. Butler, A. J. C. Chewter, J. F. C. Cocks, O. Dorvaux, S. Eeckhaudt, K. Eskola, J. Gerl, T. Grahn, N. J. Hammond, K. Hauschild, K. Helariutta, F. P. Heßberger, M. Houry, G . D. Jones, P. M. Jones, R. Julin, S. Juutinen, H. Kankaanpää, H. Kettunen, T. L. Khoo, W. Korten, P. Kuusiniemi, Y. Le Coz, M. Leino, C. J. Lister, R. Lucas, M. Muikku, P. Nieminen, M. Nyman, R. D. Page, J. Pakarinen, P. Rahkila, P. Reiter, J. Sarén, Ch. Schlegel, C. Scholey, O. Stezowski, Ch. Theisen, W. H. Trzaska and H. J. Wollersheim, Eur. Phys. J. A **28** (2006) 301

[Loe68] K. E. G. Löbner, Phys. Lett. B **26** (1968) 42

[May49] M. G. Mayer, Phys. Rev. **75** (1949) 1969

[Mig59] A. B. Migdal, Nucl. Phys. **13** (1959) 655

[Mol97] P. Möller, J. R. Nix and K.-L. Kratz, At. Dat. Nucl. Dat. Tab. **66** (1997) 131.

[Muk05] G. Mukherjee, T. L. Khoo, R. Blinstrup, D. Seweryniak, I. Ahmad, P. A. Butler, M. P. Carpenter, P. Chowdhury, J. A. Cizewski, C. N. Davids, S. J. Freeman, J. P. Greene, N. J. Hammond, A. Heinz, R.-D. Herzberg, P. J. C. Ikin, R. V. F.Janssens, M. S. Johnson, G. D. Jones, F. G. Kondev, T. Lauritsen, C. J. Lister, E. F. Moore, E. Ngijoi-Yogo, P. Reiter and S.Sinha, AIP Conf. Proc. **764** (2005) 243

[Mul97] S. M. Mullins, G. D. Dracoulis, A. P. Byrne, T. R. McGoram, S. Bayer, W. A. Seale and F. G. Kondev, Phys. Lett. B **393** (1997) 279

[Mul76] L. G. Multhauf, K. G. Tirsell, and R. A. Meyer, Phys. Rev. C **13** (1976) 771

[Naz85] W. Nazarewicz, J. Dudek, R. Bengtsson, T. Bengtsson and I. Ragnarsson, Nucl. Phys. A **435** (1985) 397

[Neu73] W. Neubert, Nucl. Data Tables **11** (1973) 531

[Nil55] S. G. Nilsson, Kgl. Dan. Viden. Selsk. Mat. Fys. Medd. **29** No.16 (1955)

[Nil69] S. G. Nilsson, Ch. F. Tsang, A. Sobiczewski, Z. Szymaski, S. Wycech, Ch. Gustafson, I.-L. Lamm, P. Möller and B. Nilsson, Nucl. Phys. A **131** (1969) 1

[Nil95] S. G. Nilsson and I. Ragnarsson, *Shapes and Shells in Nuclear Structure*, Cambridge University Press, Cambridge (1995)

[Oga91] Yu. Ts. Oganessian, Yu. V. Lobanov, A. G. Popeko, F. Sh. Abdullin, Yu. P. Kharitonov, A. A. Ledovskoy and Yu. S. Tsyganov, Z. Phys. D **21** (1991) 357

[Pag03] R. D. Page, A. N. Andreyev, D. E. Appelbe, P. A. Butler, S. J. Freeman, P. T. Greenlees, R.-D. Herzberg, D. G. Jenkins, G. D. Jones, P. Jones, D. T. Joss, R. Julin, H. Kettunen, M. Leino, P. Rahkila, P. H. Regan, J. Simpson, J. Uusitalo, S. M. Vincent, R. Wadsworth, Nucl. Instr. and Meth. B **204** (2003) 634

[Pat91] Z. Patyk, A. Sobiczewski, Nucl. Phys. A **533** (1991) 132

[Pau02] E. S. Paul, postgraduate lecture notes, University of Liverpool (2002)

[Pau95] E. S. Paul, P. J. Woods, T. Davinson, R. D. Page, P. J. Sellin, C. W. Beausang, R. M. Clark, R. A. Cunningham, S. A. Forbes, D. B. Fossan, A. Gizon, J. Gizon, K. Hauschild, I. M. Hibbert, A. N. James, D. R. LaFosse, I. Lazarus, H. Schnare, J. Simpson, R. Wadsworth and M. P. Waring, Phys. Rev. C **51** (1995) 78

[Pet06] D. Peterson, B. B. Back, R. V. F. Janssens, T. L. Khoo, C. J. Lister, D. Seweryniak, I. Ahmad, M. P. Carpenter, C. N. Davids, A. A. Hecht, C. L. Jiang, T. Lauritsen, X. Wang, S. Zhu, F. G. Kondev, A. Heinz, J Qian, R. Winkler, P. Chowdhury, S. K. Tandel and U. S. Tandel, Phys. Rev. C **74** (2006) 014316

[Pol70] S. M. Polikanov and G. Sletten, Nucl. Phys. A **151** (1970) 656

[Rah07] P. Rahkila, submitted to Nucl. Instr. and Meth. A

[Ras59] J. O. Rasmussen, Phys. Rev. **113** (1959) 1593

[Rei99] P. Reiter, T. L. Khoo, C. J. Lister, D. Seweryniak, I. Ahmad, M. Alcorta, M. P. Carpenter, J. A. Cizewski, C. N. Davids, G. Gervais, J. P. Greene, W. F. Henning, R. V. F. Janssens, T. Lauritsen, S. Siem, A. A. Sonzogni, D. Sullivan, J. Uusitalo, I. Wiedenhöver, N. Amzal, P. A. Butler, A. J. Chewter, K. Y. Ding, N. Fotiades, J. D. Fox, P. T. Greenlees, R. D. Herzberg, G. D. Jones, W. Korten, M. Leino and K. Vetter, Phys. Rev. Lett. **82** (1999) 509

[Rei05] P. Reiter, T. L. Khoo, I. Ahmad, A. V. Afanasjev, A. Heinz, T. Lauritsen, C. J. Lister, D. Seweryniak, P. Bhattacharyya, P. A. Butler, M. P. Carpenter, A. J. Chewter, J. A. Cizewski, C. N. Davids, J. P. Greene, P. T. Greenlees, K. Helariutta, R.-D. Herzberg, R. V. F. Janssens, G. D. Jones, R. Julin, H.Kankaanpää, H. Kettunen, F. G. Kondev, P. Kuusiniemi, M. Leino, S. Siem, A. A. Sonzogni, J. Uusitalo and I.Wiedenhover, Phys. Rev. Lett. **95** (2005) 032501

[Rus61] L. I. Rusinov, Sov. Phys. Usp. **4** (1961) 282

[Sch01] G. Schiwietz and P. L. Grande, Nucl. Instr. and Meth. B **175 - 177** (2001) 125

[Sch84] K. H. Schmidt, C.-C. Sahm, K. Pielenz and H.-G. Clerc, Z. Phys. A **316** (1984) 19

[Sch00] K. H. Schmidt, Eur. Phys. J. A **8** (2000) 141

[Sim86] R. S. Simon, K.-H. Schmidt, F. P. Heßberger, S. Hlavac, M. Honusek, G. Münzenberg, H.-G. Clerc, U. Gollerthan, and W. Schwab, Z. Phys. A **325** (1986) 197

[Smi03] M. B. Smith, P. M. Walker, G. C. Ball, J. J. Carroll, P. E. Garrett, G. Hackman, R. Propri, F. Sarazin and H. C. Scraggs, Phys. Rev. C **68** (2003) 031302

[Sob89] A. Sobiczewski, Z. Patyk and S. Ćwiok, Phys. Lett. B **224** (1989) 1

[Sob01] A. Sobiczewski, I. Muntian and Z. Patyk, Phys. At. Nucl. 64 (2001) 1105

[Sol91] V. G. Soloviev, A. V. Sushkov and N. Yu. Shirikova, Yad. Fiz. **54** (1991) 1232

[Ste75] F. S. Stephens, Rev. Mod. Phys. **47** (1975) 43

[Str67] V. M. Strutinsky, Nucl. Phys. A **95** (1967) 420

[Sul07a] B. Sulignano, PhD thesis, University of Mainz (2007)

[Sul07b] B. Sulignano, S. Heinz, F. P. Heßberger, S. Hofmann, D. Ackermann, S. Antalic, B. Kindler, I. Kojouharov, P. Kuusiniemi, B. Lommel, R. Mann, K. Nishio, A. G. Popeko, Š. Šáro, B. Štreicher, M. Venhart and A. V. Yeremin, Eur. Phys. J. A **33** (2007) 327

[Sul07c] B. Sulignano, private commucation (2007)

[Tan06] S. K. Tandel, T. L. Khoo, D. Seweryniak, G. Mukherjee, I. Ahmad, B. Back, R. Blinstrup, M. P. Carpenter, J. Chapman, P. Chowdhury, C. N. Davids, A. A. Hecht, A. Heinz, P. Ikin, R. V. F. Janssens, F. G. Kondev, T. Lauritsen, C. J. Lister, E. F. Moore, D. Peterson, P. Reiter, U. S. Tandel, X. Wang and S. Zhu, Phys. Rev. Lett **97** (2006) 082502

[Trz90] W. H. Trzaska, Nucl. Instr. and Meth. in Phys. Res. A **297** (1990) 223

[Wal94] P. M. Walker, G. D. Dracoulis, A. P. Byrne, B. Fabricius, T. Kibédi, A. E. Stuchbery and N. Rowley, Nucl. Phys. A **568** (1994) 397

[Wal97] P. M. Walker, D. M. Cullen, C. S. Purry, D. E. Appelbe, A. P. Byrne, G. D. Dracoulis, T. Kibédi, F. G. Kondev, I. Y. Lee, A. O. Macchiavelli, A. T. Reed, P. H. Regan and F. Xu, Phys. Lett. B **408** (1997) 42

[Wal99] P. M. Walker and G. D. Dracoulis, Nature (London) **399** (1999) 35

[Wal01] P. M. Walker and G. D. Dracoulis, Hyper. Interact. **135** (2001) 83

[Woo54] R. D. Woods and D. S. Saxon, Phys. Rev. **95** (1954) 577

[Xu04] F. R. Xu, E. G. Zhao, R. Wyss and P. M. Walker, Phys. Rev. Lett. **92** (2004) 252501